



Diplomarbeit

Multi Body System of Racing Testbed Mechanics

von Peter Holzhammer

Durchgeführt am Institut für Fahrzeugtechnik
Vorstand: Univ.-Prof. Dr.techn. W. Hirschberg

und bei

Firma AVL List GmbH
Abteilung PR Racing
Graz

Betreuer: DI Cornelia Lex

Graz, im Dezember 2010

The logo of FTG, featuring the letters 'FTG' in a bold, blue, italicized font.

Acknowledgement

I would like to express my sincere gratitude to DI Cornelia Lex for her supervision and support from side of the TU Graz.

It is a pleasure to thank DI Matthias Dank for the great support from side of AVL List GmbH.

My deepest appreciation to Christoph Windisch from AVL List GmbH in helping me analysing the measurement data and working together from the initial to the final level.

1 Abstract

Engines are mounted in a different way on engine testbeds than inbuilt in the cars. This thesis shows that the vibration situation is a different as a consequence of that. This was done by analysing the measured vibration acceleration of a race car engine on an engine testbed and comparing it to measured vibration amplitudes of an engine inbuilt in a race car. The vibration condition has an influence on the life cycle of engine components and attached parts, which leads to another fatigue life of the engine on the testbed than on the track. Goal of AVL is to design an "adaptive engine mounting system" which arranges similar vibration situations on the testbed than in real case will occur. This is of special interest in motor sport since all components are dimensioned close to the fatigue limit. Base of the design is a multi body simulation of an engine and the engine testbed, which represents the vibration behaviour. Therefore the engine is reduced to a model of rigid bodies. A comparison to real case measurements shows, that the simulated vibration conditions do not represent the reality exactly. Nevertheless it still enables to evaluate possibilities for an "adaptive engine mounting systems". This theses discusses two different systems, one is to modify the engine mounting stiffness, which has influence on the vibration amplitude. The other possibility is to induce sinusoidal forces into the engine block which either excite or reduce vibration. It's shown that the adaptive engine mounting stiffness has great influence on the vibration amplitude close to the point of resonance. Far away from the resonant frequency the influence gets smaller and smaller. The application of forces however is effective over the whole engine speed band, but a high sophisticated controller with high resolution is needed in order to detect and control the phase shift between the implied forces in short time.

2 Contents

1	Abstract	1
2	Contents	2
3	Actual situation	4
4	Assignment of task	5
5	Engine and Race Car	6
5.1	Tankia 2008 vs. Formula 1 race car.....	6
5.2	Yamaha R6 vs. Formula 1 Engine:.....	7
5.2.1	Inertia forces:.....	8
5.2.2	Moments of inertia.....	15
6	Previous projects	16
6.1	Measurement on engine testbed.....	16
6.1.1	Testbed layout.....	16
6.1.2	The Sensors:.....	17
6.1.3	Test procedure:.....	17
6.2	Measurement on chassis dyno.....	18
6.2.1	Testbed layout.....	18
6.2.2	The Sensors:.....	19
6.2.3	Test procedure:.....	20
7	Preparation of Testbed Data	21
7.1	Raw data.....	21
7.2	Filtering.....	21
7.3	FFT Transformation.....	22
7.4	Running mode analyses.....	24
7.4.1	Definition of acceleration- and vibration velocity level.....	24
7.5	Calculation of second order vibration amplitude.....	25
7.6	Calculation of cg vibration.....	26
7.6.1	Rotation of a rigid body.....	26
7.6.2	Translation of a reference frame.....	26
7.6.3	Translation and Rotation of a Reference Frame.....	28
7.6.4	Solving an over determined equation system with method of least squares.....	31
7.7	Testbed vs. Chassis Dyno.....	33
7.7.1	Vibration of engine mounting points.....	35
7.7.2	Vibration of engine cg and angular velocity.....	36
7.7.3	Conclusion:.....	39
8	Multi Body Model of Engine and Engine Testbed	41
8.1	Simplifications:.....	41
8.1.1	Valve train.....	41
8.1.2	Rigid bodies:.....	41
8.1.3	Engine friction:.....	42
8.1.4	Rubber pads.....	42
8.1.5	Driveline.....	42
8.2	Mechanical Multi Body Model in Dymola.....	43

8.2.1	Engine	44
8.2.2	Gas force calculator.....	55
8.2.3	Clutch.....	57
8.2.4	Gearbox.....	58
8.2.5	Drive shaft	61
8.2.6	Torque gauge	63
8.2.7	Engine mounting frame	64
8.2.8	Rubber pad.....	66
8.3	Simulink Model	69
8.3.1	Dymola Block.....	70
8.3.2	Engine speed controller.....	71
9	Model Validation	75
9.1	Rigid body.....	75
9.2	Plausibility Check	76
9.2.1	Piston displacement:	77
9.2.2	Firing order	77
9.2.3	Engine Characteristic Map	78
9.2.4	Crank shaft torque	78
9.2.5	Excitation force	80
9.3	Simulation vs. Testbed	81
9.4	Conclusion:.....	83
10	Adaptive engine mounting stiffness	84
10.1	Simplified model of the engine mounted on the testbed	84
10.2	Conclusion:.....	88
11	Vibration Absorber	89
11.1	Model of Vibration Absorber.....	90
11.1.1	Dymola Model of Vibration Absorber.....	90
11.1.2	Simulink Model of vibration absorber	92
11.1.3	Vibration Absorber Map.....	96
11.1.4	Results.....	98
12	Conclusion	101
13	Future projects	102
14	List of references.....	103
15	Table of figures.....	104
16	Appendix A: Previous projects	106
17	Appendix B: Measurements Data	112
18	Appendix C: Multi-Body Simulation	122
19	Appendix D: Simulation vs. Testbed	137
20	Appendix E: Simulation Results incl. vibration absorbers	141

3 Actual situation

Engine testing on testbeds is an essential tool in professional motorsport for optimizing the engines performance but also in order to test the durability. Therefore driving manoeuvres and environmental conditions which occur on the racetrack are rearranged on the testbed close to reality. But nevertheless it occurs that the fatigue life which is determined on the testbed deviates from the life cycle reached in reality. In the first instance, his concerns attached electronic devices but also critical stressed mechanical engine components. A possible reason for this is the fact that the engine is mounted on the testbed in a different way than in the race car. Consequently the vibration conditions of the engines are different, which have an influence on the life cycle of the parts. Since the critical frequency of each part is not known, the goal is to arrange similar vibration conditions already on the testbed than on the race track will occur.

Therefore it's necessary to analyse and compare the conditions of vibration of an engine on a testbed and inbuilt in a race car in a close to realty project.

AVL List GmbH has all needed measurement and test equipment but a suitable race car was not available. For this reason AVL turned to the TU Graz Racing Team, one of the Formula SAE racing teams which are supported by AVL. Since that the TU Graz Racing Team became an important project partner of AVL and several measurements and tests were done on one of the TU Graz Racing Team's race cars, the so called Tankia 2008.

4 Assignment of task

The task was to analyse the vibration situation of the engine on the testbed and inbuilt in the race car. Previous test runs have been done in order to capture the vibration situation in the two different mounting situations which are described in chapter 6.

First task was to prepare the raw data of the real case measurements and to analyse the difference in vibration between the two mounting situations.

Next step was to build a multi-body model of the engine including the mounting on the testbed. The model has to be designed in a way, that it can be easily modified and adapted to other engine layouts, numbers of cylinders and testbed layouts. The simulation shall represent the vibration situation of the engine on the testbed as close to reality as possible.

Afterwards the model was validated with the real case test data and possibilities for an “adaptive engine mounting system” were discussed. This system has the function to generate a vibration condition which is similar to the conditions inbuilt in the race car.

Finally a model of an applicable adaptive engine mounting system was designed, implemented and tested in the multi-body simulation.

5 Engine and Race Car

For this analysis one of the race cars of the TU Graz Racing Team, the Tankia 2008 was used. The TU Graz Racing Team is one of the most successful Teams of students competing in the Formula SAE Competition. Motivation for using this race car was in first instance that the car and the engine are available for measurements and road tests and all measured data can be freely used without restrictions. This makes it possible to validate and evaluate simulations and test results with the reality and enables a proof of concept. Furthermore the possibility to get all needed technical information about the race car and the engine for the simulation was a big advantage.

But since the adaptive engine mounting system will be used in commercial motorsport, it has to be taken into account, that the Tankia 2008 has different specifications than most other race cars. As the Formula SAE series is primarily a design competition for students, the main objective lies in the technical design and not in driver skills and speed like in commercial motorsport. Because of the fact that most Formula SAE racing drivers are non professionals, the safety is of high importance. For this reason the engine power is limited through restrictions in intake area and engine displacement, which means that Formula SAE race cars generally have less power output than commercial race cars. Another fact is that the racetracks are very curvy and feature no long straights compared to commercial racetracks. This limits the average speed to a much lower level than most other racing series have. However the level of technical design in formula SAE is quite high and the used high-tech materials are similar to those used in Formula 1.

The following analysis shows the differences between a Formula 1 car and the Tankia 2008 and evaluates the ability to transfer the achieved results from the Tankia 2008 to a Formula 1 race car.

5.1 Tankia 2008 vs. Formula 1 race car

Technical data:

	Tankia 2008	Formula 1 race car
Weight:	175 kg without driver	Min. 620 kg with driver [Fed10]
Top speed:	170 km/h	More than 300 km/h
Acceleration 0-100 km/h:	3.4 sec	1.7 sec
Engine:	4-cylinder Yamaha R6 2006 engine, natural aspirated MPFI injection	8-cylinder 90°V engine, naturally aspirated [Fed10] Top feed injection
Displacement volume:	598 ccm	max. 2400 ccm [Fed10]
Stroke:	42.5 mm	39.7 mm
Bore:	67	max. 98 mm [Fed10]
rod length / stroke ratio:	2.13	2.56
Max. engine speed:	13500 rpm	18000 rpm [Fed10]

BMEP:	14.1 bar	15.2 bar [Kan10]
Mean piston speed:	22.95 m/s	25.5 m/s [Kan10]
Engine weight:	56 kg	min. 95 kg [Fed10]
Piston weight:	176 g	295 g [Kan10]
Reciprocating weight:	224 g	380 g [Kan10]
Chassis:	Open wheel open cockpit construction	Open wheel open cockpit construction
	Carbon fiber monocoque	Carbon fiber monocoque

table 5.1 technical data Formula SAE vs. Formula 1 race car

Same as a Formula 1 race car, the Tankia 2008 is an open wheel open cockpit construction using a carbon fibre monocoque as frame. It can be expected, that the chassis stiffness in relation to the size and weight of the race car is approximately the same for a Formula 1 car and the Tankia 2008. The big difference is the importance of aerodynamics. As the average speed of a Formula SAE race car is much less than the speed of a Formula 1 car, wings and other aerodynamic elements do not show that much effect on a Formula SAE car than in Formula 1. Consequently the aerodynamic forces acting on the Formula SAE monocoque are much smaller. But as the aerodynamic forces do not have much influence on the vibration situation of the engine, this difference is acceptable.

5.2 Yamaha R6 vs. Formula 1 Engine:

In Formula 1, 8-cylinder V-90 natural aspirated engines are in use. These engines have a displacement volume of maximum 2400 ccm [Fed10] . In comparison a formula SAE car has a maximum allowed displacement of 610 ccm. The engine layout is not regulated and can be chosen by every team. The Tankia 2008 uses the serial engine from the Yamaha R6 motorcycle, where the intake and exhaust system as well as the cam shafts are redesigned by the TU Graz Racing Team. This engine is a 4-cylinder in-line engine with a displacement volume of 600 ccm. By rule the intake area is restricted to a maximum diameter of 20 mm. The serial Yamaha R6 engine reaches a maximum speed of 17000 rpm but because of the air intake restriction the speed is limited to 13500 rpm in the Tankia 2008. The engines performance and fuel consumption were optimized on a professional testbed at AVL List GmbH. The brake mean effective pressure (BMEP) reaches values up to 14.1 bar. The mean piston speed has a maximum of 22.95 m/s. in comparison Formula 1 engines operate at engine speeds up to 17000 rpm, reach BMEP's of 15.2 bar and mean piston speeds of 25.5 m/s [Kan10] .

The technical data show, that the engine of the Tankia 2008 in general is much smaller than a Formula 1 engine, but looking at the displacement volume specific values, for example the brake mean effective cylinder pressure (BMEP) or the mean piston speed, the Yamaha R6 engine is not far away from the Formula 1 engine. The BMEP can be interpreted as the displacement volume specific torque and is approximately the same for both engines. Since the mean piston speed is approximately the same, the two engines are geometrically similar, which makes a scaling possible.

5.2.1 Inertia forces:

One of the main effects causing vibration are the unbalanced inertia forces of the engine. The following analysis shows the difference between the inertia forces of an 8-cylinder V90 and a 4-cylinder in-line engine:

5.2.1.1 Single-cylinder engine

First of all the appearance of inertia forces is explained using the example of a single cylinder engine. The moving parts can be reduced to the following simplified model:

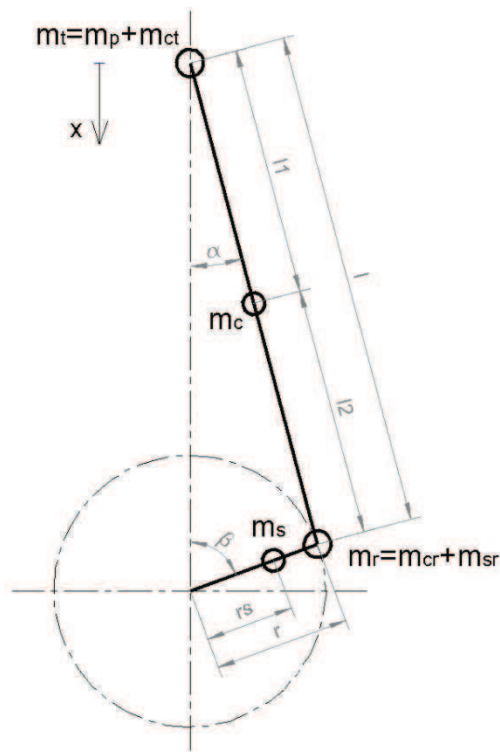


figure 5.1 simplified model of single cylinder crank mechanism

The piston follows a translational movement in direction of the cylinder axis. It can be assumed that the mass of the piston m_p concentrates in the centre of the piston pin.

The kinematics of the crank mechanism can be described with the following equations:

$$x = r + l - r \cdot \cos(\varphi) - l \cdot \cos(\beta) \tag{5.1}$$

$$\sin(\beta) = \frac{r}{l} \cdot \sin(\varphi) \tag{5.2}$$

These equations can be transformed and expanded to a Taylor series. Without proof the Taylor series explanation results in:

$$x = r \cdot (1 - \cos(\varphi) + \frac{r}{l} \cdot \frac{1}{2} \sin^2 \varphi + \left(\frac{r}{l}\right)^3 \cdot \frac{1}{8} \sin^4 \varphi + \left(\frac{r}{l}\right)^5 \cdot \frac{1}{16} \sin^6 \varphi + \dots) \tag{5.3}$$

In most cases the higher orders can be neglected because of the small value of the ratio $\frac{r}{l}$. Thus equation (5.3) reduces to the following form:

$$x = r \cdot (1 - \cos(\varphi) + \frac{r}{l} \cdot \frac{1}{2} \sin^2 \varphi) \tag{5.4}$$

By introducing the angular velocity $\omega = \frac{d\varphi}{dt}$ equation (5.4) can be written as:

$$x = r \cdot \left[1 - \cos(\omega t) + \frac{r}{l} \cdot \frac{1}{2} \sin^2(\omega t) \right] \tag{5.5}$$

The derivative of the displacement x gives the velocity of the piston v_P .

$$v_P = \frac{dx}{dt} = r \cdot \omega \cdot \left[\sin\varphi + \frac{1}{2 \cdot r} \cdot \sin(2\varphi) \right] \tag{5.6}$$

And the derivation of the velocity gives the piston acceleration a_P :

$$a_P = \frac{dv_P}{dt} = r \cdot \omega^2 \cdot \left[\cos\varphi + \frac{1}{r} \cdot \cos(2\varphi) \right] \tag{5.7}$$

The movement of the connecting rod is a combination of rotation and translation. As a simplification the connecting rod is split into two point masses, one is concentrated in the centre of the piston pin (m_{ct}) and the other in the centre of the crank pin (m_{cr}). So m_{ct} just perform a translational movement and m_{cr} a rotational. The amount of each part is calculated using the following equations:

$$m_{cr} + m_{ct} = m_c \tag{5.8}$$

$$m_{cr} \cdot l_1 = m_{ct} \cdot l_2 m_c \tag{5.9}$$

Equation (5.8) in (5.9) gives:

$$m_{ct} = \frac{l_1}{l} \cdot m_c \tag{5.10}$$

$$m_{cr} = \frac{l_2}{l} \cdot m_c \tag{5.11}$$

The mass of the crank shaft m_s is reduced to a point mass m_{sr} concentrated in the centre of the crank pin in a way that the centrifugal force remains the same.

$$m_{sr} = \frac{r_s}{r} \cdot m_s \tag{5.12}$$

Now the whole system is simplified to two point masses, one moving in a translational (m_t) and the other in a rotational (m_r) way.

where:

$$m_t = m_p + m_{ct} \tag{5.13}$$

and:

$$m_r = m_{cr} + m_{sr} \tag{5.14}$$

Consequently there are two masses which can cause inertia forces.

First we consider the translational masses m_t . The inertia force equals to the mass times the acceleration:

$$F_t = -m_t \cdot a_p \tag{5.15}$$

Substitution of the piston acceleration from equation (5.7) in equation (5.15) results the translational inertia force:

$$F_t = \underbrace{-m_t \cdot r \cdot \omega^2 \cdot \cos\varphi}_{F_I} - \underbrace{m_t \cdot r \cdot \omega^2 \cdot \frac{r}{l} \cdot \cos(2\varphi)}_{F_{II}} \tag{5.16}$$

The inertia force can be split into two parts: the first order inertia force (F_I), which oscillates with the crank shaft frequency and the second order inertia force (F_{II}) which oscillates with the double crank shaft frequency.

$$F_I = -m_t \cdot r \cdot \omega^2 \cdot \cos\varphi \tag{5.17}$$

$$F_{II} = -m_t \cdot r \cdot \omega^2 \cdot \frac{r}{l} \cdot \cos(2\varphi) \tag{5.18}$$

The rotational masses accelerate with constant value in radial direction. Thus the inertia force can be calculated using following equations:

$$a_r = r \cdot \omega^2 \tag{5.19}$$

$$F_r = m_r \cdot r \cdot \omega^2 \tag{5.20}$$

This force is constant in radial direction at constant engine speed and can be easily compensated. Because of the fact that rotational inertia forces are balanced in nearly every engine, these forces are not taken into consideration in the further analyses.

5.2.1.2 4-cylinder in-line engine:

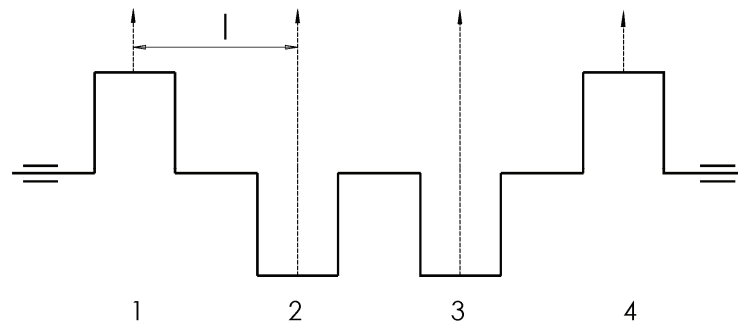


figure 5.2 layout crank shaft 4-cylinder in-line engine

The crank angles of cylinders one to four, beginning with one are 0, 180, 540 and 360 degrees. The resulting inertia forces are visualized in the following vector diagrams:

First order inertia forces:

In the following diagram the first order inertia forces are visualised as rotation vectors. The force of cylinder two is 180 degrees cranked in respect to cylinder one. The force of cylinder three is 540 degrees and of cylinder four 360 degrees cranked.

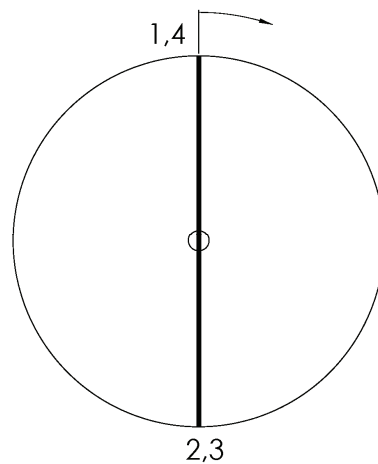


figure 5.3 vector diagram 1st order inertia forces 4-cylinder in-line engine

The first order mass force of cylinder one and four are acting in the positive cylinder axis direction. The mass force of cylinder two and three are acting in contrariwise direction. Since the amount of every force is the same, cylinder two and three compensate the inertia force of cylinder one and four. That means that a four cylinder in-line engine is completely balanced in first order.

Second order inertia forces:

The second order inertia forces rotate in double frequency to the crank shaft. That means that in the vector diagram the second order inertia forces have to be rotated by the double crank angle. Hence the second order inertia forces of each cylinder occur with 360 degrees of phase shift.

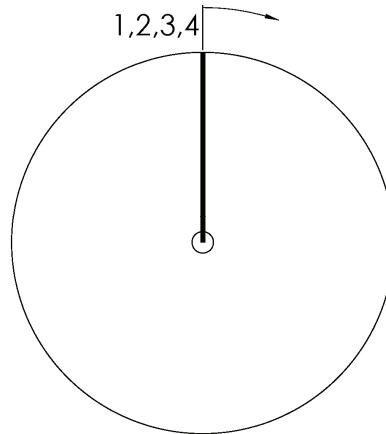


figure 5.4 vector diagram 2nd order inertia forces 4-cylinder in-line engine

The second order inertia forces of all cylinders act in positive cylinder axis direction. Consequently the resulting second order excitation force equals four times the second order inertia force and acts in direction of the cylinder axis.

$$F_{ex,4cyl} = 4 \cdot F_{II} \tag{5.21}$$

The excitation of the 4-cylinder in-line engine equals according equation (5.18) and equation (5.21) to:

$$F_{ex,4cyl} = -4 \cdot m_t \cdot r \cdot \omega^2 \cdot \frac{r}{l} \cdot \cos(2\varphi) \tag{5.22}$$

5.2.1.3 8-cylinder 90°V engine:

The crank shafts of 8-cylinder engines exist in two different layouts, the cross-plane and the flat-plane layout. The cross-plane crank shaft has crank angles of 90 degrees. It has the advantage, that there are no first and second order inertia forces. Only first order moments of inertia occur. The flat-plane layout has crank angles of 180 degrees. This gives a flat, symmetric crank shaft similar to a 4-cylinder in-line engine.

In motorsport mostly flat-plane layouts are in use, so also in Formula 1. The main advantage is that flat-plane crank shafts are lighter compared to cross-plane shafts. Consequently also the rotational inertia is reduced which provides a sharper response. But the balance of the inertia forces is a different.

The flat-plane crank shaft of an 8-cylinder V engine has a similar layout than the crank shaft of a 4-cylinder in-line engine, with the only difference that two con-rods are connected to each crank pin. Consequently the 8-cylinder V engine can be considered as two inclined 4-cylinder in-line engines which make use of the same crank shaft.

First order inertia forces:

Since the first order inertia forces of a 4-cylinder in-line engine are balanced, they are balanced for the 8-cylinder V90° engine too.

Second Order inertia forces:

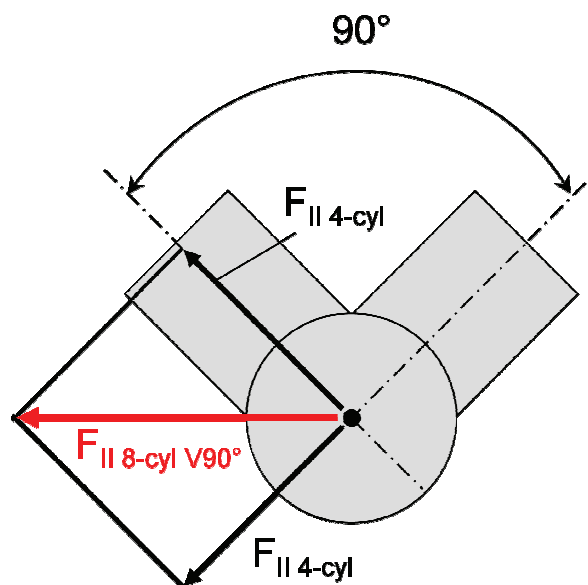


figure 5.5 Second order inertia forces 8-cylinder V90° engine

According chapter 5.2.1.2 the second order inertia forces of a 4-cylinder in-line engine act in positive cylinder axis direction. The second 4-cylinder in-line engine has an inclination of 90 degrees compared to the first one. Hence the second order inertia force has a phase shift of about the double of the inclination angle and consequently acts in negative cylinder axis direction. This is visualised in figure 5.5.

The resultant force is the vectorial summation of the inertia forces of the two 4-cylinder engines. The result is a force, which acts in transversal direction with the value according equation (5.23).

$$F_{II\ 8-cyl\ V90^\circ} = \sqrt{2} \cdot F_{II\ 4-cyl}$$

(5.23)

5.2.1.4 Inertia forces Formula 1 vs. Formula SAE

The previous chapters describe the relation between the unbalanced inertia forces of a 4-cylinder in-line engine which is used in the Tankia 2008 and the in Formula 1 used 8-cylinder V90 engine. The Substitution of the corresponding values in table 5.1 in equation (5.18) and equation (5.23) result the second order inertia forces of the Formula 1 engine $F_{II\ F1}$ and the Yamaha R6 engine $F_{II\ R6}$ which is used in the Tankia 2008.

$$F_{II\ F1} = 0.01667 \cdot \omega^2 \cdot \cos(2\varphi)$$

$$F_{II\ R6} = 0.00893 \cdot \omega^2 \cdot \cos(2\varphi)$$

(5.24)

Putting these two values into relation it can be assume that the second order inertia force of a Formula 1 engine equals 1.864 times the inertia force of the Yamaha R6 engine at the same engine speed.

$$F_{II\ F1} / F_{II\ R6} = \frac{0.01667 \cdot \omega^2 \cdot \cos(2\varphi)}{0.00893 \cdot \omega^2 \cdot \cos(2\varphi)} = 1.864$$

(5.25)

Conclusion:

Despite the fact that the engine which is used in the Tankia 2008 has much less power output than a Formula 1 engine, these engines show analogies in many fields. Both engines are free of first order inertia forces and moments of inertia. Only second order inertia forces occur but with the difference that they act in transverse direction for the 8-cylinder V90° engine and in vertical direction for the 4-cylinder in-line engine, with a scaling factor of 1.864 according equation (5.25). Since the displacement volume specific values are similar, a direct comparison is possible. Because of these facts we can assume that a Formula 1 engine will have similar vibration behaviour than the engine of the Tankia 2008 but the direction of the path is a different.

5.2.2 Moments of inertia

Since both engines are completely symmetric, no moments of inertia occur.

6 Previous projects

6.1 Measurement on engine testbed

Since the year 2005 the TU Graz Racing Team optimizes the performance of their engine on a professional engine testbed of AVL. In 2008 additional to the standard measurements the accelerations in all three directions of all four engine mounting points were measured. These measurements were done by AVL List GmbH under the direction of Josef Retzl in cooperation with the TU Graz Racing Team. Therefore acceleration sensors were attached nearby the mounting points. An additional sensor measures the movement of the base frame.

6.1.1 Testbed layout

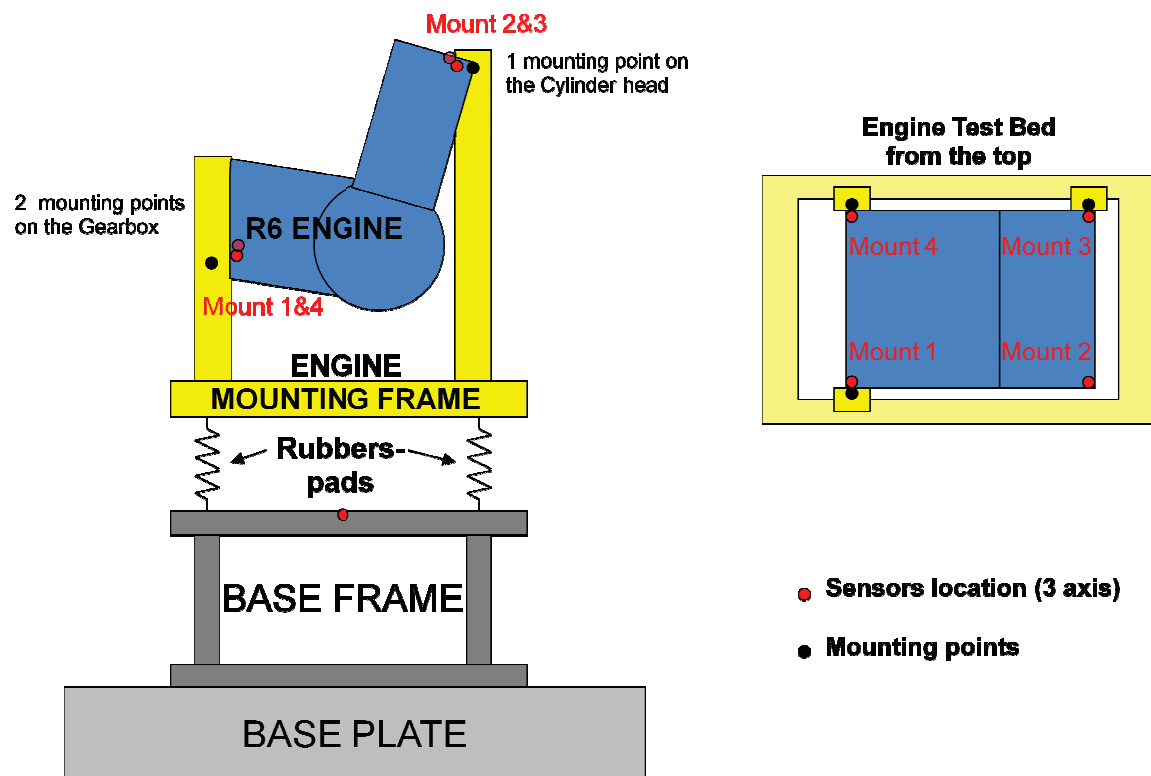


figure 6.1 layout engine testbed

The engine is mounted on a steel mounting frame which is attached with rubber pads on the solid base frame and finally on the testbed base plate. First it was planned to mount the engine on four points on the mounting frame but as the second mounting of the mounting frame collided with the exhaust system just three points could be used. This does not exactly represent the mounting situation in the race car, where the engine is connected to the chassis on all four points.

Position of acceleration sensors:

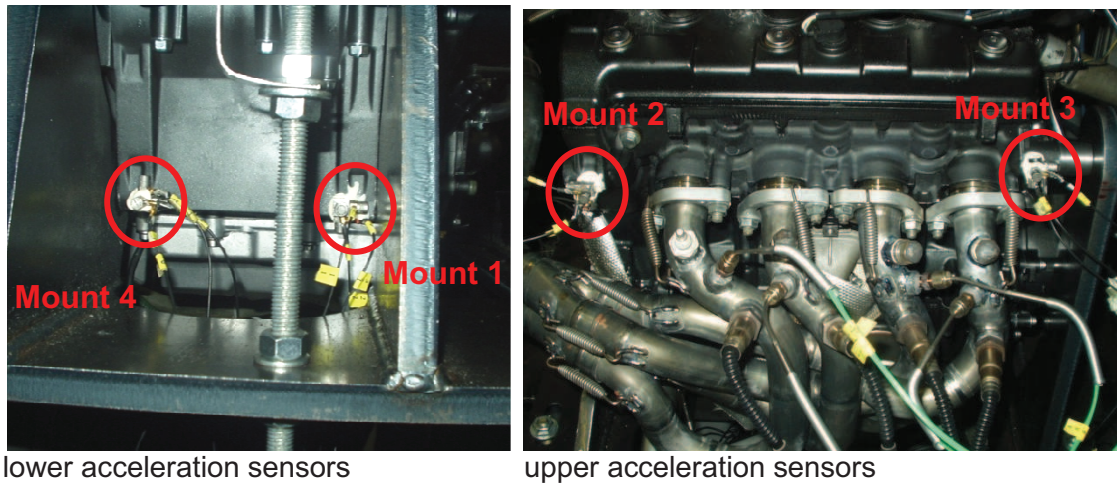


figure 6.2 sensor position on engine testbed

Four acceleration sensors were mounted on the engine block, two nearby the upper mounting points on the cylinder head and two close to the lower mounting points. An additional sensor measures the acceleration of the base frame which turned out to be negligible and wasn't taken into account in the model.

6.1.2 The Sensors:

For the measurement the three dimensional piezoelectric charge accelerometers "B&K 4393" from Bruel & Kjaer were used. A data sheet is attached in the appendix.

The measurement system was the Vibro acoustic measurement system (PAK 5.4 sr 9) from Müller BBM.

The sample frequency was 25600 Hz.

6.1.3 Test procedure:

The acceleration was measured at full throttle and halve throttle. The engine speed was varied in a linear run up from 4000 to 13500 rpm in 200 seconds according figure 6.3. The engine speed was controlled by the testbed-dynamometer. This test was done at different gear ratios in order to show the influence of the gear number on the vibration. One test run was also done at unfired operation. After that the mean value of the vibration velocity was plotted in a graph for all test runs. This graph can be found in the appendix. It can be seen, that the influence of the gear ratio is not significant, but there is a difference if the engine is fired or unfired. For this reason the gear has not been changed during one run-up.

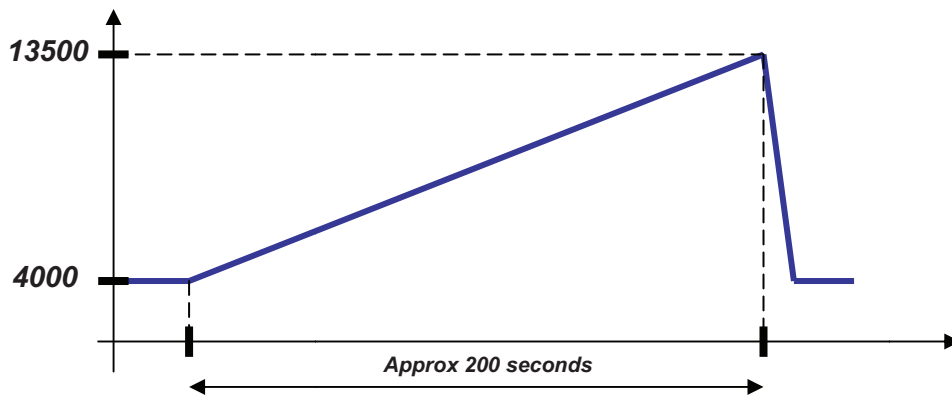


figure 6.3 test procedure engine testbed

6.2 Measurement on chassis dyno

The accelerations of the mounting points were measured in the race car. The measurements were done on a chassis dyno, as road tests would be too complex. For road tests it would be necessary to take along the measurement signal amplifier, the data acquisition system and the power supply for the sensors on the race car. This would influence the weight of the car and the centre of gravity and consequently the natural frequency of the car which influences the vibration situation of the engine. Thus the measured data would not represent the reality. Because of these facts the tests were done on the chassis dyno. Another advantage of the chassis dyno is that the test can be done at defined ideal conditions without environmental influences, for instance vibrations caused due to roughness of the road which disturb the measurement.

6.2.1 Testbed layout

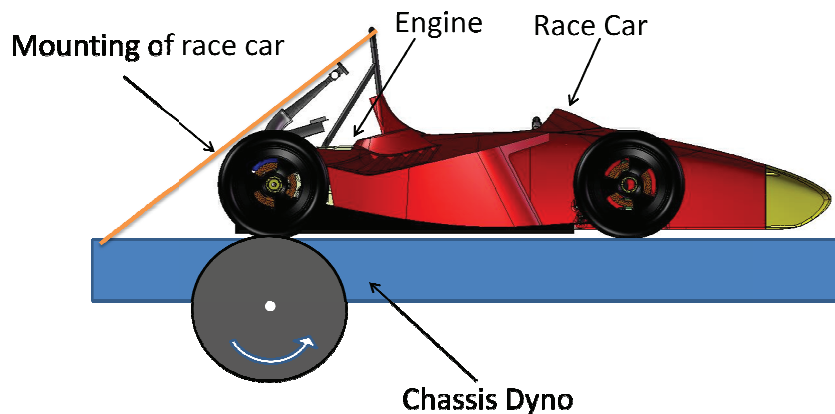


figure 6.4 schematic diagram of chassis dyno

figure 6.4 schematically shows the layout of the chassis dyno. The race car was restrained with lashing straps in order to avoid movement of the car. The lashing straps were mounted on the top of the main roll hoop as there was no other possible position. Because of the high position of the restrain belt a torque is generated, which loads the rear tires and unloads the front tires. This has the advantage that the risk of wheelspin is reduced because of the higher contact force of the rear tires, but it doesn't represent the real situation on the track exactly. The risk is that the rear suspension goes into complete bump and the dampers reach its final position at the bump stops. In this case the vibration from the unsuspended masses is nearly undamped when being transformed into the chassis. By analyzing the measured data it has to be taken into account that the oscillation of the chassis heterodynes the oscillation of the engine.

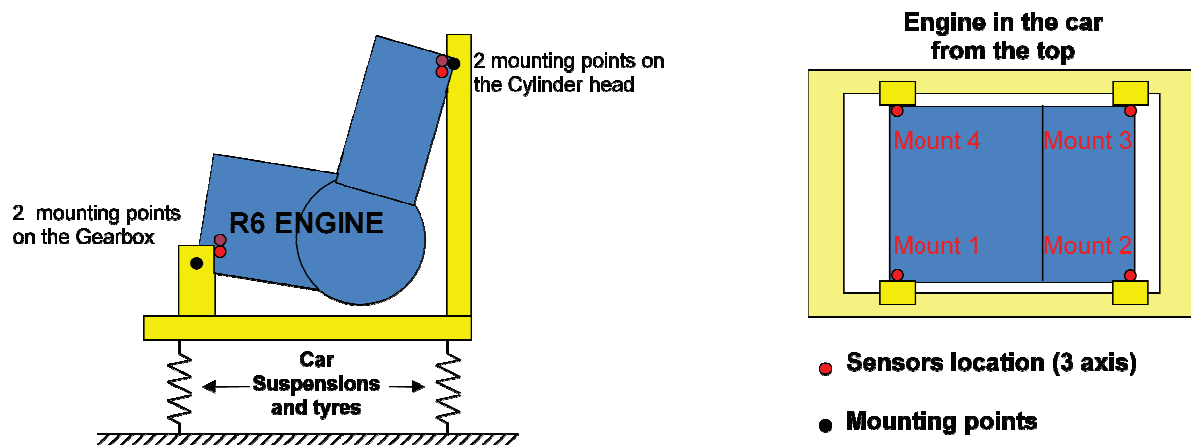


figure 6.5 mounting situation on chassis dyno

The mounting of the engine is different than on the engine testbed. In one hand the engine is mounted on four points and in the other hand the stiffness of the chassis is a different than the stiffness of the engine mounting frame attached to the rubber pads on the engine testbed.

The accelerations were measured on the same positions than on the engine testbed which has been done in the previous project. Four sensors are glued nearby the mounting points.

6.2.2 The Sensors:

For the measurement on the chassis dyno the same sensors and measurement system where used than described in chapter 6.1.2.

The sample frequency was 32768 Hz.

6.2.3 Test procedure:

The testrun was done in a similar way than on the engine testbed which is described in chapter 6.1.3. The only difference is that the runup was done in a time range of approximately 10 seconds.

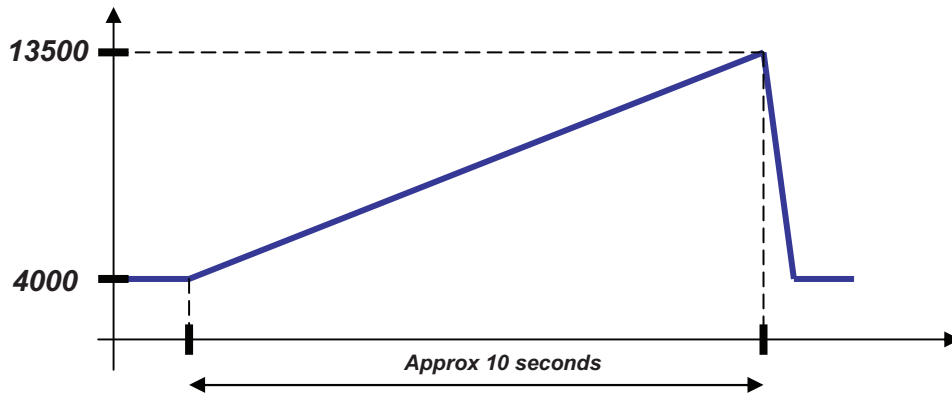


figure 6.6 test procedure on chassis dyno

7 Preparation of Measurement Data

7.1 Raw data

Both on the testbed and on the chassis dyno the accelerations were measured using four acceleration sensors which were fixed nearby the engine mounting points. Each sensor outputs a voltage which is proportional to the acceleration in three channels for the three directions x, y and z. As the chosen coordinate system is a different than the used in the simulation, the coordinates had to be transformed. For further calculations a coordinate system was used which has same directions than the ISO 70000 system but the origin is chosen in the engine reference point. The engine reference point is situated concentrically in the central crank shaft bearing. Consequently the x-axis shows in the direction of motion of the car, the z-axis in vertical direction and the y-axis in lateral direction.

The measurement was done with the Vibro acoustic measurement system (PAK 5.4 sr 11) from Müller BBM. This system doesn't only output the acceleration, but also the internal computed integration of the acceleration, the vibration velocity. Problem was that the raw data show high measurement noise and a big zero offset. For this reason an offset compensation and filtering was necessary.

The raw data were stored in a matrix with 13 columns. The first column is the time vector; the second column begins with the x-acceleration of mounting point 1. The following columns content the acceleration vectors in y- and z- direction of mounting point 1 and the accelerations of the other points in ascending order.

Same data are available for the vibration velocity.

$$\begin{pmatrix} t & a_{1,x} & a_{1,y} & a_{1,z} & a_{2,x} & a_{2,y} & a_{2,z} & a_{3,x} & a_{3,y} & a_{3,z} & a_{4,x} & a_{4,y} & a_{4,z} \\ \vdots & \vdots & \vdots & \vdots & \vdots & \vdots & \vdots & \vdots & \vdots & \vdots & \vdots & \vdots & \vdots \end{pmatrix}$$

figure 7.1 shape of raw data matrix

7.2 Filtering

The raw data were filtered with a highpass Butterworth filter. The highpass filter reduces vibration amplitudes in low frequency range and let high frequent signals pass. Reason for the filtering was that the data show high amplitudes in a frequency range of 1 to 3 Hz at the chassis dyno measurements. This is due to the natural frequency of the chassis, which lies in this range. As these oscillations are not caused as consequence of the excitation of the engine, these vibrations are not of interest and were filtered out. A cutoff frequency of 25 Hz means that the attenuation of the magnitude equals to 3 dB at a frequency of 25 Hz.

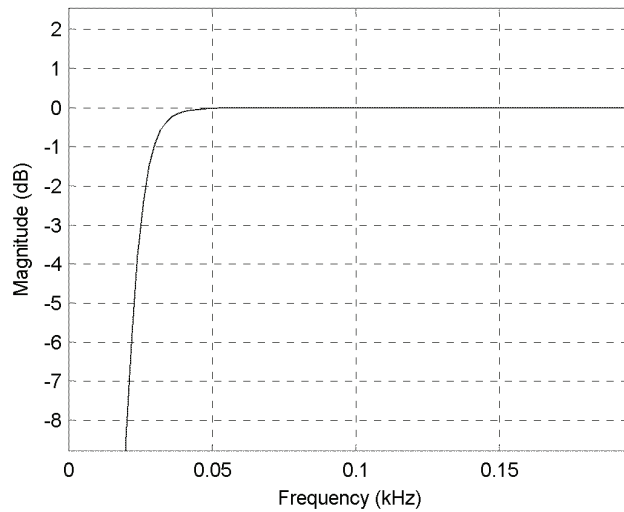


figure 7.2 lowpass Butterworth filter design

The figure shows that the magnitude is attenuated at frequencies below approximately 50Hz. In this case the low frequent errors but also the zero-offset are eliminated without doing modifications on the vibration due to the second order excitation, which lies in a range between 130 and 450 Hz.

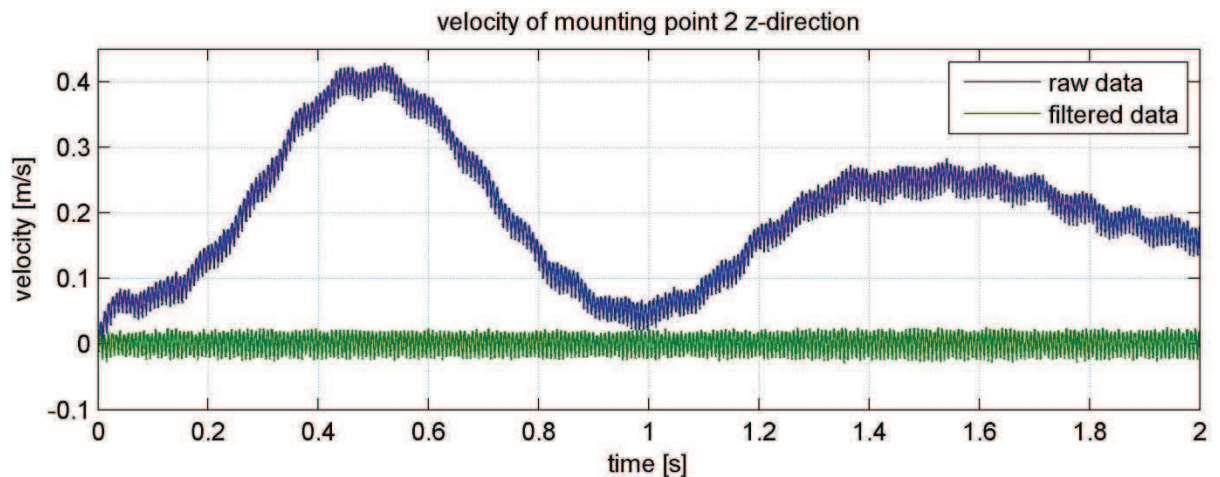


figure 7.3 raw data vs. Filtered data

7.3 FFT Transformation

A Fast Fourier Transformation (FFT) was done in order to allocate the vibration amplitude spectrum to the corresponding frequency at the specific engine speed. As the engine speed was varied in a run-up from 4000 rpm to 13500 rpm, the data were split into 512 classes. The mean value of the engine speed of each class was defined as the

corresponding engine speed. Of each class a FFT was done in order to detect the characteristic vibrations at the specific engine speed.

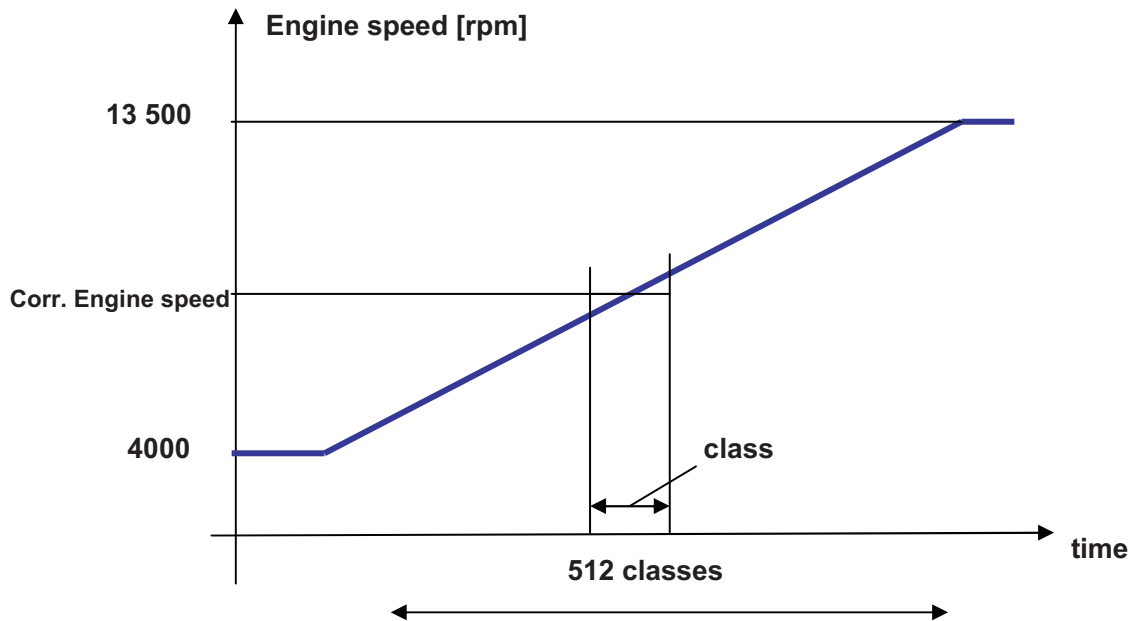


figure 7.4 Classification of data for FFT

First of all the raw data had to be cut at the beginning and the end of the runup. Also the time vector was deleted as it is not used for the FFT. Then the data are split into its classes. This was done using the Matlab function “reshape”. Thereby the 2-dimension raw data matrix is transformed into a 3-dimensional matrix, where each plane in the third direction represents one measurement channel. By using 512 classes the reshaped matrix equates a length x 512 x 12 matrix, where “length” represents the number of measurements in each class.

After that for each channel a FFT was done by using the Matlab function “fft(X,n)”. This function returns the n-point discrete Fourier transformation of the matrix X. If X is a matrix, fft returns the Fourier transformation of each column. For the number of points n the sample frequency fs of the recorded measurements was chosen. In this case the result matrix Y has the same width than the input matrix X and the length equals the sample frequency. The frequency resolution $d_f = \frac{f_a}{n}$ equals 1 what means that one step in the resultant matrix Y equates to a frequency step of 1 Hz.

$$Y = \text{fft}(X, fs) \quad [\text{Mat10}]$$

(7.1)

The amplitude spectrum of the oscillations equals to two times the absolute value of the result matrix divided by the length of the input matrix X.

$$IY = 2 \cdot \text{abs}(Y) / \text{lenght}(X) \quad [\text{Mat10}] \quad (7.2)$$

The frequency vector equals:

$$f = 0: d_f: f_a - d_f \quad (7.3)$$

7.4 Running mode analyses

Plotting the amplitude spectrum over the frequency vector and the engine speed in a 3-dimensional mesh gives a view over the vibration response of the system at the corresponding excitation. This is called a running mode analyses.

For a better visualization the results are plotted as a vibration level in logarithmic scale.

As an example the acceleration level of mounting point 1 in z-direction is shown in figure 7.9. The results of the other mounting points are attached in the appendix. The running mode analysis of the acceleration level was available from the previous project under the direction of Josef Retzl. The plots of the vibration velocity level had to be prepared by myself and can be found in the appendix.

The plotted results show the acceleration level in [dB] of the engine mounting points. Therefore the vibration frequency measured in the mounting points is plotted over the engine speed. In other words, the ordinate demonstrates the frequency of the excitation and the abscissa shows the corresponding system response. These figures demonstrate the vibration situation and its dependency on the engine speed for the testbed and the chassis dyno.

7.4.1 Definition of acceleration- and vibration velocity level

The acceleration level is often used to characterize structure-borne noise. Therefore the movement of the surface of a body has to be quantified. Like the noise level the acceleration level is plotted in a logarithmic scale as a level measured in Decibel [dB]. The acceleration is based on an acceleration value a_0 of 10^{-6} m/s^2 according ISO R 1683.

$$L_a = 20 \cdot \log\left(\frac{a}{a_0}\right) \text{ dB} \quad [\text{Kol00}]$$

Through integration of the acceleration level, the vibration velocity level can be defined. For a sinusoidal oscillation the velocity amplitude is $\frac{1}{\omega}$ times the acceleration.

$$L_v = 20 \cdot \log\left(\frac{v}{v_0}\right) \text{ dB} \quad [\text{Kol00}]$$

The base value for the vibration velocity v_0 level according to ISO R 1683 is 10^{-9} m/s.

7.5 Calculation of second order vibration amplitude

For further analyses the amplitude of the second order vibration is of interest. For this reason a plot has to be defined where only the second order vibration is apparent. That was done by filtering out the second order vibration and visualising it in a 2-dimensional plot.

The FFT returns the vibration amplitude to the corresponding frequency. Now we just need to look at the amplitude which occurs at a frequency which equates two times the engine speed. If we look on one plane in the 3rd direction of the 3-dimensional result vector from the FFT, we get the amplitude spectrum at a specific engine speed. figure 7.5 shows the amplitude spectrum at an engine speed of 10 000 rpm of the engine testbed measurements.

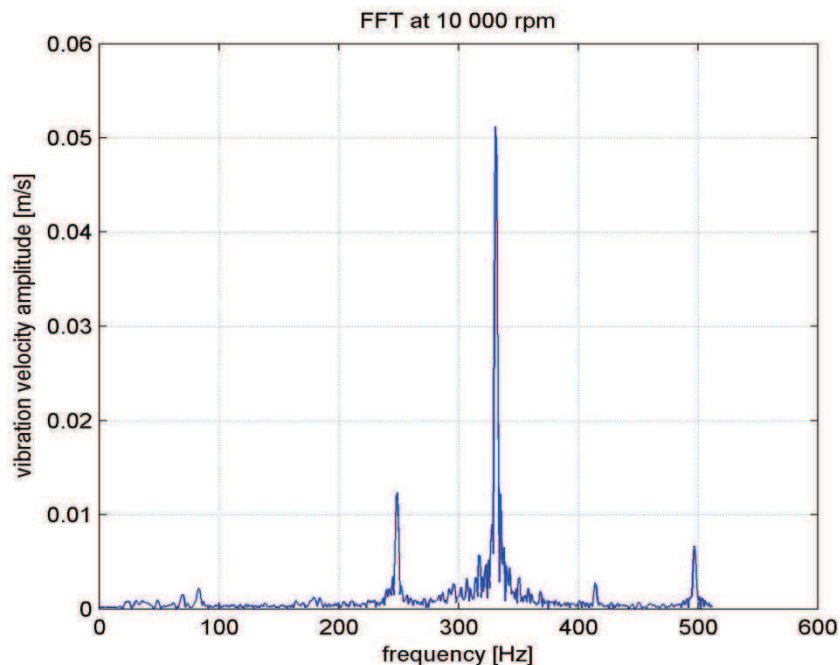


figure 7.5 FFT at 10 000 rpm on engine testbed

It's obvious that there is a maximum at a frequency which equals the double engine speed. This maximum is the amplitude we are looking for. Since the corresponding engine speed is not exactly at the right position, we are looking for the maximum in a vicinity of 20 steps before and after the specific engine speed. This was done for all of the 512 classes. The results are plotted in figure 7.10. The complete result plots can be found in the appendix.

7.6 Calculation of cg vibration

The previous measurement gives information about the vibration of the mounting points, but the movement of the whole system is not evident. In order to get this information, the vibration of centre of gravity and the angular velocity is of interest.

7.6.1 Rotation of a rigid body

The following derivations describe the movement of a frame of reference in an inertial system. The analyses are based on the book "Technische Mechanik 3" from Hauger, Schnell and Gross [Hau02].

We consider the rotation of a point P of a rigid body around a fixed point A. The unit vector \vec{e}_ω describes the instantaneous location of the rotation axle. The rigid body rotates about the angle $d\varphi$ at a time range dt . The displacement of point P is $d\vec{r}_P$ and can be described with the following equation:

$$d\vec{r}_P = (\vec{e}_\omega \times \vec{r}_{AP})d\varphi \quad (7.4)$$

Where $\vec{e}_\omega \times \vec{r}_{AP}$ describes a vector which is normal to \vec{e}_ω and \vec{r}_{AP} and the amount equals the distance from the rotation axle to the point P.

Introducing the angular velocity

$$\vec{\omega} = \frac{d\varphi}{dt} = \dot{\varphi} \cdot \vec{e}_\omega = \omega \cdot \vec{e}_\omega \quad (7.5)$$

results for the velocity $\vec{v}_P = \frac{d\vec{r}_P}{dt}$ of point P:

$$\boxed{\vec{v}_P = \vec{\omega} \times \vec{r}_{AP}} \quad (7.6)$$

7.6.2 Translation of a reference frame

We analyse the movement of a point P in respect to two frames. The x, y, z frame is fixed and in that case an inertial system. The ξ, η, ζ -systeme is moved in respect to the inertial system.

First of all we just consider a translational movement of frame ξ, η, ζ .

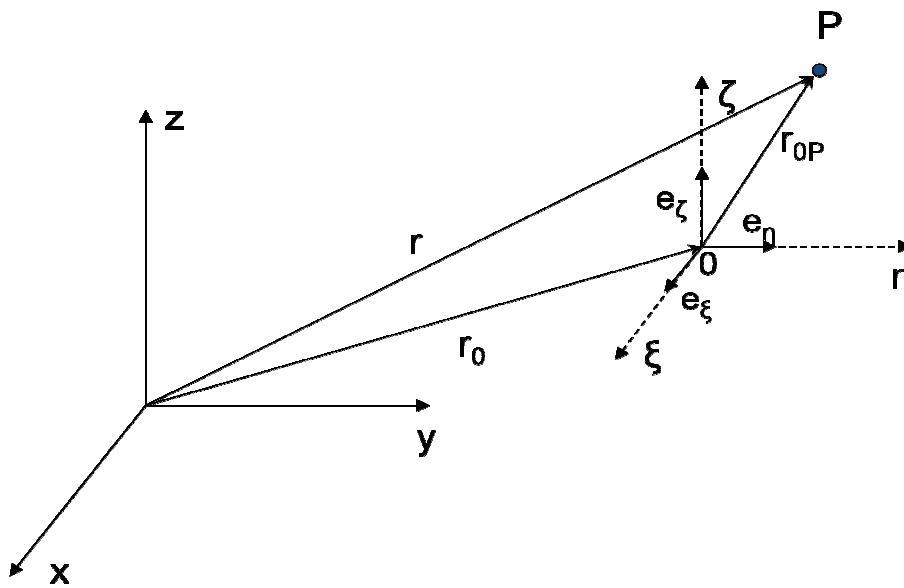


figure 7.6 translation of a reference frame

The position vector to point P equals

$$(7.7)$$

The vector can be written as:

$$(7.8)$$

With the unit vectors , and of the moved frame.

The velocity of point P measured in the inertial frame is called the absolute velocity and can be determined through derivation in respect to the time.

$$(7.9)$$

With . The unit vectors do not change as there is no rotation.

7.6.3 Translation and Rotation of a Reference Frame

Now we consider that the frame ξ, η, ζ does perform a translation and rotation in respect to the fixed frame.

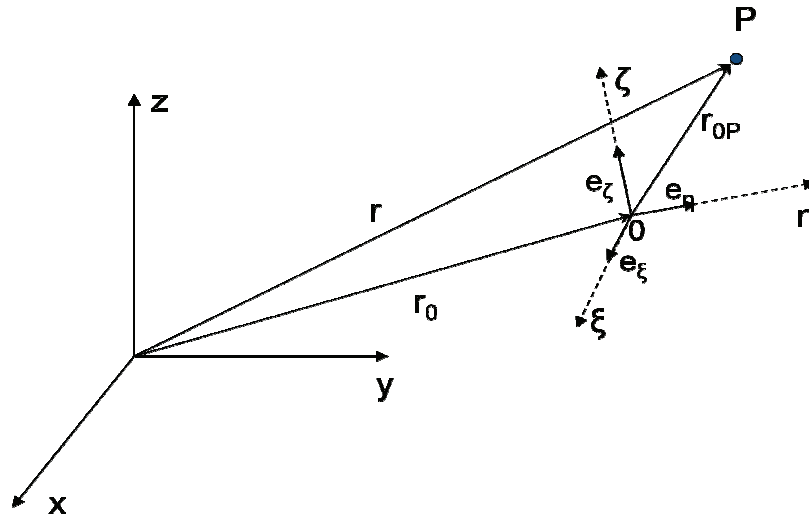


figure 7.7 translation and rotation of a reference frame

Again the position vector of point P equals:

$$(7.10)$$

With

The absolute velocity of point P can be determined through derivation of . In this case the unit vectors cannot be assumed to be constant, as there is a rotation.

$$(7.11)$$

With:

$$(7.12)$$

The frame of reference is rotating with the angular velocity $\vec{\omega}$. In this case the periodic change of the unit vectors equals according equation (7.6)

$$\dot{\vec{e}}_{\xi} = \vec{\omega} \times \vec{e}_{\xi}, \quad \dot{\vec{e}}_{\eta} = \vec{\omega} \times \vec{e}_{\eta}, \quad \dot{\vec{e}}_{\zeta} = \vec{\omega} \times \vec{e}_{\zeta}$$

Consequently:

$$\begin{aligned} \xi \cdot \dot{\vec{e}}_{\xi} + \eta \cdot \dot{\vec{e}}_{\eta} + \zeta \cdot \dot{\vec{e}}_{\zeta} &= \xi \vec{\omega} \times \vec{e}_{\xi} + \eta \vec{\omega} \times \vec{e}_{\eta} + \zeta \vec{\omega} \times \vec{e}_{\zeta} \\ &= \vec{\omega} \times (\xi \cdot \vec{e}_{\xi} + \eta \cdot \vec{e}_{\eta} + \zeta \cdot \vec{e}_{\zeta}) \\ &= \vec{\omega} \times \vec{r}_{0P} \end{aligned}$$

(7.13)

Substitute this in equation (7.12) gives:

$$\dot{\vec{r}}_{0P} = (\dot{\xi} \cdot \vec{e}_{\xi} + \dot{\eta} \cdot \vec{e}_{\eta} + \dot{\zeta} \cdot \vec{e}_{\zeta}) + \vec{\omega} \times \vec{r}_{0P}$$

(7.14)

The expression $(\dot{\xi} \cdot \vec{e}_{\xi} + \dot{\eta} \cdot \vec{e}_{\eta} + \dot{\zeta} \cdot \vec{e}_{\zeta})$ represents the periodic change of the vector \vec{r}_{0P} in respect to the moving frame and is indicated as $\frac{d^* \vec{r}_{0P}}{dt}$.

$$\frac{d^* \vec{r}_{0P}}{dt} = (\dot{\xi} \cdot \vec{e}_{\xi} + \dot{\eta} \cdot \vec{e}_{\eta} + \dot{\zeta} \cdot \vec{e}_{\zeta})$$

(7.15)

Finally the velocity of point P in respect to the moving frame equals:

$$\dot{\vec{r}}_{0P} = \frac{d^* \vec{r}_{0P}}{dt} + \vec{\omega} \times \vec{r}_{0P}$$

(7.16)

Entering equation (7.16) in (7.11) gives the absolute velocity of point P:

$$\boxed{\vec{v}_a = \dot{\vec{r}} = \dot{\vec{r}}_0 + \vec{\omega} \times \vec{r}_{0P} + \frac{d^* \vec{r}_{0P}}{dt}}$$

(7.17)

This equation can be applied to our system. If the origin of the moved frame is placed in the centre of gravity of the engine, the following assertion can be done:

equals the measured absolute velocity of a mounting point, equals the translation velocity of the centre of gravity of the engine in respect to the inertial frame and equals the angular velocity of the engine.

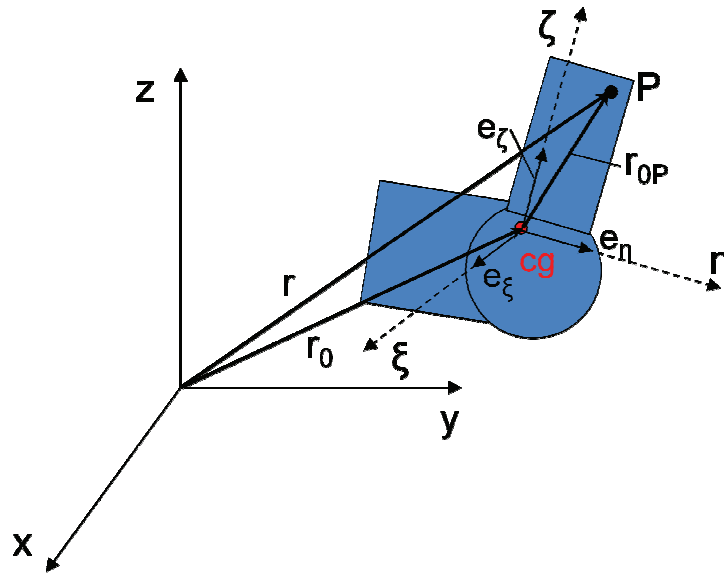


figure 7.8 translation and rotation of engine cg

The term \dot{r}_{0P} represents the velocity of point P in respect to the moving frame, or applied to our system the velocity of the mounting point in respect to the centre of gravity. As the engine is assumed to be a rigid body, the distance between the engine cg and the mounting points is constant and consequently \dot{r}_{0P} equals zero.

In this case equation (7.17) can be reduced to:

$$\dot{r} = \dot{r}_0 + \omega \times r$$

(7.18)

This equation system has 2 unknown vectors, the angular velocity and the translation velocity of the centre of gravity in all three directions.

That means that the movement of the whole system can be determined, if the velocities of two points of the system are known.

As we measure the velocities at four points, we have an over determined system of equations.

7.6.4 Solving an over determined equation system with method of least squares

If there are more measurement points than needed for solving the equation system, it cannot be expected that all points exactly fulfil the solution. In this case the task is to find a solution which approximates the observed solution best, for example with help of the method of least squares.

The method of least squares is based on the assumption that the square of the difference of the exact solution and the approximated solution, the so called residuum becomes a minimum.

In equation (7.18) the relation between the velocity of a mounting point and the velocity of the centre of gravity is defined. Substitute the values of mounting point i results in equation (7.19):

$$\begin{pmatrix} v_{i,x} \\ v_{i,y} \\ v_{i,z} \end{pmatrix} = \begin{pmatrix} v_{cg,x} \\ v_{cg,y} \\ v_{cg,z} \end{pmatrix} + \begin{pmatrix} \dot{\phi} \\ \dot{\psi} \\ \dot{\theta} \end{pmatrix} \times \begin{pmatrix} r'_{i,x} \\ r'_{i,y} \\ r'_{i,z} \end{pmatrix} \quad (7.19)$$

Where $v_{i,j}$ describes the velocity of mounting point i in j -direction in respect to the inertial system, $v_{cg,j}$ the velocity of the centre of gravity in j -direction in respect to the inertial system, $\begin{pmatrix} \dot{\phi} \\ \dot{\psi} \\ \dot{\theta} \end{pmatrix}$ the angular velocity vector resolved in the inertial system and $r'_{i,j}$ the position in j -direction of mounting point i in respect to the moving coordinate system.

Solving the cross product of equation (7.19) results:

$$\begin{pmatrix} v_{i,x} \\ v_{i,y} \\ v_{i,z} \end{pmatrix} = \begin{pmatrix} v_{cg,x} \\ v_{cg,y} \\ v_{cg,z} \end{pmatrix} + \begin{pmatrix} \dot{\psi} \cdot r'_{i,z} - \dot{\theta} \cdot r'_{i,y} \\ \dot{\theta} \cdot r'_{i,x} - \dot{\phi} \cdot r'_{i,z} \\ \dot{\phi} \cdot r'_{i,y} - \dot{\psi} \cdot r'_{i,x} \end{pmatrix} \quad (7.20)$$

If considering four measurement points, the result are twelve equations with the three unknowns of the velocity vector of the centre of gravity and the three unknowns of the angular velocity vector. This linear equation system can be written in matrix syntax according to equation (7.21).

$$\underbrace{\begin{bmatrix} v_{1,x} \\ v_{1,y} \\ v_{1,z} \\ v_{2,x} \\ v_{2,y} \\ v_{2,z} \\ v_{3,x} \\ v_{3,y} \\ v_{3,z} \\ v_{4,x} \\ v_{4,y} \\ v_{4,z} \end{bmatrix}}_d = \underbrace{\begin{bmatrix} 1 & 0 & 0 & 0 & r'_{1,z} & -r'_{1,y} \\ 0 & 1 & 0 & -r'_{1,z} & 0 & r'_{1,x} \\ 0 & 0 & 1 & r'_{1,y} & -r'_{1,x} & 0 \\ 1 & 0 & 0 & 0 & r'_{2,z} & -r'_{2,y} \\ 0 & 1 & 0 & -r'_{2,z} & 0 & r'_{2,x} \\ 0 & 0 & 1 & r'_{2,y} & -r'_{2,x} & 0 \\ 1 & 0 & 0 & 0 & r'_{3,z} & -r'_{3,y} \\ 0 & 1 & 0 & -r'_{3,z} & 0 & r'_{3,x} \\ 0 & 0 & 1 & r'_{3,y} & -r'_{3,x} & 0 \\ 1 & 0 & 0 & 0 & r'_{4,z} & -r'_{4,y} \\ 0 & 1 & 0 & -r'_{4,z} & 0 & r'_{4,x} \\ 0 & 0 & 1 & r'_{4,y} & -r'_{4,x} & 0 \end{bmatrix}}_C \cdot \underbrace{\begin{bmatrix} v_{cg,x} \\ v_{cg,y} \\ v_{cg,z} \\ \dot{\phi} \\ \dot{\psi} \\ \dot{\theta} \end{bmatrix}}_x$$

(7.21)

Now we have a linear equation system of the shape:

$$C \cdot x - d = 0$$

If considering a system of N equations with n unknowns, the system is overdetermined if $n < N$. Accordingly C is an $N \times n$ matrix. We assume that the matrix C has the rank n what means that its columns are linear independent.

As there is no exact solution for this system we have to define an error vector r , called the residual. The residual describes the deviation between the observed solution and the computed solution.

$$r = C \cdot x - d$$

(7.22)

Now we want to find a solution for the unknowns x so that the square of the residual approaches a minimum. The following deductions are based on the book "Numerische Mathematik" [Sch97].

$$r^T r := \min$$

(7.23)

Substituting equation (7.22) in equation (7.23) gives:

$$\begin{aligned}
 r^T r &= (C \cdot x - d)^T (C \cdot x - d) \\
 &= x^T C^T C x - x^T C^T d - d^T C x + d^T d \\
 &= x^T C^T C x - 2(C^T d)^T x + d^T d
 \end{aligned}
 \tag{7.24}$$

For simplification we define the matrixes:

$$A := C^T C \quad b := C^T d$$

So the function to minimize $F(x)$ is reduced to:

$$F(x) = r^T r = x^T A x - 2b^T x + d^T d$$

In order to get the minimum the derivative of function $F(x)$ is set equal to zero.

$$\begin{aligned}
 \frac{dF(x)}{dx} &= 0 \\
 \frac{dF(x)}{dx} &= 2Ax - 2b := 0
 \end{aligned}
 \tag{7.25}$$

Substitution of the factors A and b results in the following equation:

$$\boxed{(C^T C) \cdot x = C^T d}
 \tag{7.26}$$

This is called the “normal equation”. Where $C^T C$ and $C^T d$ are $n \times n$ matrixes. Accordingly there exists an explicit solution for x . The equation system was solved in Matlab.

7.7 Testbed vs. Chassis Dyno

It's obvious that mounting situation of the engine in the race car is a different than on the engine testbed. On the one hand the stiffness of the mounting frame on the engine testbed is different than the stiffness of the chassis of the race car, on the other hand the engine is mounted on four points in the race car and on only three points on the testbed. The following graphs show the difference of the vibration situations of the two mounting systems by comparison of the running mode analysis.

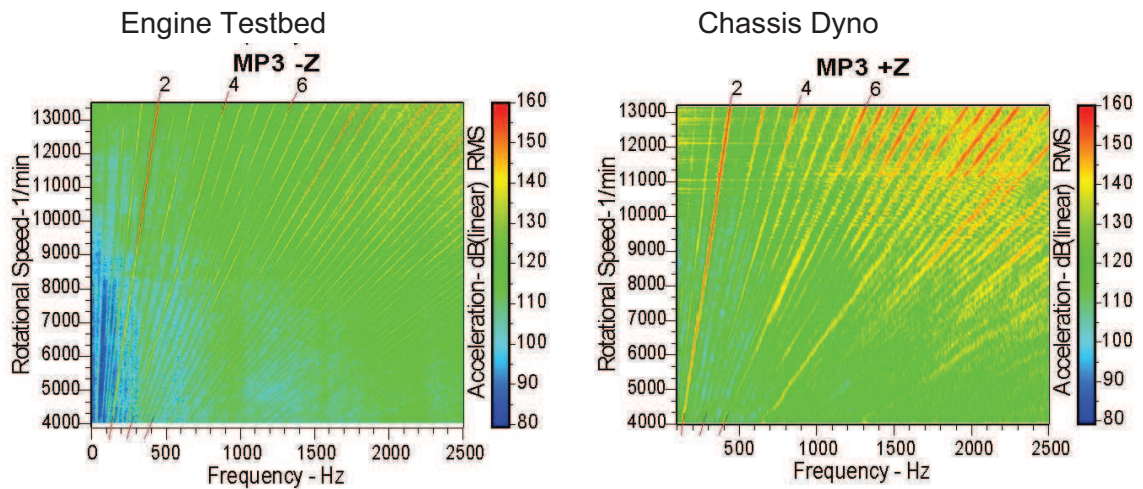


figure 7.9 running mode analysis of mounting point 3 in z-direction

The result of the running mode analyses of the z-acceleration of the mounting point 3 is illustrated in figure 7.9 representing the behavior of all measurement points. The result of the other mounting points in all three directions can be found in the appendix.

It can be clearly seen, that the acceleration level is not the same on the testbed and the chassis dyno. But both diagrams show a dominating amplitude at frequencies which equals the double frequency of the excitation. This is due to the second order inertia forces which are significant for 4-cylinder in-line engines, but also 4th and 6th order can be identified. Furthermore high frequent resonances occur at both measurements. This can probably be ascribed to vibration of attaching parts like cover plates since it occurs at both measurements and at high frequencies.

Since the second order vibration is dominating the focus of the assignment lies in analysing and finding a solution for an adaptive engine mounting system which generates the desired second order vibration. For this reason the vibration of higher orders are not taken into account in the further analyses. Hence in the running mode analyses plots of the vibration velocity level only a frequency range from 130 to 500 Hz is visualized.

7.7.1 Vibration of engine mounting points

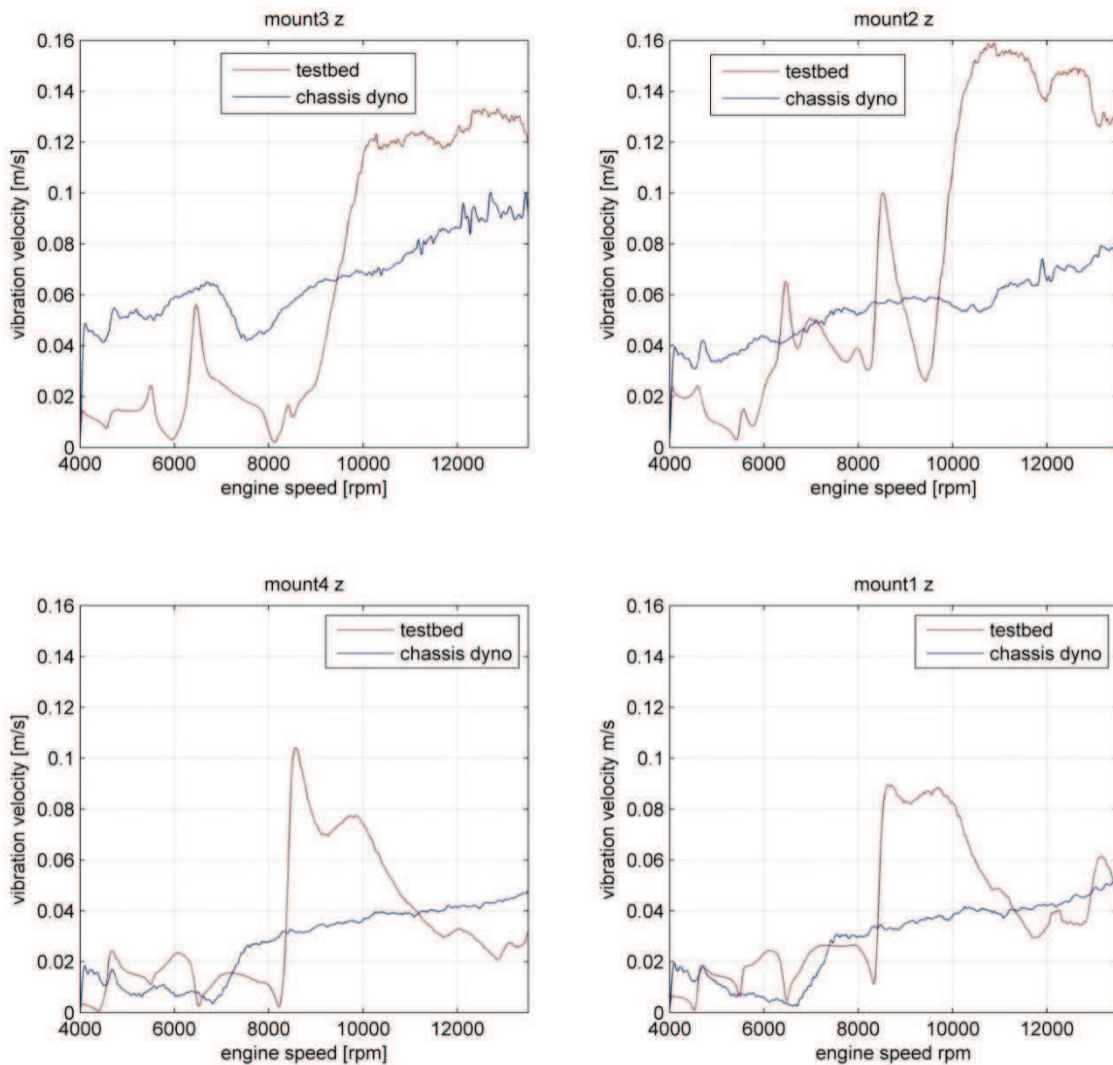


figure 7.10 second order vibration velocity on testbed and chassis dyno in z-direction

figure 7.10 demonstrate the amplitude of the second order vibration velocity over the engine speed in z-direction. The diagrams which content the vibration velocity in the other directions show a similar behaviour and can be found in the appendix.

In this figure it can be clearly seen that the vibration velocity on the chassis dyno increases nearly linear over the engine speed, the vibration velocity on the testbed however shows resonances at different points.

By looking at the results of the chassis dyno , its obvious that the velocity amplitudes of mounting point 1 and 4 are generally smaller than the amplitudes of mounting 2 and 3. Additionally the left side of the engine (mounting point 3 and 4) does nearly the same

movement than the right side (mounting point 1 and 2), that means that the movement is approximately symmetric to the zx -plane. Because of these facts there is evidence that the engine does a rotational movement around an axis which is parallel to the y -axis and close to the mounting points 1 and 4. Because of the symmetry it can be assumed that the rotation around the x -axis is relatively small.

Also on the engine testbed a symmetry between left and right side is apparently. However the upper mounting points (mounting points 2 and 3) have a different vibration behavior than the lower mounting points (mounting points 1 and 4). Demonstrative are the resonance, while the the upper mounting points show resonances at engine speeds higher 10 000 rpm, the resonance of the lower mounting points occurs at engine speeds between 8 000 and 10 000 rpms.

One problem is that the resonances cannot be clearly allocated to a specific movement by looking at figure 7.10. For example the resonance which occure at an engine speed of about 9000 rpm can eighter result due to resonance in translation in z -direction or as a consequence of resonance in angular displacement around the y -axis.

7.7.2 Vibration of engine cg and angular velocity

Looking on the vibration of the centre of gravity and the angular velocity gives more information about the source of the resonances.

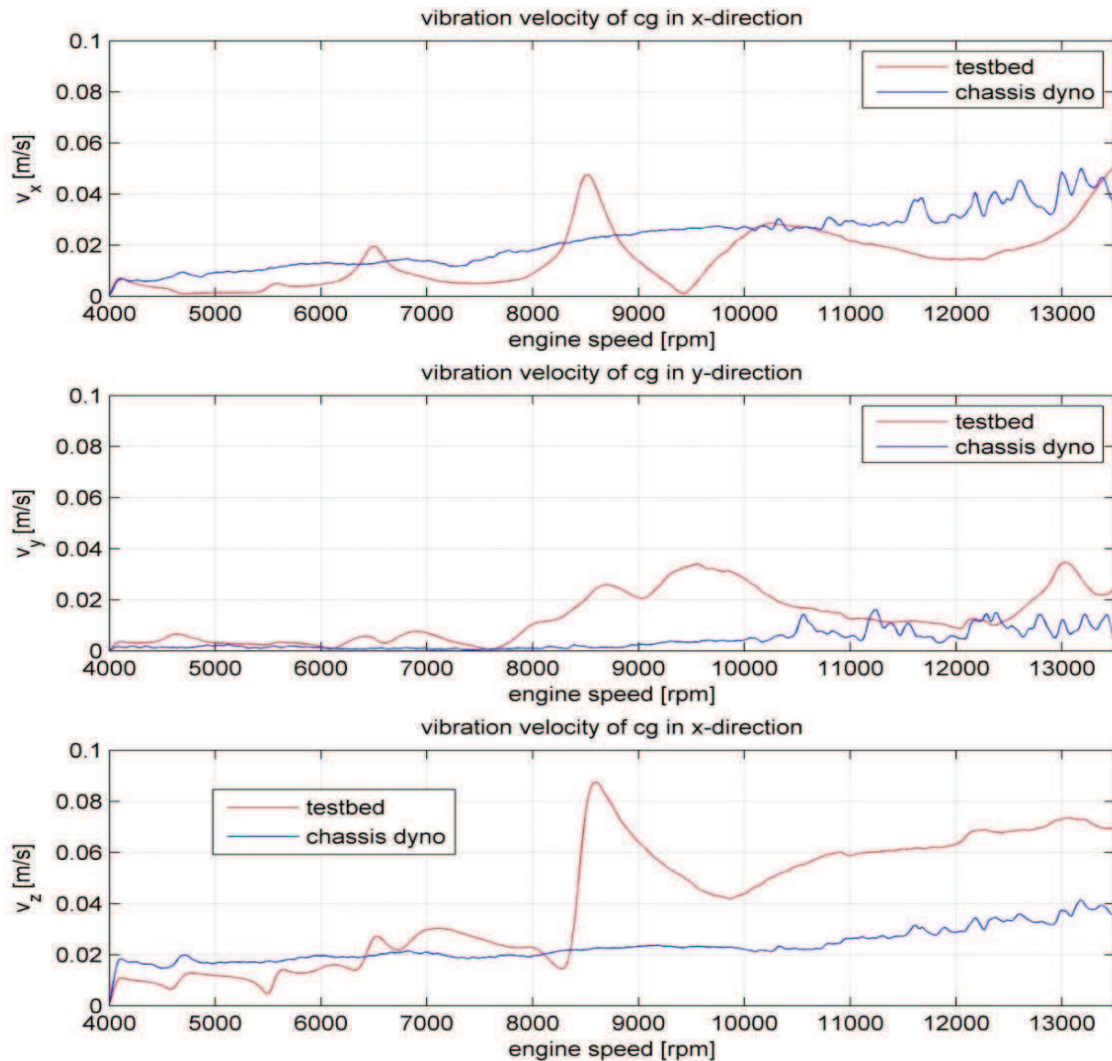


figure 7.11: second order vibration velocity of cg on testbed and chassis dyno

In figure 7.11 the second order vibration velocity amplitude of the centre of gravity of the engine is plotted versus the engine speed. The transformation from the measured amplitudes in the mounting points to the centre of gravity was done according chapter 7.6

The vibration situation of the engine on the chassis dyno shows similar characteristics than in the figures before. Also the vibration velocity of the centre of gravity increases nearly linear over the engine speed in all directions. No peaks can be found which indicate resonances.

If we look at the vibration velocity of the engine testbed data in z-direction, a significant peak can be seen at an engine speed of approximately 8590 rpm. A peak at same engine speed occurs also in x-direction but with smaller magnitude. A possible reason for this is

the 15 degree inclination of the cylinder axis with respect to the z-axis. In this case the resulting excitation force has components in x- and z-directions. Since there are no peaks in any rotational direction at the same engine speed, it's obvious that the peak is caused due to resonance in translation in direction of the cylinder axis. That means that the natural frequency of the testbed system in direction of the excitation equals to the frequency of the second order excitation at an engine speed of 8590 rpm. Accordingly the natural frequency of the testbed system in direction of the cylinder axis equals approximately to 286 Hz.

The vibration amplitude in y-direction does not show any significant peaks. In general the amplitudes are low compared to the vibration in z-direction. Explanation for this phenomena can be that there is no excitation due to the second order inertia forces in this direction.

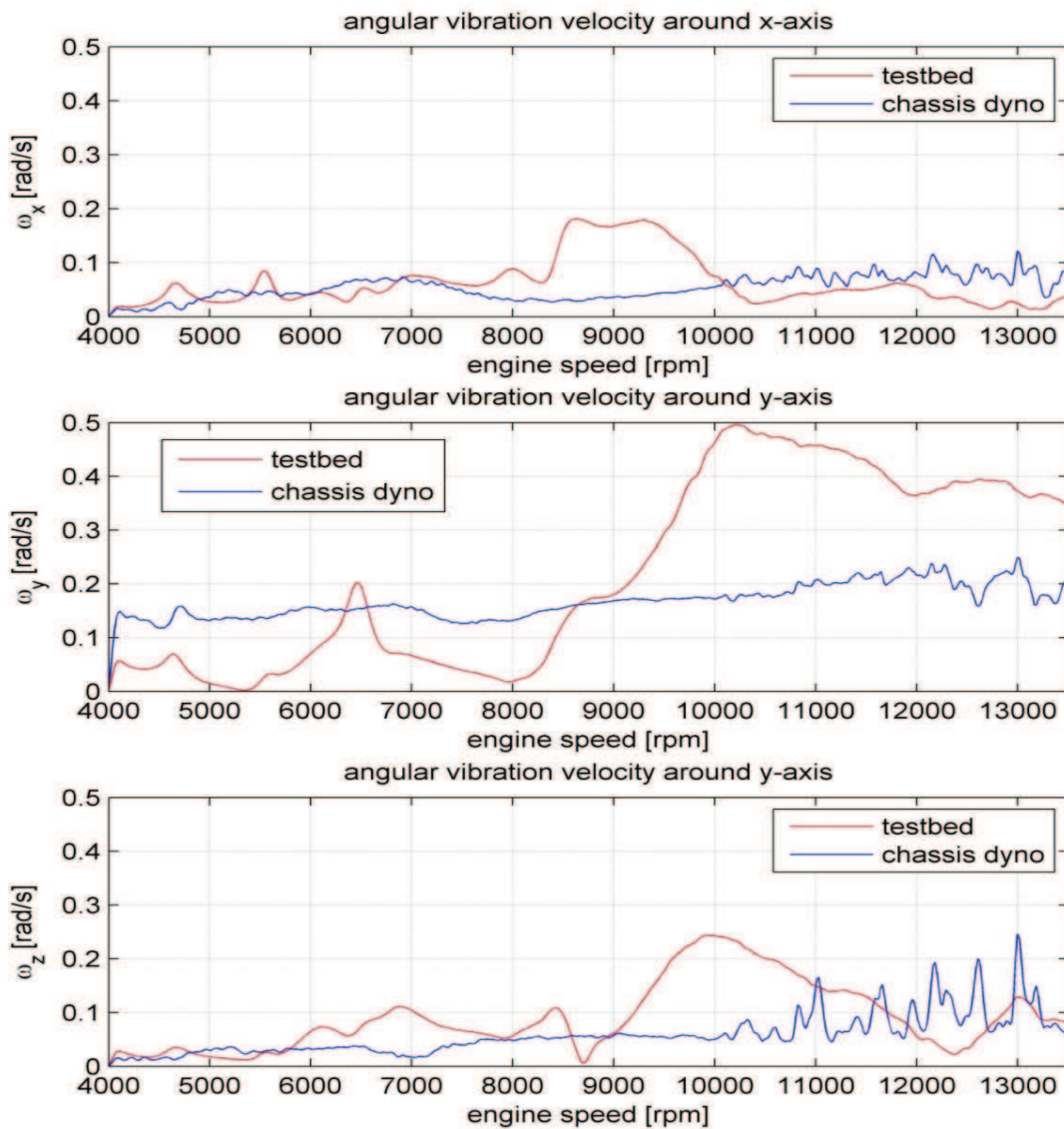


figure 7.12: second order angular velocity of cg on testbed and chassis dyno

In figure 7.12 the second order angular velocity amplitude is plotted versus the engine speed. If we consider the engine as a rigid body, the angular velocity is the same for every single point of the body.

It can be clearly seen that the highest amplitudes occur at vibrations around the y-axis at both measurements. That means that the engine mainly does movement around the crank shaft axis, while the angular movements around the other axis are of small importance.

7.7.3 Conclusion:

The analysis clearly shows that the vibration situation of the engine on the engine testbed is a different than inbuilt in the race car.

Engine Testbed:

Resonances occur in direction of the cylinder axis at a frequency of 286 Hz and in rotation around the y-axis at a frequency of 340 Hz. That means that the stiffness of the chosen rubber pads and the engine mounting frame are in a range where resonance occur due to the second order excitation. That proves that the chosen rubber pads were absolutely inappropriate for this application. Since the stiffness of the rubber pads which are used in commercial motorsport are usually chosen in a range where resonance is avoid over the whole speedband, the analysed case represents a worst case scenario.

Chassis dyno:

The mounting on the chassis dyno does not cause resonances. Consequently the natural frequency of the engine mounted in the race car is either much higher or much less than the excitation frequency caused due to the second order mass forces. Since the engine is mounted on soft rubber pads on the testbed and on solid carbon fibre in the race car it can be expected that the mounting in the race car is stiffer than the mounting on the testbed. That leads to a lower natural frequency on the engine testbed than on the chassis dyno.

8 Multi Body Model of Engine and Engine Testbed

The developed model consist of the multi body system of the engine and the testbed including the mounting and bedding on rubber pads, the clutch, the gearbox, the drive shaft, the torque measuring gauge and the dynamometer with its entire controller. Objective was to design the model as universal as possible, to enable easy adaptations to other engine layouts, engine mounting systems and testbed layouts. All mechanical elements are modelled in Dymola. Afterwards the complete mechanical Dymola model is implemented in Matlab/Simulink, where all controller, for example the PID-controller for the engine speed and the controller for the vibration absorber, are modelled. The Simulink model can be directly implemented in the AVL test bed software and gives a better possibility to do further calculations and signal processing in Matlab.

Dymola is a object orientated simulation tool for simulating dynamic behaviour and complex interactions between systems of many engineering fields such as mechanical, electrical thermodynamic, hydraulic and control systems. The Dymola environment gives the advantage of using the versatile Modelica library, which includes plenty of predefined models of multibody elements. The open modelling language allows the user to free redesign and adapt existing models as well as the programming of new models in object-orientated code.

A detail description of the used blocks of the Modelica library can be found in the appendix. This description is quoted from the Modelica documentation.

8.1 Simplifications:

8.1.1 Valve train

Since the Yamaha R6 engine has two symmetric overhead camshafts the generated mass forces are zero in the ideal case. As the valves are made out of titanium, the inertia forces are expected to be marginal compared to the second order mass forces. Because of these facts the influence of the valve train can be neglected.

8.1.2 Rigid bodies:

All bodies, like the engine block, the con rod, the pistons, the crank shaft and the engine mounting frame are assumed to be rigid. That means that no elongation and bending are allowed. In reality there will be a deformation of more or less all parts, but not all will influence the vibration behaviour. For example deformation of the piston and the con rod will not have any effect on the vibration situation of the engine block.

However the bending of the crank shaft will in reality result a permanent elongation and shortening of the shaft and consequently vibration in y-direction. The measurements on the testbed show, that the vibration in y-direction has lower amplitudes compared to x- and z-direction. This vibration only exists because of the bending of the crank shaft as there is no other excitation in this direction. It has to be taken into account that this vibration cannot be reproduced correctly by the simulation.

The engine block is made of aluminium die-cast which does not have a good vibration absorbing capability. But the vibration of the die-cast block is expected to be in a much higher frequent range than the second order mass forces. Because of this fact this vibrations can be neglected in the analysis. However the displacement of the mounting points to each other and in respect to the centre of gravity influences the whole movement of the engine and is of great importance. For this case the model validation will prove that a simplification to a rigid body is acceptable.

The engine mounting frame is made of solid steel and is much stiffer than all other elements. Because of this fact a simplification to a rigid body is expected to be sufficient for this basic analysis. The model validation will verify this assumption. For more detailed vibration analysis a FEM analysis of the mounting frame is necessary.

8.1.3 Engine friction:

The friction of every single part, for example friction of piston, crank bearing, and fluidic friction are combined to one friction torque acting on the crank shaft. This torque was measured on the AVL testbed in 2008 by measuring the brake mean effective torque and the indicated mean effective torque. Through this simplification the amount of the total friction is simulated correct but the friction torque does not act on the same place in the simulation as it is generated in reality. That means that the forces in the con rod and each crank shaft segment will be about the amount of the friction higher than in reality. As the very exact load of these engine components is not of interest, this simplification is acceptable.

8.1.4 Rubber pads

The used rubber pad is a caoutchouc natural rubber pad from the company Stöfl Rudolf Ges.m.b.H. The model of this element is highly simplified. The damping coefficient and the spring stiffness are considered as constant over the deformation and the vibration frequency. But studies conducted in other areas show, that this is not the case in reality. The spring stiffness of natural rubbers is also depending on the deflection, vibration frequency, vibration amplitude and insignificant from the temperature.

In order to achieve an exact model of the rubber, lots of material tests would be necessary. For this reason, a very simplified model was realized with being aware not representing the reality. The model validation will prove if this simplification is acceptable.

Another simplification is that the rotational stiffness and damping rates are zero. In case of rotation the torque produced by the rotational stiffness of the rubber is negligible low compared to the torque due to the translational stiffness of the other rubbers because of the small rotation angles. For this reason this simplification is acceptable.

8.1.5 Driveline

The driveline after the crank shaft bearing is modelled only with only one rotational degree of freedom. Translational vibration produced by the gearbox, the clutch the driveshaft the torque gauge and the dynamometer are not taken into account.

8.2 Mechanical Multi Body Model in Dymola

The multi body model is a simplified model of the engine and the most important test bed components. Special attention was given to the mounting of the engine on the testbed. The model basically consists of a model of the engine, including the clutch and the gearbox, the drive shaft to the dynamometer, the torque gauge and the dynamometer itself. Furthermore the mounting of the engine, including the engine mounting frame and the rubber pads were modelled and connected to the fix basement of the testbed.

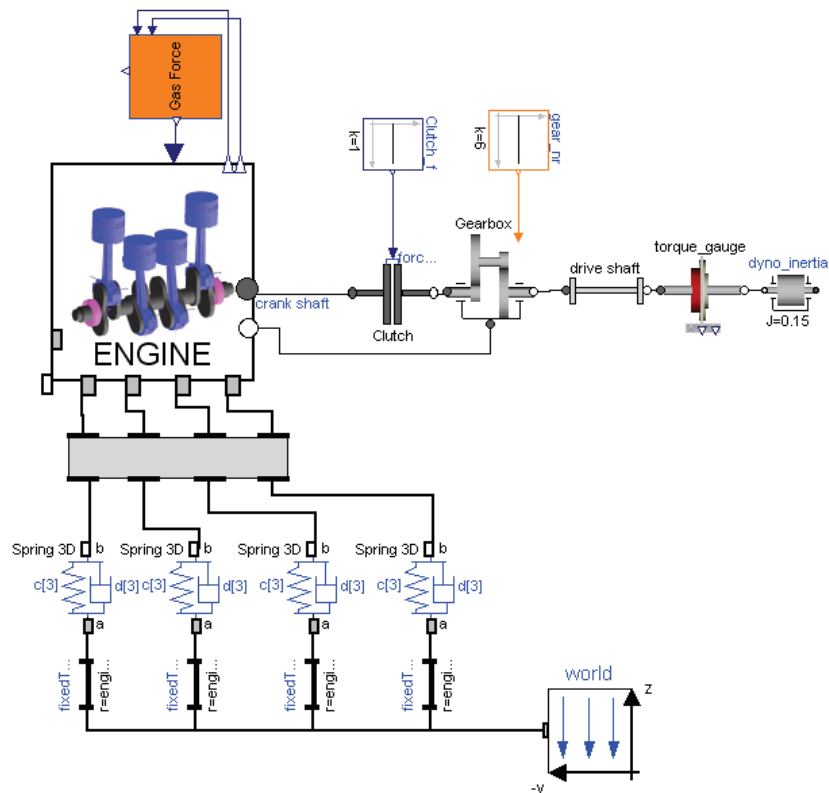


figure 8.1 Dymola model of test bed

The Block “Engine” in figure 8.1 contains the model of the Yamaha R6 four cylinder inline engine. In this model all pistons, con rods and the crank shaft are modelled as rigid bodies. A gas force is acting on the top of every piston. The engine block is a rigid body and includes four mounting points, where the engine is fixed connected to the engine mounting frame. The out port “crank shaft” represents the flange of the crank shaft. From this point towards the driveline the model has only one rotational degree of freedom around the crank shaft axle. This flange is connected to the input shaft of the Clutch and transforms the torque and angular velocity of the crank shaft. The second flange has the function to induce torques into the engine block.

The Clutch gives the possibility to decouple the crank shaft from the driveline and to limit the maximum transmissible torque.

The output Shaft of the clutch is fixed connected to the gearbox, which shifts the ratio between the engine speed and the driveshaft speed. At the same time the torque is shifted inversely proportional to the speed. Since the equilibrium conditions have to be fulfilled, the differential torque has to be inducted into the engine block via a third flange (see chapter 8.2.4).

The drive shaft is the interface between the gear box and the dynamometer. This element has one degree of freedom in rotation due to elasticity in torsion.

Between the drive shaft and the dynamometer the torque is measured. This is represented in the "torque_gauge" model. The torque gauge is considered as inertia free.

The dynamometer controls the speed of the engine. It can be used both as powering and braking device. In the Dymola Model the dynamometer is only described by its inertia and with an output flange since the controller is modelled in Simulink.

8.2.1 Engine

The model of the engine consists out of different sub models, which describe the cylinders including the piston and con-rod, the crank shaft and its bearings, the engine block as a rigid body mass, a block which that adds the friction and the mounting points.

In reality the crank shaft is supported by five bearings which results an over determined system if the crank shaft is considered as a rigid body. Therefore the five bearings are reduced to one bearing with one rotational degree of freedom in the model.

From the crank shaft bearing towards the dynamometer, the drive line is modeled only with respect to the rotational degree of freedom, what means, that the drive line only considers inertias around the rotation axis which do not produce translational vibrations. The masses of the drive line elements like the clutch and the gearbox are added to the engine body mass.

- Degrees of freedom:

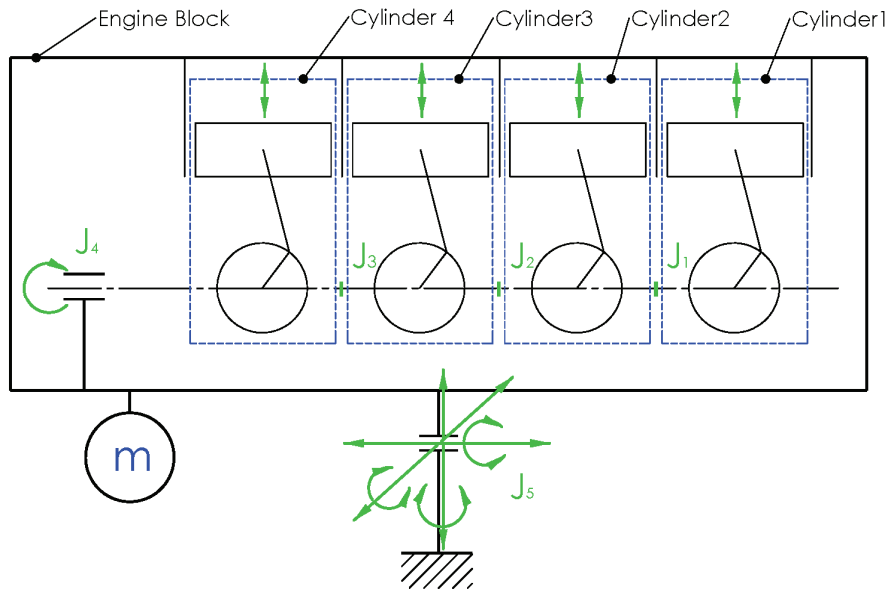


figure 8.2 degrees of freedom of engine model

As the engine block is supported on elastic rubber pads, the mounting allows movement in all three directions and rotation around all three axes. In this case the number of constraints is zero. Additionally the four cylinders have to be taken into account. The crank shaft segments of each cylinder are fixed connected to each other on three points (J_1 - J_3), thus the number of constraints is six for each Joint. The crank shaft bearing allows rotation around the crank axle thus the number of constraints is five. This gives a total of five bodies and 23 constraints.

Joint Nr.	Type	Number of constraints
J_1	fixed	6
J_2	fixed	6
J_3	fixed	6
J_4	Revolute	5
J_5	Elastic	0
Total		23

table 8.1 number of constraints of engine model

The degrees of freedom are calculated using equation (8.1).

$$f = 6 \cdot n - q$$

(8.1)

f...degrees of freedom
 n...number of rigid bodies
 q...number of constraints

According to equation (8.1) the engine model has seven degrees of freedom.

- Used blocks from the Modelica library

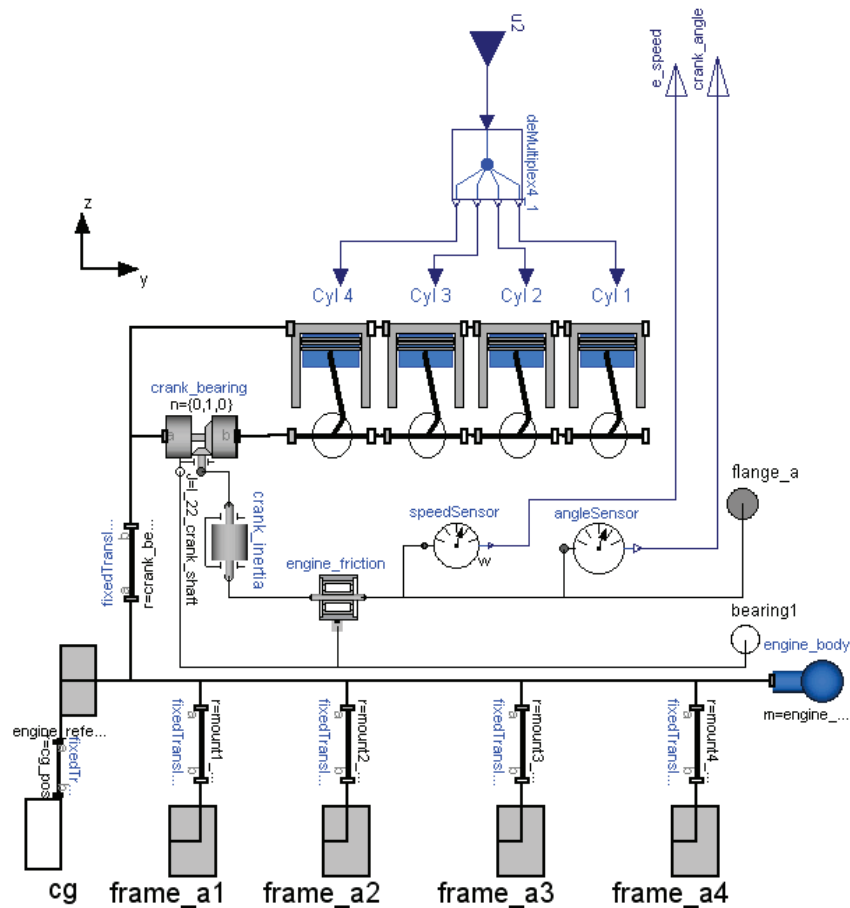


figure 8.3 Dymola model of engine

Engine_body: The mass properties of the engine block are modelled in a “body” element. This includes the mass and inertia tensor of the engine block with the cylinder head, the valve train, the crank shaft, the intake system all fluids and the gear box, if gearbox is internal, but not of the piston and the con rod. The position vector of the centre of gravity refers to the engine reference point.

Crank_Inertia: This element considers the inertia of the crank shaft around its rotation axis. The mass of the crank shaft is taken into account in the engine body mass.

Crank_bearing: This “ActuatedRevolute” joint connects the crankshaft with the engine body and allows rotation around the y-axis. Additionally the bearing can be driven with rotational elements from the Modelica library on two flanges, where the flange “axis” represents the driving flange (in this case the crank shaft) and flange “bearing” the bearing which is fixed on frame_a. After this element the driveline has just rotational degrees of freedom around its axis.

fixedTranslation1: Describes the position vector of the mounting point 1 resolved in the engine reference point.

fixedTranslation2: Describes the position vector of the mounting point 2 resolved in the engine reference point.

fixedTranslation3: Describes the position vector of the mounting point 3 resolved in the engine reference point.

fixedTranslation4: Describes the position vector of the mounting point 4 resolved in the engine reference point.

fixedTranslation: Describes the position vector of the left crank shaft bearing resolved in the engine reference point.

speedSensor: The speed sensor is connected with the flange of the crank shaft and outputs the angular velocity of the crank shaft in [rad/s].

angleSensor: The angle sensor is connected with the flange of the crank shaft and outputs the continuous angle [rad] of the crank shaft. The angle is zero at simulation start.

Parameters

Name	Type	Unit	Default	Description
cg_crank_shaft[3]	Position	[m]	{0.00,0.25,0.00}	Vector from left crank shaft bearing to center of gravity of the crank shaft, when piston 1 is in top dead center
I_22_crank_shaft	Inertia	[kgm ²]	0.014	22 component of inertia tensor of the crank shaft resolved in crank shaft cg
cg_pos[3]	Position	[m]	{-0.042,-0.0784,0.053}	Vector from engine reference point to center of gravity of the engine block
engine_mass	Mass	[kg]	56.4	Mass of the engine block incl. all fluids and crank shaft excl. con rod and piston
mount1_pos[3]	Position	[m]	{-0.156,0.098,-0.12}	Vector from engine reference point to mount 1
Mount2_pos[3]	Position	[m]	{0.136,-0.191,0.170}	Vector from engine reference point to mount 2
Mount3_pos[3]	Position	[m]	{0.118,0.165,0.176}	Vector from engine reference point to

				mount 3
Mount4_pos[3]	Position	[m]	{-0.175,0.062,-0.121}	Vector from engine reference point to mount 4
crank_bearing_pos[3]	Position	[m]		Vector from engine reference point to left bearing of the crank shaft
I_11_engine	Inertia	[kgm ²]	1.263	11 component of inertia tensor of the engine block
I_22_engine	Inertia	[kgm ²]	1.129	22 component of inertia tensor of the engine block
I_33_engine	Inertia	[kgm ²]	1.109	33 component of inertia tensor of the engine block
I_21_engine	Inertia	[kgm ²]	0.116	21 component of inertia tensor of the engine block
I_31_engine	Inertia	[kgm ²]	0.248	31 component of inertia tensor of the engine block
I_32_engine	Inertia	[kgm ²]	-0.0023	32 component of inertia tensor of the engine block
Bore	Distance	[m]	0.067	Engine bore

Connectors

Type	Name	Description
Frame_a	Engine_Reference	Describes the engine reference point. It's situated in the central crank shaft bearing.
Frame_a	Frame_a1	Describes the mounting point 1 of the engine. On this point the engine is connected to the mounting frame and the acceleration sensor 1 is attached
Frame_a	Frame_a2	Describes the mounting point 2 of the engine. On this point the engine is connected to the mounting frame and the acceleration sensor 2 is attached
Frame_a	Frame_a3	Describes the mounting point 3 of the engine. On this point the engine is connected to the mounting frame and the acceleration sensor 3 is attached
Frame_a	Frame_a4	Describes the mounting point 4 of the engine. On this point the engine is connected to the mounting frame and the acceleration sensor 4 is attached
Frame_b	CG	Describes the centre of gravity of the engine body.
Flange_a	flange_a	Describes the connection point for rotational drive line elements to the crank shaft.
Flange_b	Bearing1	Represents the connection to the fixed part of the crank shaft bearing. Reinforced torques in the cylinder block can be introduced in this flange.
RealInput	U2	This is the in port for the gas force signal in [N], coming from the "Gas_force_calculator". The signal is of type Real and has a size of 4. The "deMultiplex" Element splits the signal into the gas force signal of each cylinder
RealOutput	E_speed	This describes the out port of the engine speed signal in [rad/s] measured after the engine friction. The value equates to the actual angular speed of the crank shaft.
RealOutput	Crank_angle	This describes the out port of the crank angle. The value is zero at the simulation start.

8.2.1.1 Cylinder

The cylinder model consists of two rigid bodies, the piston and the con-rod. The crank shaft is modelled as a kinematic relation, which is connected with a rigid rotational inertia element outside the cylinder model. On the top of the piston, a gas force is acting, which is defined in the model „gasforcecalculator“. The cylinder is defined as ideal and free of friction.

- Degrees of freedom:

The degrees of freedom are calculated using equation (8.1).

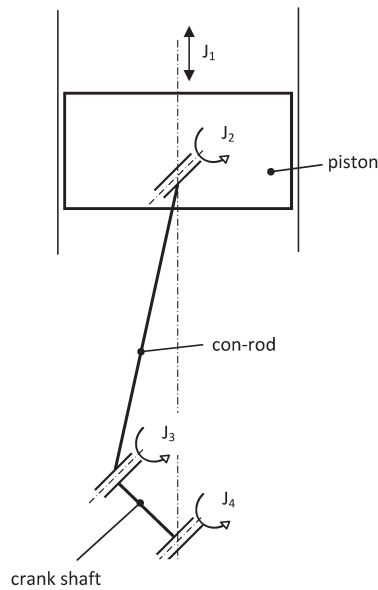


figure 8.4 degrees of freedom cylinder

The cylinder consists of 3 bodies: the piston, the con rod and the crank shaft. Thus $n=3$.

Joint Nr.	Type	Number of constraints
J ₁	Prismatic	5
J ₂	Revolute	5
J ₃	Revolute	5
J ₄	Revolute	5
Total		20

table 8.2 number of constraints cylinder model

This substitute in equation (8.1) results -2 degrees of freedom, what means, that there are 3 constraints too much. In order to achieve the desired one degree of freedom, 3

constraints are removed in the revolute joint J_3 . This is done by setting the parameter `planarCutJoint` in the "Advanced" menu of the Revolute3 joint to true.

- Used blocks from the Modelica library:

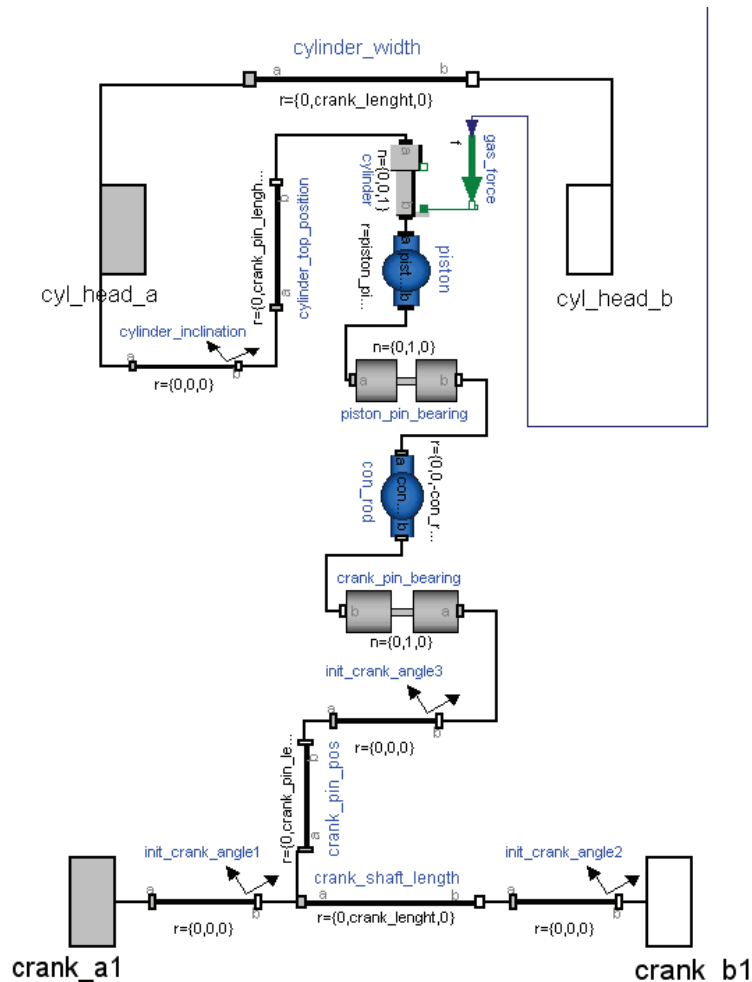


figure 8.5 Dymola model of Cylinder

Piston: The piston is modelled as a "BodyShape" element, which consist of a body and a "frameTranslation" element. The body contains the mass of the piston, an inertia tensor in respect to the centre of gravity and a position vector from frame_a to the centre of gravity. The "frameTranslation" element describes the vector from "frame_a" (top of the piston) to frame_b (piston pin).

Con_rod: For the model of the con rod a "BodyShape" element is used. The body contains the mass of the con rod, the position vector of the centre of gravity from "frame_a" and the inertia tensor in respect of the centre of gravity. The "frameTranslation" element contains the vector from frame_a (piston pin) to frame_b (crank pin).

Crank_shaft_lenght: describes the vector from the left end of the current crank shaft segment to the left end of the following crank shaft segment. This equates to the length of the crank shaft segment

crank_pin_pos: describes the position of the crank pin. (position vector from left crank shaft connection point „Crank_a1“ resolved in a coordinate system rotated by the initial crank angle)

Cylinder_top_position: This “fixedTranslation” element describes the position vector from the cyl_head_a frame (equates to left crank shaft bearing or rather the left connection point to the previous cylinder) to the top centre of the cylinder.

Cylinder_width: describes the distance vector from the connection point of the current cylinder to the connection point of the next cylinder. This equates to the crank shaft length.

Init_crank_angle1: describes the angular position of the crank pin related to the cylinder axis.

Init_crank_angle2 and **init_crank_angle3:** These elements are used to transform the rotated coordinate system by the initial crank angle back to its initial position. Thus the angular position of each crank pin can be defined in root coordinates.

cylinder_inclination: This “fixedRotation” element rotates the coordinate system of the cylinder around the crank shaft axle in a desired inclination angle.

Crank_pin_bearing: This „Revolute“ joint describes the bearing between the crank pin and the con rod. It allows only rotation around the y-axis.

Piston_pin_bearing: describes the piston pin. This „revolute“ joint connects the con rod with the piston and allows rotation around the y-axis. Additional two degrees of freedom are required, because rotation of the con rod around its own axis and translation in y-direction prevents already the crank pin bearing. In Modelica this is done by setting the parameter “planarCutJoint” true. The effect is that from the five constraints of a usual revolute joint, three are removed and replaced by appropriate known variables.

Cylinder: This prismatic joint describes the movement of the piston along the cylinder axis. It has five constraints and one translational degree of freedom along the cylinder axis.

Gas_force: This element describes the gas force. It transforms the gas force signal, which is computed in the gas force calculator in a force which is acting on the top of the piston in direction of the cylinder axis. The value of the force is determined by measurements of the indicated cylinder pressure on the AVL engine test bed.

Parameters:

Name	Type	Unit	Default	Description
Cyl_inclination	Angle	[deg]	15	Inclination of cylinder axis regarding z-axis by rotation around crank shaft axis
Piston_pin_position[3]	Position	[m]	{0,0,-0.025}	Vector from the centre of the piston top to the centre of the piston pin
Dead_length	Distance	[m]	0.0003	Distance between cylinder head and piston top, when piston is in top dead centre
Cg_piston[3]	Position	[m]	{0,0,-0.02}	Vector from the centre of the piston top to the centre of gravity of the piston
Piston_mass	Mass	[kg]	0.176	Mass of the piston incl. Piston pin and compression rings
Con_rod_length	Distance	[m]	0.0905	Length of con rod
Cg_con_rod[3]	Position	[m]	{0,0,-0.0719}	Vector from centre of piston pin to the centre of gravity of the con rod.
Con_rod_mass	Mass	[kg]	0.234	Mass of the con rod
I_11_con_rod	Inertia	[kgm ²]		xx element of inertia tensor of the con rod
I_22_con_rod	Inertia	[kgm ²]		yy element of inertia tensor of the con rod
I_33_con_rod	Inertia	[kgm ²]		zz element of inertia tensor of the con rod
I_21_con_rod	Inertia	[kgm ²]	0	yx element of inertia tensor of the con rod
I_32_con_rod	Inertia	[kgm ²]	0	zy element of inertia tensor of the con rod
Stroke	Distance	[m]	0.0426	Engine stroke
Crank_pin_length	Distance	[m]	0.036	Distance from the left crank shaft bearing to the centre of the crank pin
Crank_length	Distance	[m]	0.072	Distance from the left crank shaft bearing to the right crank shaft bearing
Crank_angle	Angle	[deg]	0	Initial crank angle

8.3 Simulation Parameter of Cylinder Model**Connectors**

Type	Name	Description
Flange_a	Crank_a1	Describes the connection between the crank shaft segment of the current cylinder and the crank shaft segment of the prior cylinder or rather the left crank shaft bearing
Flange_b	Crank_b1	Describes connection between the current crank shaft segment to the crank shaft segment of the next cylinder
Flange_a	Cyl_head_a	Describes the link between the cylinder and the engine block. The chosen position is in the centre of the left crank shaft bearing of the current cylinder, what means that the position of Cyl_head_a coincides with the crank_a1 frame, with the difference that Cyl_head_a is fixed

Flange_b	Cyl_head_b	Describes the fixed link to the next cylinder if next cylinder exists
reallInput	U2	This is the import for the gas force signal coming from the gas force calculator

8.2.1.2 Engine friction

The engine friction is modelled as a torque acting on the crank shaft contrariwise the rotation direction. The value equates the friction mean effective torque (FMET), which was determined on the AVL test bed. This includes the complete friction between piston and cylinders, the crank shaft bearings, the valve train, the gear box and the clutch and the fluidic friction but also the energy demand of all additional components like the alternator and water and oil pumps. The data are stored in a lookup table as a function of the engine speed. The lookup method is linear inter- and extrapolation of intermediate values.

The friction mean effective torque is the difference of the indicated mean effective torque (IMET) and the brake mean effective torque (BMET). The BMET was measured with the torque gauge and the IMET was determined through the indicated mean effective cylinder pressure (IMEP), which was measured on the AVL test bed. The relation between the IMET and the IMEP for four stroke engines describes equation (8.2).

$$M_{ind} = \frac{V_H \cdot p_{ind}}{4\pi}$$

(8.2)

M_{ind} ... indicated mean effective torque
 V_H ... displacement volume
 p_{ind} ... indicated mean effective pressure

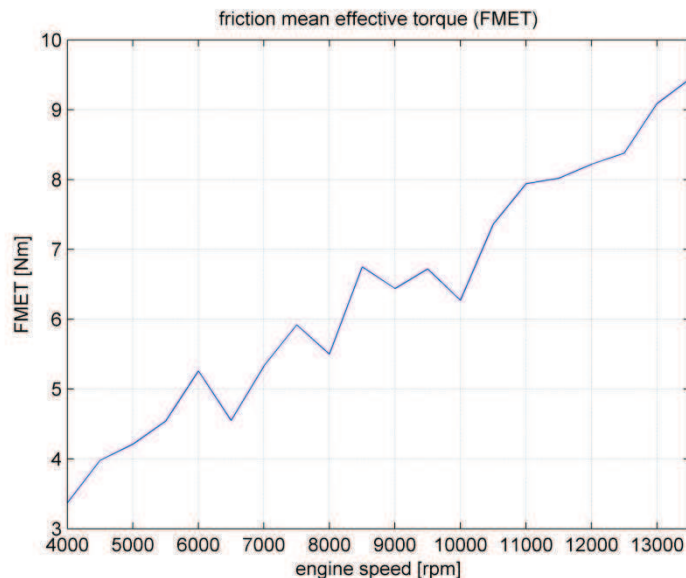


figure 8.6 friction mean effective torque

In order to realize the friction in Dymola, a predefined block for bearing friction from the Modelica library was used. This block gives the possibility to implement a lookup table for the friction torque acting between a flange and the housing. The housing is connected with the fixed part of the crank shaft bearing.

8.2.1.3 Engine body

The Engine body is modelled as a rigid body with mass and inertia tensor.

- Mass properties:

The mass of the engine was determined on a scale. The centre of gravity was determined by slowly moving the engine over the edge of a table until it tilts. In this position the table edge lies in a vertical line under the centre of gravity. This was done in x- and y- direction. The z- component was determined by tilting the engine over a sharp edge (in this case the edge of the oil sump) and measuring the tilting angle. The height of the centre of gravity can be calculated with help of equation (8.3).

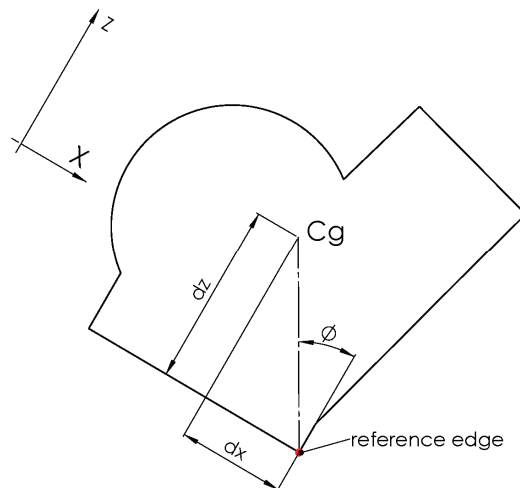


figure 8.7 measurement of engine cg height

$$dz = \frac{dx}{\tan(\phi)}$$

(8.3)

The inertia tensor was calculated in a simplified CAD model in Solid Works. The CAD model includes solid bodies in the shape of the engine with the centre of gravity in the same position than in the real engine. The density was chosen so that the mass equals the real mass of the engine.

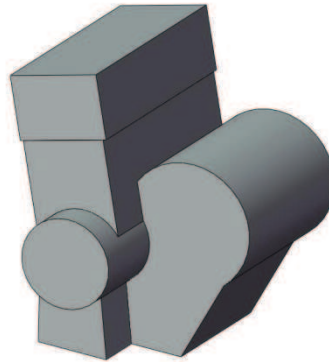


figure 8.8 CAD-model of engine

8.2.2 Gas force calculator

The amount of the gas force is based on the measurement of the indicated cylinder pressure on the AVL test bed in 2008. The pressure was measured crank angle resolved with piezoelectric pressure sensors over the whole engine characteristic map. In this study it's sufficient to focus on the full throttle characteristic because the highest amplitudes of excitation accrue there. As the gas forces of the cylinders are not the same, each cylinder has to be taken into account separately. As can be seen in figure 8.9 the raw data of the measured pressure shows high frequent measurement noise especially at the point when the intake valve opens. This noise is based on a local pressure fluctuation caused due to the opening of the inlet valve since the sensor is located nearby the valve. This fluctuation is locally and doesn't reflect the global pressure situation. Because of this fact the pressure signal was filtered with a Savitzky and Golay filter.

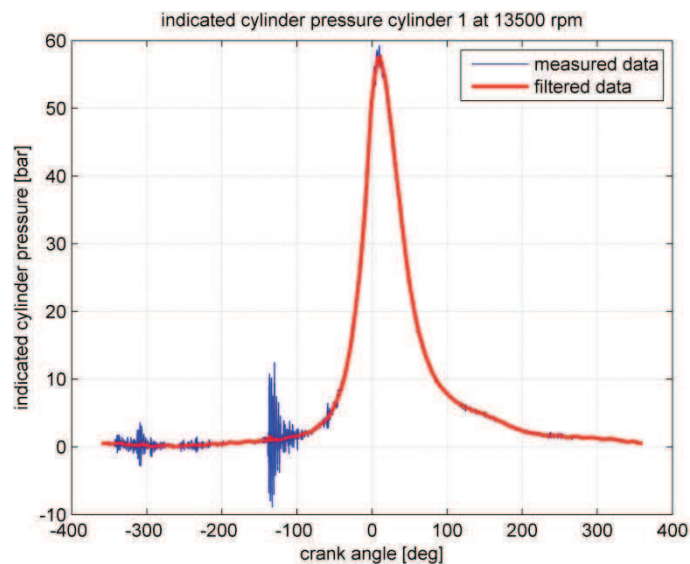


figure 8.9 indicated cylinder pressure of cylinder 1

The gas force equals the indicated cylinder pressure times the piston area. The data are stored in a 2D look up table with dependence on the engine speed and the crank angle. Lookup method is linear inter- and extrapolation of intermediate values.

- Used blocks from the Modelica library:

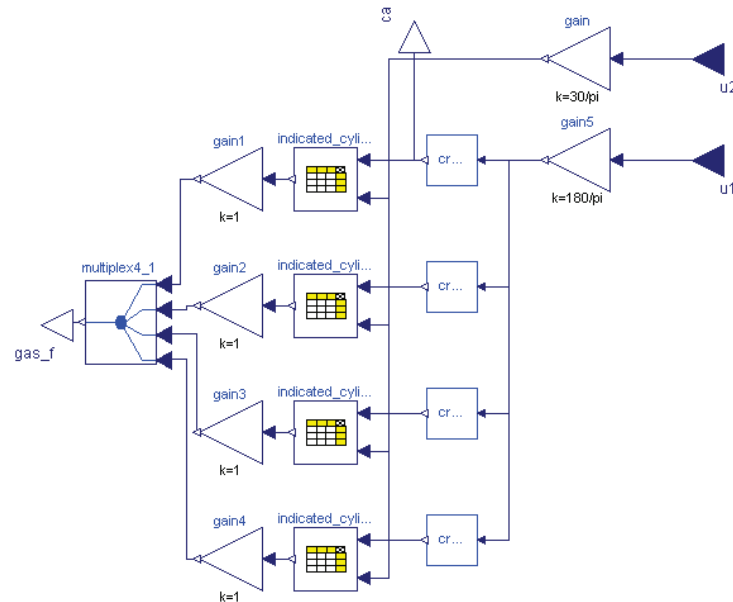


figure 8.10 Dymola Model of gas force calculator

Indicated_cylinder_pressure 1-4: The data for the indicated cylinder pressure for each cylinder is stored in this lookup tables. The data are imported from a .txt file with the name PI1_F in the following format: The first row vector demonstrates the crank angle from zero to 720 degrees and the first line the engine speed from zero to 13500 rpm. The data between represent the amount of the indicated cylinder pressure for the corresponding engine speed and crank angle. The crank angle is zero, when the actual cylinder is in upper dead centre. The lookup table has two in ports, one for the engine speed and one for the crank angle. The output is the indicated cylinder pressure in [bar] to the corresponding inputs.

Gain1-4: This gain elements multiply the indicated pressure signals from the lookup tables by the piston area and converts the pressure signal from [bar] to [Pa]. Output is a gas force signal in [N].

Gain: This block converts the engine speed signal in [rad/s] into a speed signal in [rpm].

Gain5: This element converts the crank angle signal in [rad] into an angle signal in [deg]

- Self designed blocks:

Crank_angle_Calculator: The crank angle calculator transforms the continuing crank angle signals from the angle sensor in a sliding signal from zero to 720 degrees. As the crank angle signal refers to cylinder one, the phase has to be shifted for cylinders two to four.

Connectors

Type	Name	Description
RealInput	U1	Describes the in port for the crank angle signal coming from the crank angle sensor
RealInput	U2	Describes the in port for the engine speed signal coming from the engine speed sensor
RealOutput	Gas_f	Describes the out port for the gas force signal coming from the lookup table. It includes the gas force signals of all four cylinders
RealOutput	ca	Describes the out port for the sliding crank angle signal after the crank angle calculator

8.2.3 Clutch

The clutch consists of two inertias, one representing the driving shaft and the other representing the driven shaft, and a predefined clutch block from the Modelica library. As the clutch has not much influence on the vibration situation, a very exact model is not needed. In this study a releasing of the clutch is not necessary, but the possibility to release the clutch is implemented in the model for further investigations. Input signal is a normalized signal for the clutch closing force. This force equates to the force which presses the two flanges of the clutch together.

- Used Blocks from the Modelica library

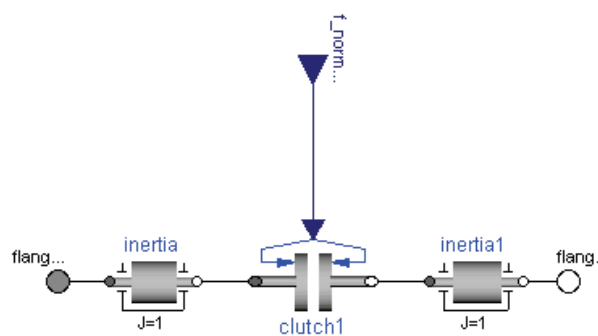


figure 8.11 Dymola Model of Clutch

Inertia: This block describes the inertia of the driving shaft around its rotation axis.

Inertia1: This block describes the inertia of the driven shaft around its rotation axis

Clutch1: Is a predefined block for a clutch from the Modelica library.

Connectors

Type	Name	Description
Flange_a	Flange_a1	Describes the connection to the driving axle, in this case the crank shaft
Flange_b	Flange_b1	Describes the connection to the driven shaft, in this case the Gearbox
RealInput	F_normalized1	The normalized force signal describes the force, which presses the two flanges of the clutch together. This signal is a value between zero and one, where one means that the clutch is fully closed and zero represents a full opened clutch.

8.2.4 Gearbox

The model should allow the possibility to change the gear transmission ration during simulation. The Yamaha R6 engine has a manual six-speed gearbox. The model exists out of a rotational inertia representing the input axle and another rotational inertia representing the output axle. For the transmission a predefined gearbox block of the Modelica library was used. But this block has the disadvantage that the gear ratio is constant, what means that a shifting between different speeds is not possible. Therefore a switch had to be defined which allows a change of the gear ratio during simulation. The different rotational inertia of input and output shaft at different gear ratios is not considered.

- Used Blocks from the Modelica library

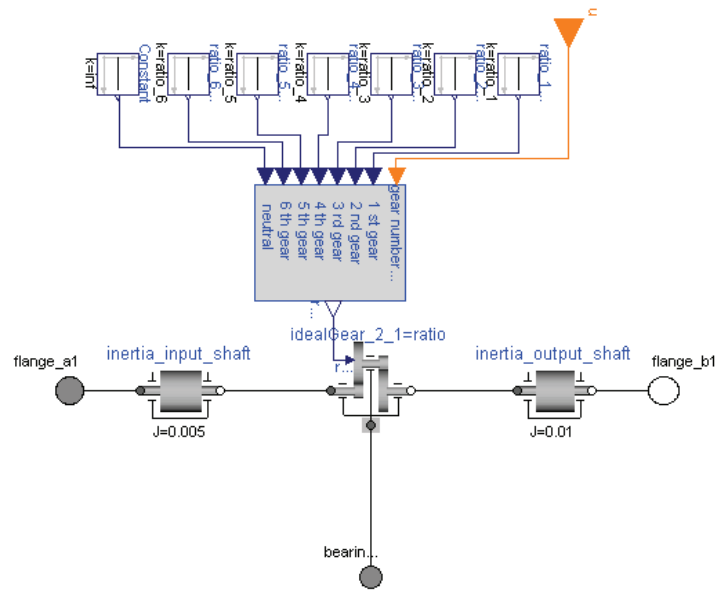


figure 8.12 Dymola Model of Gearbox

idealGear_2: This block is connected to the input shaft on the left end and to the output shaft on the right end. The model characterises an ideal gearbox without mass, inertia, friction and elasticity. This block uses a real input signal representing the ratio between input speed and output speed and therefore the output torque to the input torque. To fulfil equilibrium conditions the differential torque is acting on the bearing flange, which is connected to the engine block.

- Self designed blocks

Gear switch: The input “gear number input” of this switch is an integer variable from one to six, representing the gear number. All other values cause the neutral gear, which means no transmission.

The real in ports “1st gear to 6th gear” require the values of the corresponding gear ratio to the gear number. The real in port “neutral” requires the value of the gear ratio in neutral position which is infinity.

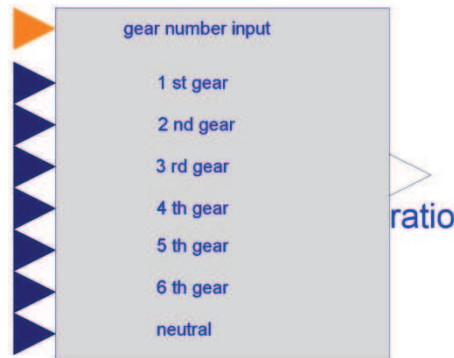


figure 8.13 model of gear switch

The switch outputs either the ratios of the 1st to 6th gear or the neutral gear depending on the integer input “gear number input”.

The Dymola source code of this switch is attached in the appendix.

Parameters

Name	Type	Unit	Default	Description
Ratio_1	real	[]	16.829	Ratio between input speed and output speed at 1 st gear
Ratio_2	real	[]	13.03	Ratio between input speed and output speed at 2nd gear
Ratio_3	real	[]	10.861	Ratio between input speed and output speed at 3rd gear
Ratio_4	real	[]	9.408	Ratio between input speed and output speed at 4th gear
Ratio_5	real	[]	8.378	Ratio between input speed and output speed at 5th gear
Ratio_6	real	[]	7.492	Ratio between input speed and output speed at 6th gear
Inertia_input_shaft	inertia	[kgm^2]	0.005	Rotational Inertia of input shaft around rotation axis.
Inertia_output_shaft	inertia	[kgm^2]	0.01	Rotational Inertia of output shaft around rotation axis.

Connectors

Type	Name	Description
Flange_a1	Flange_a1	Describes the connection to the driving axle
Flange_b1	Flange_b1	Describes the connection to the driven shaft
IntegerInput	u	This integer Input represents the desired gear number. Values from 1 to 6 result the corresponding gear, all other values cause the neutral gear.

8.2.5 Drive shaft

The drive shaft is a circular hollow shaft with two flanges and is modelled as two inertias connected with a spring damper element. Each of the inertia is assigned to be half the inertia of the whole drive shaft around its rotation axis. The spring damper element allows contortion between the two inertias, which means that the model gets an additional degree of freedom.

The inertia of the whole shaft was determined in a CAD model in Solid Works. The calculation of the spring stiffness is based on the book "Festigkeitslehre" [Wit01] :

According [Wit01] equals the torsional stiffness of a circular shaft as follows:

$$G \cdot I_p = \frac{M_t \cdot l}{\varphi} \quad (8.4)$$

where G equates the modulus of rigidity, I_p the polar second moment of area of the shaft, M_t the applied torque, l the length of the axle and φ the angular displacement.

The torsional stiffness equals the torque M_t divided by the angular displacement φ and can be written as follows:

$$c = \frac{M_t}{\varphi} = \frac{G \cdot I_p}{l} \quad (8.5)$$

The polar second moment of area of a circular ring cross-section can be calculated by using the following equation:

$$I_p = \frac{1}{2} \cdot \pi \cdot (r_o^4 - r_i^4) \quad [\text{Wit01}] \quad (8.6)$$

where r_o equals to the outer radius and r_i to the inner radius of the shaft.

The material of the drive shaft is steel, which has a modulus of rigidity G of about 81 GPa. [Rol09]

Substitution of the values for the inner and outer diameter of the shaft of 16 and 25mm, the shaft length of 430mm and the modulus of rigidity in equation (8.6) gives the torsional stiffness of 6010 Nm/rad.

For the damping coefficient no suitable data were available. The book "Maschinenelemente 2" [Sch10] gives experienced data for the damping ratio of shafts. Accordingly equal the damping ratios D of shafts with a diameters <100mm to 0.005. The damping coefficient d of a harmonic two-mass oscillator can be calculated according [Sch10] as follows:

$$d = 2 \cdot D \cdot \eta \cdot \sqrt{c \cdot \frac{J_1 \cdot J_2}{J_1 + J_2}} \quad (8.7)$$

where c equals to the spring stiffness, J_i to the moments of inertia of inertia i and η to the frequency ratio between the natural frequency and the excitation frequency. Since the damping is most effective in case of resonance, the factor η can be set to 1 as an approximation.

According equation (8.7) equals the damping coefficient d to 0.051 Nms/rad.

- Used blocks from the Modelica library:

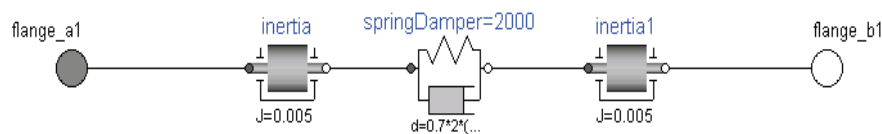


figure 8.14 Dymola Model of drive shaft

Inertia: This element describes the inertia of the half drive shaft around its rotation axis.

Inertia1: This element describes the inertia of the other half of the drive shaft around its rotation axis.

SpringDamper: The block consists of rotational spring and damper, which describes the torsional rigidity of the drive shaft.

Parameters

Name	Type	Unit	Default	Description
inertia	inertia	[kgm ²]	0.006	Inertia of half drive shaft around rotation axis
Inertia1	inertia	[kgm ²]	0.006	Inertia of half drive shaft around rotation axis
c	real	[Nm/rad]	6010	Torsional stiffness of drive shaft
d	real	[Nms/rad]	0.051	Damping coefficient in rotational direction of the drive shaft

Connectors

Type	Name	Description
Flange_a1	Flange_a1	Describes the connection to the driving axle
Flange_b1	Flange_b1	Describes the connection to the driven shaft

8.2.6 Torque gauge

The torque gauge includes a predefined torque sensor from the Modelica library. The torque signal is fluctuating depending on the crank angle. But in most cases the mean value over a whole stroke is of interest. Because of this fact, the signal is filtered with a lowpass Butterworth filter. Thus the torque gauge has two out ports, one for the unfiltered and one for the filtered signal.

- Used blocks from the Modelica library:

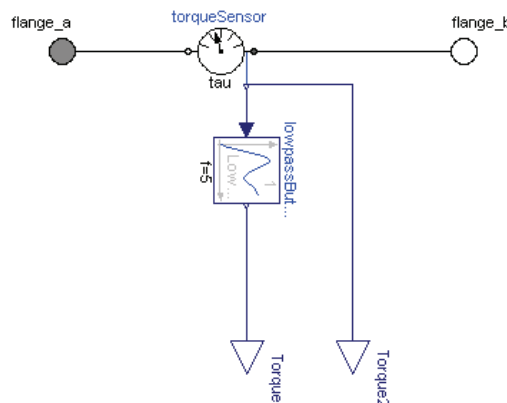


figure 8.15 Dymola model of torque gauge

torqueSensor: This is a predefined block from the Modelica library which displays the acting torque between flange_a and flange_b.

lowpassButterworth: The lowpass Butterworth filter filters the fluctuating crank shaft torque to a continuous mean torque signal. The cut off frequency is 5 Hz, which means that all oscillations higher than 5 Hz are cut off.

Parameters

Name	Type	Unit	Default	Description
n	integer	[]	2	Order of filter
f	real	[Hz]	5	Cutoff frequency of Butterworth filter

Connectors

Type	Name	Description
Flange_a	Flange_a	Describes the connection to the driving axle
Flange_b	Flange_b	Describes the connection to the driven shaft

8.2.7 Engine mounting frame

The engine mounting frame is considered as a solid block with mass and inertia tensor. It includes all mounting points for the engine and the connection to the rubber pads. This part is a construction made of solid steel. Elasticity is not taken into account. The validity of this simplification is shown in the model validation.

The values of the inertia tensor and the mass were determined in a CAD model in Solid works.

- Used blocks from the Modelica library:

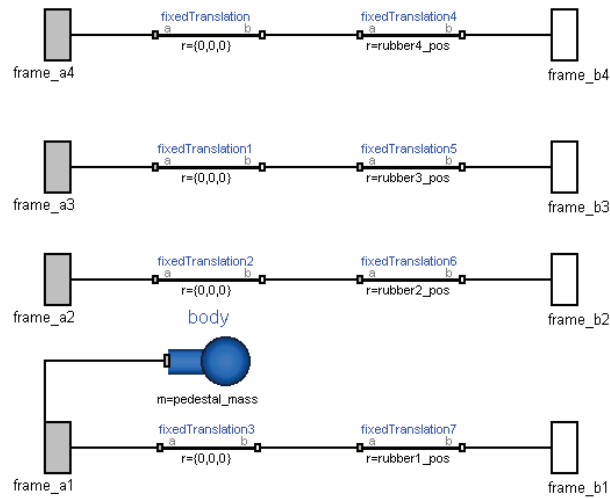


figure 8.16 Dymola Model of engine mounting frame

Body: This element consists of the mass and the inertia tensor of the mounting frame and the vector from mounting point 1 of the engine to the centre of gravity of the mounting frame.

fixedTranslation – fixedTranslation3: These elements describe the vectors from the engine mounting points 1-4 to the engine reference point.

fixedTranslation4 – fixedTranslation7: These elements describe the vector from the engine reference point to the mounting of the rubber pads 1-4.

Parameters

Name	Type	Unit	Default	Description
l_11_ped	inertia	[kgm^2]	1.72	xx component of inertia of the engine mounting frame in respect of the center of gravity
l_22_ped	inertia	[kgm^2]	1.23	yy component of inertia of the engine mounting frame in respect of the center of gravity
l_33_ped	inertia	[kgm^2]	2.26	zz component of inertia of the engine mounting frame in respect of the center of gravity
l_21_ped	inertia	[kgm^2]	0.345	yx component of inertia of the engine mounting frame in respect of the center of gravity
l_31_ped	inertia	[kgm^2]	0.07	zx component of inertia of the engine mounting frame in respect of the center of gravity
l_32_ped	inertia	[kgm^2]	0.069	xy component of inertia of the engine mounting frame in respect of the center of gravity
rubber1_pos[3]	position	[m]	{-0.271,-0.291,-0.196}	Position vector from engine reference point to rubber pad 1

Rubber2_pos[3]	position	[m]	{-0.271,0.255,-0.196}	Position vector from engine reference point to rubber pad 2
Rubber3_pos[3]	position	[m]	{0.08,0.255,-0.196}	Position vector from engine reference point to rubber pad 3
Rubber4_pos[3]	position	[m]	{0.08,-0.291,-0.196}	Position vector from engine reference point to rubber pad 4
cg_mounting frame[3]	position	[m]	{-0.008,0.08,-0.077}	Position vector from mount1 to the centre of gravity of the engine mounting frame
mounting frame_mass	mass	[kg]	{37.2}	Mass of engine mounting frame

Connectors

Type	Name	Description
Frame_a	Flange_a1	Describes the connection to engine mounting point 1
Frame_a	Flange_a2	Describes the connection to engine mounting point 2
Frame_a	Flange_a3	Describes the connection to engine mounting point 3
Frame_a	Flange_a4	Describes the connection to engine mounting point 4
Frame_b	Flange_b1	Describes the connection to the rubber pad 1
Frame_b	Flange_b2	Describes the connection to the rubber pad 2
Frame_b	Flange_b3	Describes the connection to the rubber pad 3
Frame_b	Flange_b4	Describes the connection to the rubber pad 4

8.2.8 Rubber pad

As mentioned in chapter 8.1, the model of the rubber pads is highly simplified.

Since there was no suitable predefined model available in the Modelica library, the block had to be self designed.

- Self designed block

The model of the rubber pad is a spring damper element, which allows deflection in all 3 directions. The rubber pad is not supposed to take up torques, what means in case of rotation, the rubber does not resist a torque. This behaviour can be demonstrated with three springs and dampers (one for every direction) and a universal joint according to figure 8.17.

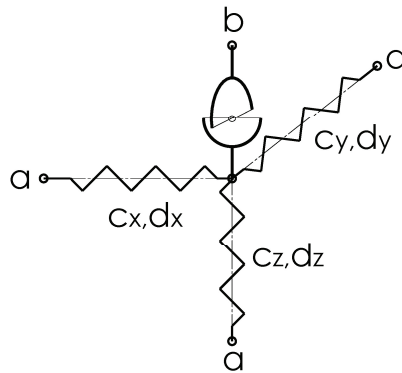


figure 8.17 schematic diagram of rubber pad model

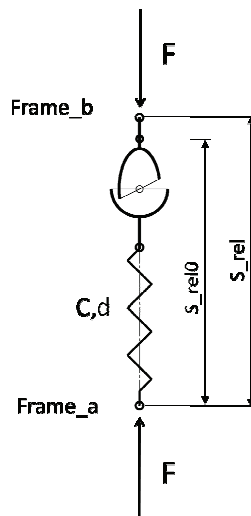


figure 8.18: 1D schematic diagram of rubber pad model

For a clearly visualization the spring/damper is displayed in one dimension in figure 8.18. The vector s_rel demonstrates the displacement vector of frame_a in respect to frame_b. S_rel0 represents the vector of the unstretched spring length.

The system has to fulfil the equilibrium conditions in the connection points frame_a and frame_b.

The Equilibrium condition in frame_a and frame_b give:

$$\rightarrow \text{Frame_a.f} = F, \quad \text{Frame_b.f} = F$$

$$\rightarrow \text{Frame_a.t} \quad , \quad \text{Frame_b.t}$$

(8.8)

In this equations Frame_a.f represents the 3-dimensional force vector and Frame_a.t the 3-dimensional torque vector which are acting in frame_a . The same applies to frame_b .

The force F equals a stiffness tensor C times the relative displacement plus a velocity dependent damping stiffness tensor D times the relative velocity of frame_b in respect to frame_a .

$$F = C \cdot (s_{\text{rel}} - s_{\text{rel}0}) + D \cdot (\dot{s}_{\text{rel}} - \dot{s}_{\text{rel}0})$$

$$F = \underbrace{\begin{pmatrix} c_{11} & c_{21} & c_{31} \\ c_{12} & c_{22} & c_{32} \\ c_{13} & c_{23} & c_{33} \end{pmatrix}}_C \cdot \begin{pmatrix} s_{\text{rel}_x} - s_{\text{rel}0_x} \\ s_{\text{rel}_y} - s_{\text{rel}0_y} \\ s_{\text{rel}_z} - s_{\text{rel}0_z} \end{pmatrix} + \underbrace{\begin{pmatrix} d_{11} & d_{21} & d_{31} \\ d_{12} & d_{22} & d_{32} \\ d_{13} & d_{23} & d_{33} \end{pmatrix}}_D \cdot \begin{pmatrix} \dot{s}_{\text{rel}_x} - \dot{s}_{\text{rel}0_x} \\ \dot{s}_{\text{rel}_y} - \dot{s}_{\text{rel}0_y} \\ \dot{s}_{\text{rel}_z} - \dot{s}_{\text{rel}0_z} \end{pmatrix}$$

(8.9)

The initial position of frame_b is computed by the component that is connected to it by default, but there is also the possibility to define an initial position of frame_b if the parameter “initialization” is set to “true” in the “general” menu. In this case the initial position of frame_b equals to $s_{\text{rel}0}$ resolved in frame_a by default. If additional a preload of the springs is desired, the start value of s_{rel} has to be changed. The springs are preload if the start value of s_{rel} does not equal to $s_{\text{rel}0}$. This can be done by defining a start value $s_{\text{rel}}(\text{start}=i)$, where i does not equal to $s_{\text{rel}0}$ in the “add modifiers” menu.

The source code of the element is attached to the appendix.

Parameters

Name	Type	Unit	Default	Description
c11	Real	[N/m]	83000	xx component of spring stiffness tensor
c22	Real	[N/m]	83000	yy component of spring stiffness tensor
c33	Real	[N/m]	500000	zz component of spring stiffness tensor
d11	Real	[Ns/m]	100	xx component of damping coefficient tensor
d22	Real	[Ns/m]	100	yy component of damping coefficient tensor
d33	Real	[Ns/m]	500	zz component of damping coefficient tensor
s_rel[3]	Position	[m]	{0,0,0}	Unstretched spring length vector

Connectors

Type	Name	Description
Frame_a	Flange_a	Describes the connection flange to engine mounting frame
Frame_b	Flange_b	Describes the connection flange to the world

8.3 Simulink Model

For a better possibility to do further calculations and signal processing in Matlab the mechanical Dymola model was implemented in Simulink as a Dymola block. Simulink gives the advantage that the model can be directly implemented in the test bed software. Also the more powerful tools for signal processing, controller design and the more user friendly environment were reasons for using Simulink. figure 8.19 gives an overview over the Simulink model.

The mechanical Dymola block has one input; the torque U on the drive shaft that is induced by the dynamometer. The outputs are the displacement, the velocity and the acceleration of the four engine mounting points. Additionally the centre of gravity of the engine, the acting torque on the crank shaft, the actual crank angle and the angular velocity of the crank shaft are put out.

The engine speed is controlled by a PID feedback controller defined in the speed controller sub model. The actual speed value is filtered with a Butterworth lowpass filter, because the actual angular velocity of the crank shaft is highly fluctuating over the crank angle. But for the engine speed controller the mean value over one stroke is of interest.

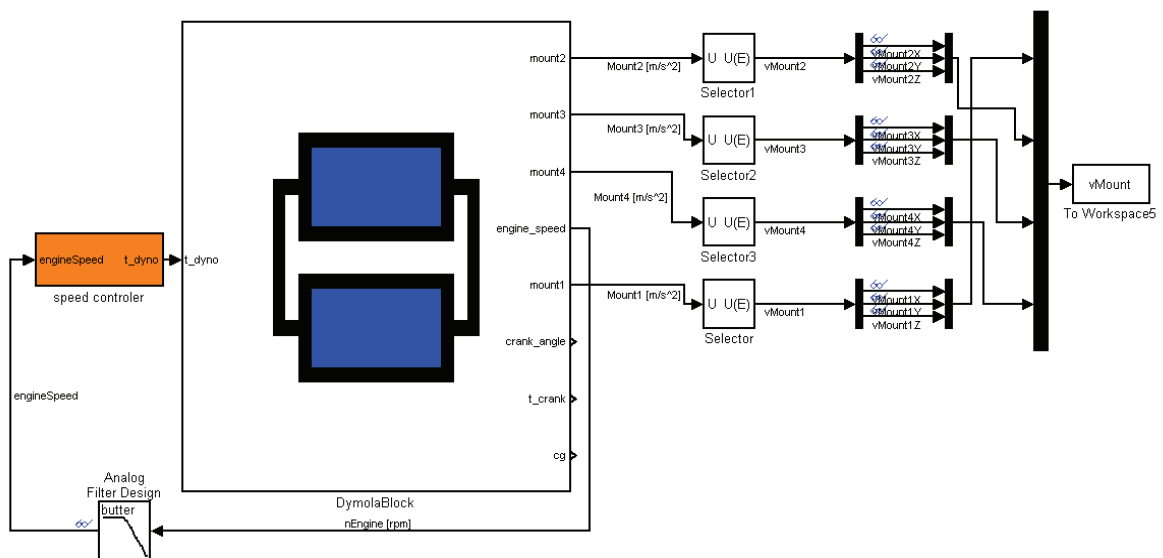


figure 8.19 Simulink Model of engine and testbed

The Out ports Mount1-Mount4 each include the displacement vector the velocity vector, the acceleration vector in x, y and z-direction, the angular displacement vector, the angular velocity vector and angular acceleration vector around the x, y and z axis. Thus the size of the output signal is 18. For the analysis basically is only the velocity vector of interest. Because of that, the Selector blocks only select the velocity components of the output signal. The velocity signals of all mounting points are merged to a velocity matrix, which is exported to the Matlab workspace.

8.3.1 Dymola Block

The mechanical Dymola model was implemented in Simulink as a Dymola block with the following in ports and out ports:

- In ports:

T_dyno: This in port represents the connection of the driveshaft to the dynamometer. The torque of the dynamometer is acting on this flange and controls the desired engine speed.

- Out ports:

Mount1-Mount4: These out-pots visualize the displacement, the velocity and the acceleration of the mounting points 1-4 of the engine in all three directions and the angular displacement, velocity and acceleration around all three axis resolved in the engine coordinate system. Thus the size of this out port is 18.

Cg: This out port visualizes the displacement, the velocity and the acceleration of the centre of gravity of the engine resolved in engine coordinate system.

Engine_speed: This out port displays the unfiltered actual angular velocity of the crank shaft. This value is the input variable for the engine speed controller.

Crank_angle: This out port displays the sliding crank angle signal from zero to 720 degrees.

T_crank: This value represents the acting torque on the driveshaft after the gearbox.

8.3.2 Engine speed controller

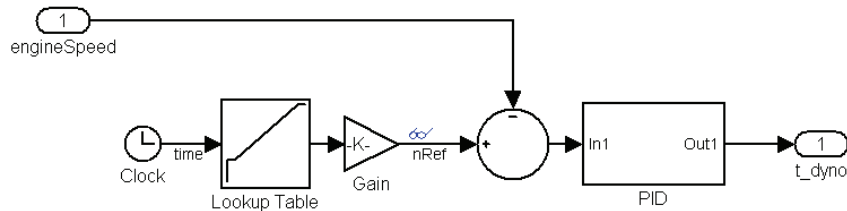


figure 8.20 Simulink Model of engine speed controller

The reference input variable is the desired engine speed, which is defined in a lookup table over the time. This value subtracted from the actual engine speed results the error signal, which is controlled with an ordinary PID controller. The resulting control factor is proportional to the produced torque of the dynamometer.

8.3.2.1 PID-controller

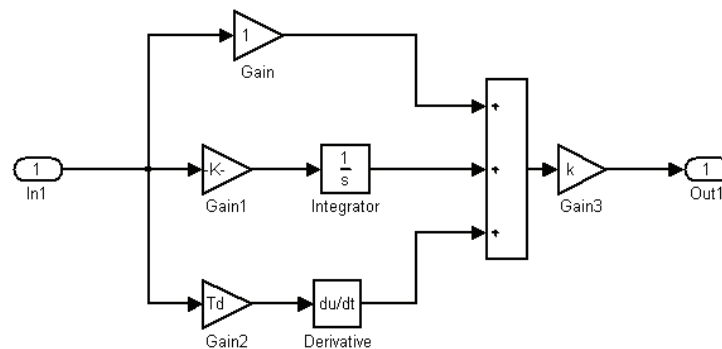


figure 8.21 Simulink Model of PID controller

A PID controller is a control loop feedback mechanism which calculates an error as the difference between an observed variable and a desired setpoint.

The controller involves a proportional, an integral and a derivative part. The proportional part determines the reaction to the current error. The integral part determines the reaction based on the sum of recent errors and the derivative part determines the reaction based on the gradient of the error.

- PID controller design

In order to find good basic values for the parameters of the PID controller, the method of Ziegler and Nichols was used. This is an empirical method in order to get basic values for the proportional, the integral and the derivative parameter. This method was progressed according to the book "Reglerteknik Grundläggande Teori" [Gla07].

For this method the loop control circuit is closed only with the proportional part. The proportional part is varied until a constant oscillation occurs with the critical cycle duration T_{crit} and the critical proportional factor k_{crit} .

According to Ziegler/Nichols the integral and the derivative factors are determined by the following equations:

$$k = 0.6 \cdot k_{crit}$$

$$T_i = 0.5 \cdot T_{crit}$$

$$T_d = 0.125 \cdot T_{crit}$$

(8.10)

The model has a critical cycle duration of 0.335 sec at a critical proportional factor of 0.1235.

According to Ziegler/Nichols the basic values for the proportional, integral and derivative factor are:

k	0,0741	Proportional factor according Ziegler/Nichols
Ti	0,1675	integral factor according Ziegler/Nichols
Td	0,041875	derivative factor according Ziegler/Nichols

table 8.4: PID controller parameter according to Ziegler/Nichols

These values result the step response shown in figure 8.22:

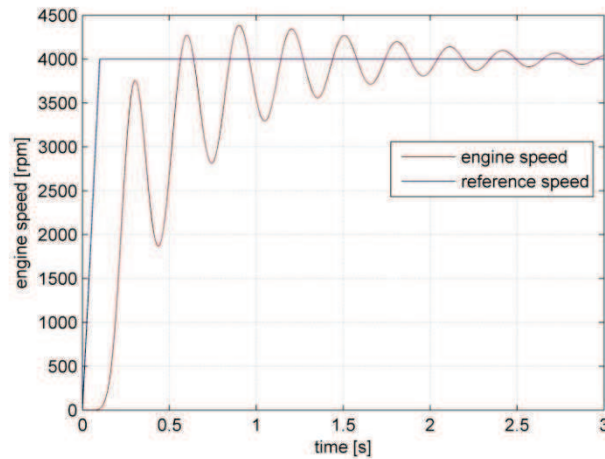


figure 8.22 Step response according Ziegler/Nichols

These settings for the PID controller do not result in a quick enough step response. For this reason a fine tuning of the parameters was necessary. Especially the oscillation does not attenuate quickly enough. This problem can be solved by increasing the derivative part. The derivative part can be seen as an equivalent of the damping of a vibration. An increase of the damping should eliminate the vibration. This is done by decreasing the T_d factor which is inverse proportional to the damping.

An increase of the integral part causes a quicker response. This is done by decreasing the T_i factor.

The fine tuning resulted in the following parameters:

k	0,04	Proportional factor according Ziegler/Nichols
T_i	0,065	integral factor according Ziegler/Nichols
T_d	0,03	derivative factor according Ziegler/Nichols

table 8.5: PID controller parameter after fine tuning

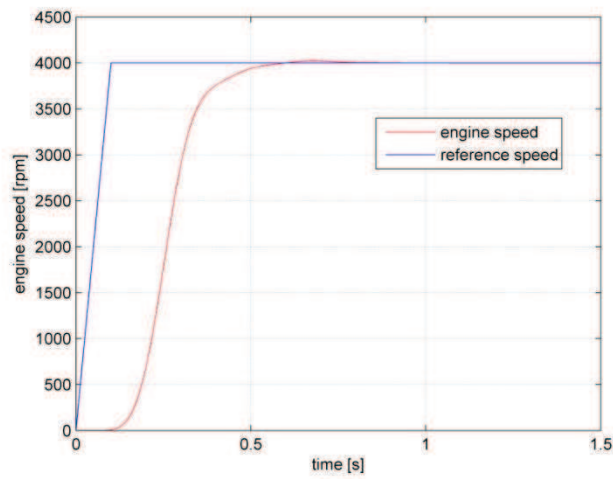


figure 8.23 Step response with improved PID controller

The desired engine speed can be reached in approximately 0.6 seconds. The vibration could be eliminated and the overshoot can be kept within a limit.

9 Model Validation

A Simulation will never represent the reality exactly; the goal is to approach the real behaviour as close as possible. The model validation visualizes the discrepancy of simulation and reality and disclosure mistakes in the model. First of all a basic plausibility check was done in order to check if the model is defined in a right way. Later on the simulation was compared to a simplified calculation of mass forces in order to check if the values of mass forces are in a plausible range. Finally the simulation was checked against the measured values on the testbed.

9.1 Rigid body

This analysis proves if the consideration of the engine block as a rigid body is valid. Therefore we are looking on the residual vector described in chapter 7.6.4. The calculation of the vibration velocity of the centre of gravity of the engine was based on the assumption, that the engine is a rigid body. The calculated residual vector is the deviation between the observed solution, that is the measured mounting point velocity and the computed solution. Reasons for the deviation are in one hand measurement errors and in the other hand wrong assumptions concerning the rigidity of the engine block. Thus the residual vector can be written as the sum of the measurement errors e_{mes} and the errors due to wrong rigidity assumptions r_{rig} .

$$r = e_{mes} + e_{rig}$$

Since we cannot determine the measurement error the residual is a statement for the sum of errors. But if the sum of errors is small, we can assume that each of the errors is small.

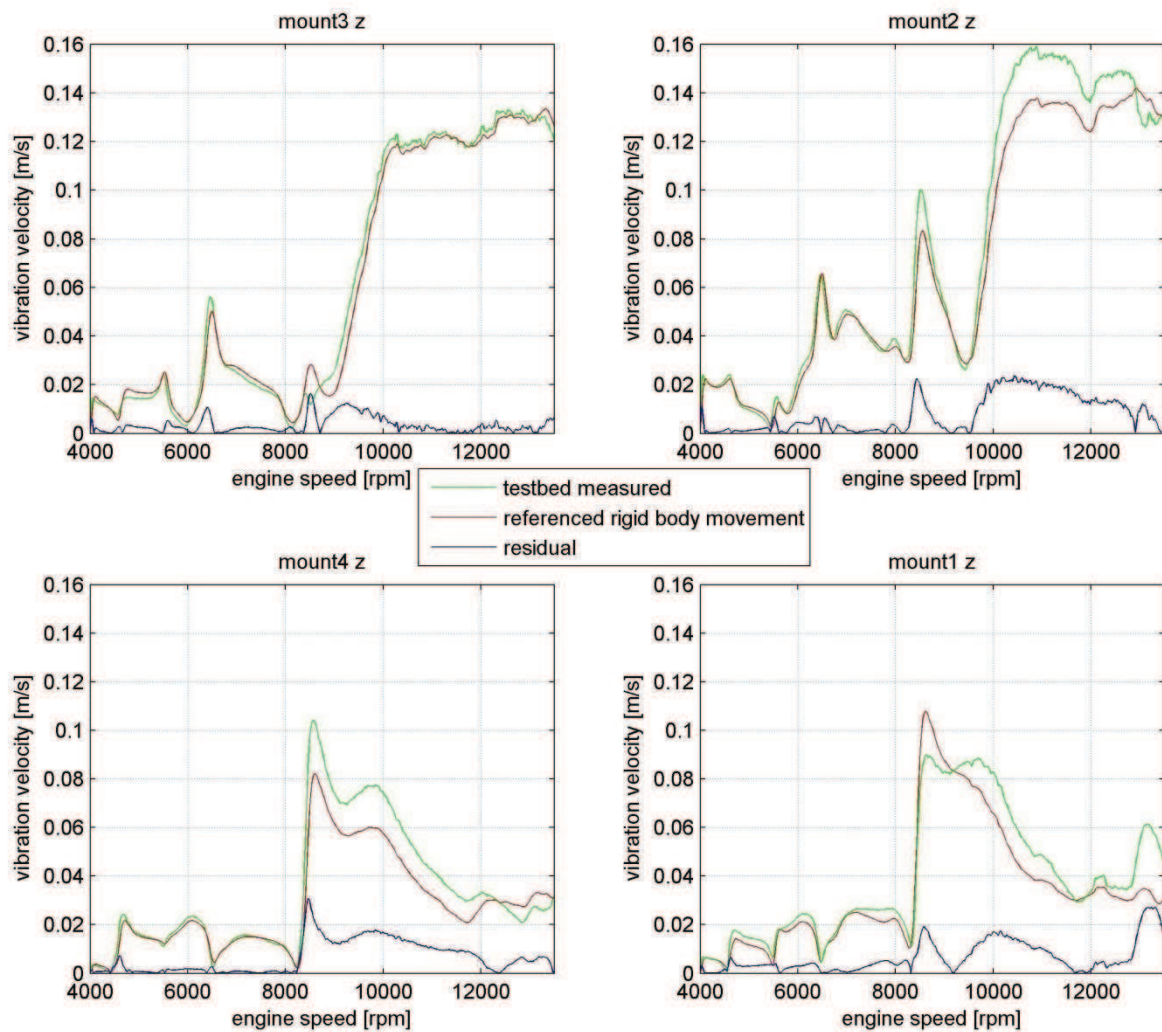


figure 9.1 residual of vibration velocity amplitude in z-direction

In figure 9.1 the measured versus the referenced rigid body movement as well as the residual vector of all mounting points in z-direction are plotted. Since the residual is comparatively small, the simplification to a rigid body is valid.

9.2 Plausibility Check

The plausibility check show if the results of the simulation are basically plausible and all parameters are defined in right order and direction. For example if the firing order is correct, the movement of the pistons is right and all input values like the calculated gas force signal are in a feasible range.

9.2.1 Piston displacement:

Since the cylinder axis has an inclination of 15 degrees to the vertical axis, the expected z-displacement of the piston is the cosine of 15 times the stroke which results a z-displacement of 41mm. The initial crank angles of cylinder 1 to 4 are 0, 180, 540 and 360 degrees. That means that cylinder 1 and 4 are in same phase and cylinder 2 and 3 are 180 degrees phase shifted.

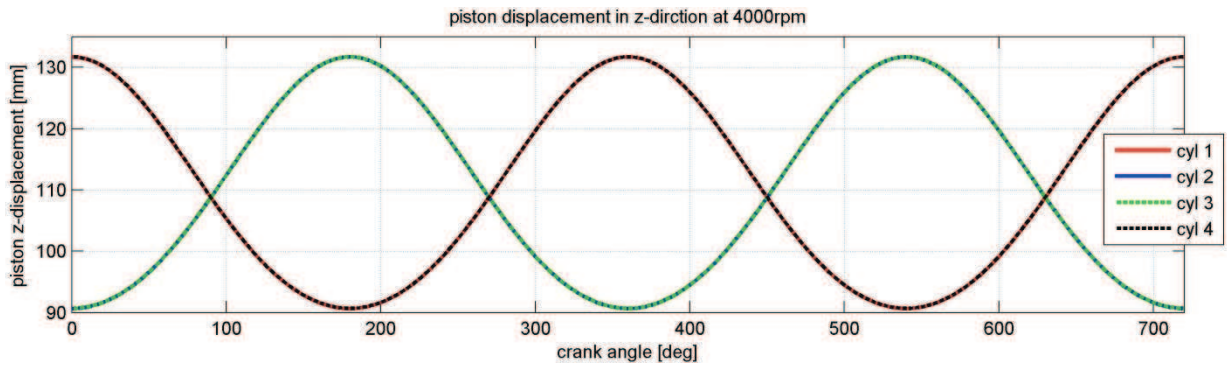


figure 9.2 piston displacement simulation at 4000rpm

figure 9.2 shows that the displacement and the phase shift of all cylinders are modelled correctly.

9.2.2 Firing order

The cylinders fire in order 1, 2, 4 and 3 beginning with cylinder 1. The resulting peak in the cylinder pressure is about 12 degrees after the cylinder was in upper dead centre. Consequently the peak of the cylinder pressure of cylinder 1 should be at approximately 12 degree crank angle, of cylinder 2 at 192 degree, of cylinder 3 at 552 degree and of cylinder 4 at approximately 372 degree crank angle.

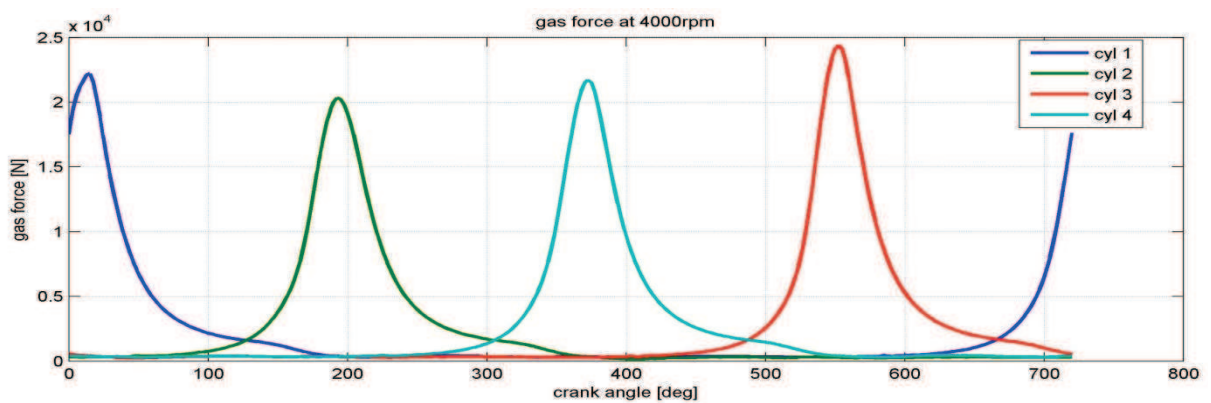


figure 9.3 firing order simulation at 4000rpm

figure 9.3 shows the simulated gas force of all 4 cylinders versus the crank angle. It can be seen that the cylinders fire in the prior described order.

9.2.3 Engine Characteristic Map

The real torque curve of the engine was measured on the AVL testbed in the year 2008.

In the simulation, the torque on the crank shaft is generated through the gas forces of the cylinders and reduced by the engine friction torque. If the simulated torque curve shows the same characteristics than the measured one, it can be assumed that the value of the gas forces and the engine friction are modelled in a correct way.

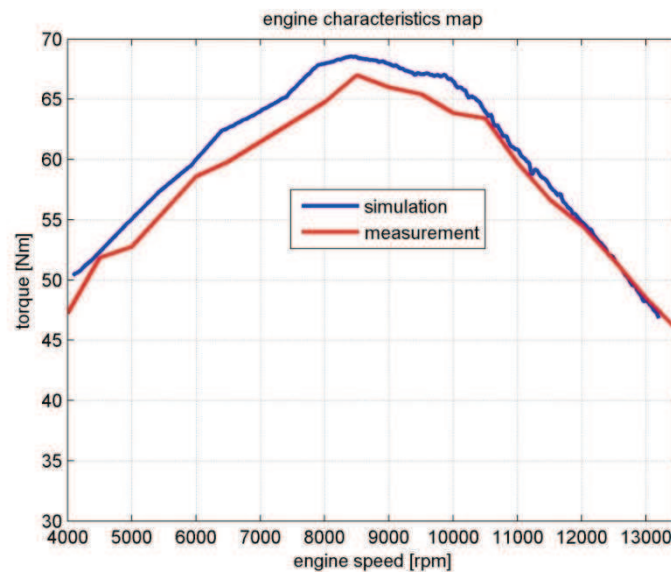


figure 9.4 engine characteristics map

As we can see in figure 9.4 are the engine characteristics of the simulation and the measurements quite similar. In this case we can assume that the gas force and the friction are modelled correctly.

9.2.4 Crank shaft torque

A comparison between the simulated crank shaft torque and the crank shaft torque of a simplified calculation proves if the simulated value lies within a plausible vicinity.

Base for the calculations is the simplified model of the crank mechanism described in chapter 5.2.1.1. In this model the crank shaft is reduced to rotation point mass.

The equilibrium conditions result in the following equation:

$$\sum T_A = J_A \cdot \ddot{\varphi} = F_T(\varphi) \cdot r - T_c \quad (9.1)$$

If we consider a constant angular velocity of the crankshaft, the derivative of the angular velocity, the angular acceleration $\ddot{\varphi}$ equals to zero and consequently equation (9.1) can be written as follows:

$$T_c = F_T(\varphi) \cdot r \quad (9.2)$$

The tangential force $F_T(\varphi)$ can be determined with help of the equilibrium conditions in z-direction of the translational mass.

$$\sum F_z = m_t \cdot a_p = F_{gas}(\varphi) - F_t \cdot \cos(\beta) \quad (9.3)$$

Substitution of the piston acceleration according equation (5.7) results in:

$$m_t \cdot r \cdot \omega^2 \cdot \left[\cos(\varphi) + \frac{1}{r} \cdot \cos(2\varphi) \right] = F_{gas}(\varphi) - F_t \cdot \cos(\beta) \quad (9.4)$$

Equation gives the relation between the angle β and the crank angle φ . Substitution and rewriting of equation (9.4) gives the tangential force F_t .

$$F_T = \left\{ F_{gas}(\varphi) - m_t \cdot r \cdot \omega^2 \cdot \left[\cos(\varphi) + \frac{1}{r} \cdot \cos(2\varphi) \right] \right\} \cdot \left[1 - \frac{r}{l \cdot \sin(\varphi)} \right]^{-1/2} \quad (9.5)$$

This follows because: $\cos(\beta) = \frac{1}{\sqrt{1 - \sin(\beta)}}$

The value for the gas force $F_{gas}(\varphi)$ comes from the measurements on the engine testbed.

The crank shaft torque of all cylinders is a superposition of four times the torque of the single cylinder engine with a phase shift of 180 degrees of each cylinder.

The calculated and the simulated crank shaft torque of the 4-cylinder in-line engine are plotted versus the crank angle at an engine speed of 13000 rpm and illustrated in figure 9.5.

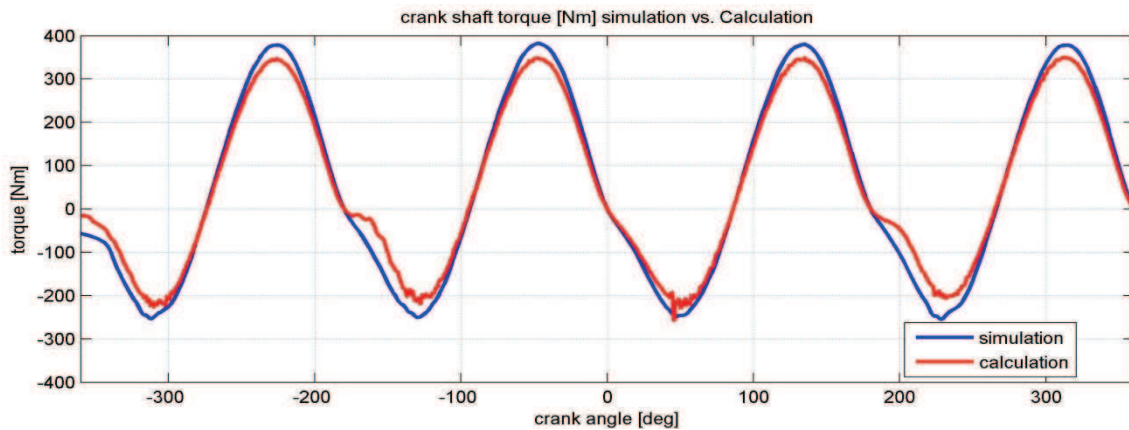


figure 9.5 crank shaft torque at 13000 rpm simulation vs. Calculation

In figure 9.5 one can see that the simulated torque has slightly higher amplitudes than the calculated one. This can be a consequence of the simplifications which were done in the calculation, like the reduction to a two point-mass system and the constant angular velocity. But in general the two functions have a similar shape and it can be assumed that the simulation outputs plausible results.

9.2.5 Excitation force

Already in chapter we calculated the excitation force of the 4-cylinder in-line engine. Now a comparison to the simulated forces shows, if the simulation is plausible. For this reason we look on the forces acting on the fixed mounting of the crank shaft bearing of the simulation at an engine speed of 4000 rpm.

Using equation (5.22) and substituting the values of table 5.1 results in the equation of the excitation force of the Yamaha R6 engine as follows:

$$F_{ex,4cyl} = -784.4 \cdot \cos(2 \cdot \omega \cdot t)$$

The simulated excitation force in direction of the cylinder axis is illustrated in figure 9.6 at an engine speed of 4000 rpm.

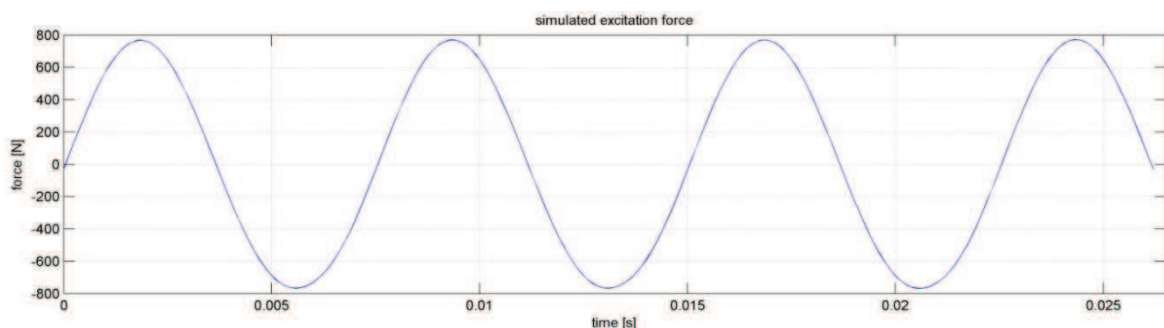


figure 9.6 simulated excitation force, engine speed 4000 rpm

It can be seen that the Amplitude of the simulated and the calculated excitation force is in plausible vicinity. Also the cycle duration, which equals to $T = \frac{1}{f} = \frac{30}{n} = 0.0075$ sec seems to be simulated correct.

9.3 Simulation vs. Testbed

First of all a simulation was done using the input parameters described in chapter 8. The procedure was a linear runup from 4000 rpm to 13500 rpm in 10 seconds, that's the same procedure than was done on the chassis dyno. The resulting vibration velocity amplitude is plotted in the following graphs and compared to the measured data of the engine testbed.

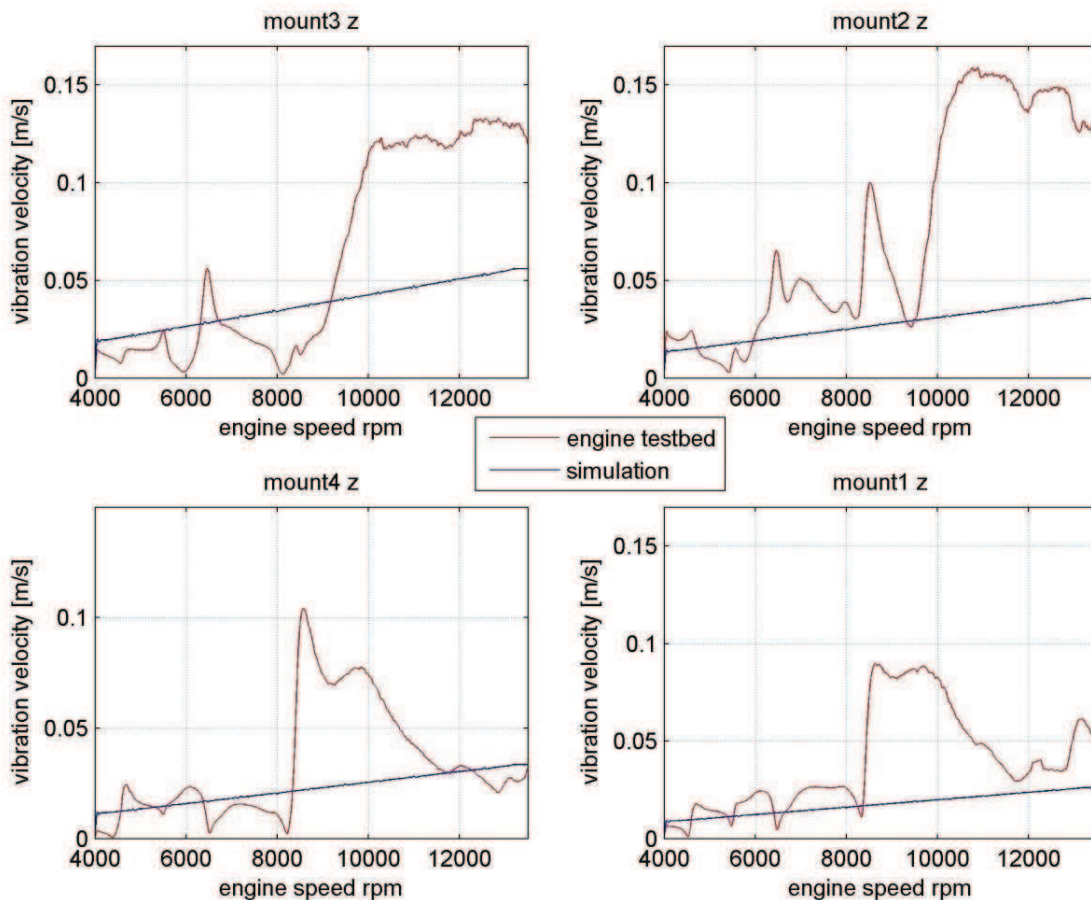


figure 9.7 vibration velocity amplitude on engine testbed, measurement vs.simulation

As one can see, the simulation does not reproduce the vibration situation on the engine testbed. The vibration amplitudes increase nearly linear over the engine speed in the simulation. Hence the resonances which occur on the engine testbed cannot be simulated. Since the excitation is simulated correctly, the error must either be in the model of the rubber pads or the simplification of reducing the engine mounting frame to a rigid body is not valid. Since no resonances occur, either the stiffness of the rubber pads is

much higher than expected or the spring stiffness of the engine mounting frame is in vicinity, where resonances occur. In the second case, the overall stiffness of the mounting equals to the connection in series of the spring stiffness of the rubber pad and the stiffness of the mounting frame.

The overall spring stiffness c_{tot} of two springs with the stiffness c_1 and c_2 connected in series is calculated using equation (9.6).

$$c_{tot} = \frac{c_1 \cdot c_2}{c_1 + c_2} \tag{9.6}$$

In this equation the overall stiffness c_{tot} is always smaller than the stiffness of each spring stiffness c_1 and c_2 . That means that an additional spring connected in series always reduces the overall spring stiffness. In other words the influence of an elastic mounting frame would reduce the overall spring stiffness and shift the resonant point to an even lower frequency and consequently the amplitudes would be even lower. Because of this fact we can assume that the simplification to the rigid body of the mounting frame does not cause the discrepancy between the simulation and the measurements. Rather the error must be caused due to an insufficient model of the rubber pad.

As described in chapter 8.1 the model of the rubber pads is very simplified. Especially the dynamic stiffness in dependency on the frequency is not taken into account which is apparently of higher influence than expected.

A more qualified model of the rubber pads requires complex material tests. Since these tests are too extensive the path was to adapt the spring stiffness of the rubber pads in the simulation manually, so that the simulation approaches the real case behaviour.

The adaptation resulted in the following values:

Mount 1		Mount 2		Mount 3		Mount 4	
C x [N/mm]	55000	C x [N/mm]	55000	C x [N/mm]	55000	C x [N/mm]	55000
C y [N/mm]	35000	C y [N/mm]	35000	C y [N/mm]	35000	C y [N/mm]	35000
C z [N/mm]	100000	C z [N/mm]	60000	C z [N/mm]	60000	C z [N/mm]	100000
D x [Ns/m]	700	D x [Ns/m]	200	D x [Ns/m]	200	D x [Ns/m]	700
D y [Ns/m]	2000	D y [Ns/m]	2000	D y [Ns/m]	2000	D y [Ns/m]	2000
D z [Ns/m]	9000	D z [Ns/m]	5000	D z [Ns/m]	10000	D z [Ns/m]	15000

table 9.1 adapted stiffness values of rubber pads

The results of the vibration velocity amplitude in z-direction of the simulation versus the real case measurements are visualized in the following graphs. The vibration velocities in x-direction show similar characteristics and can be found in the appendix.

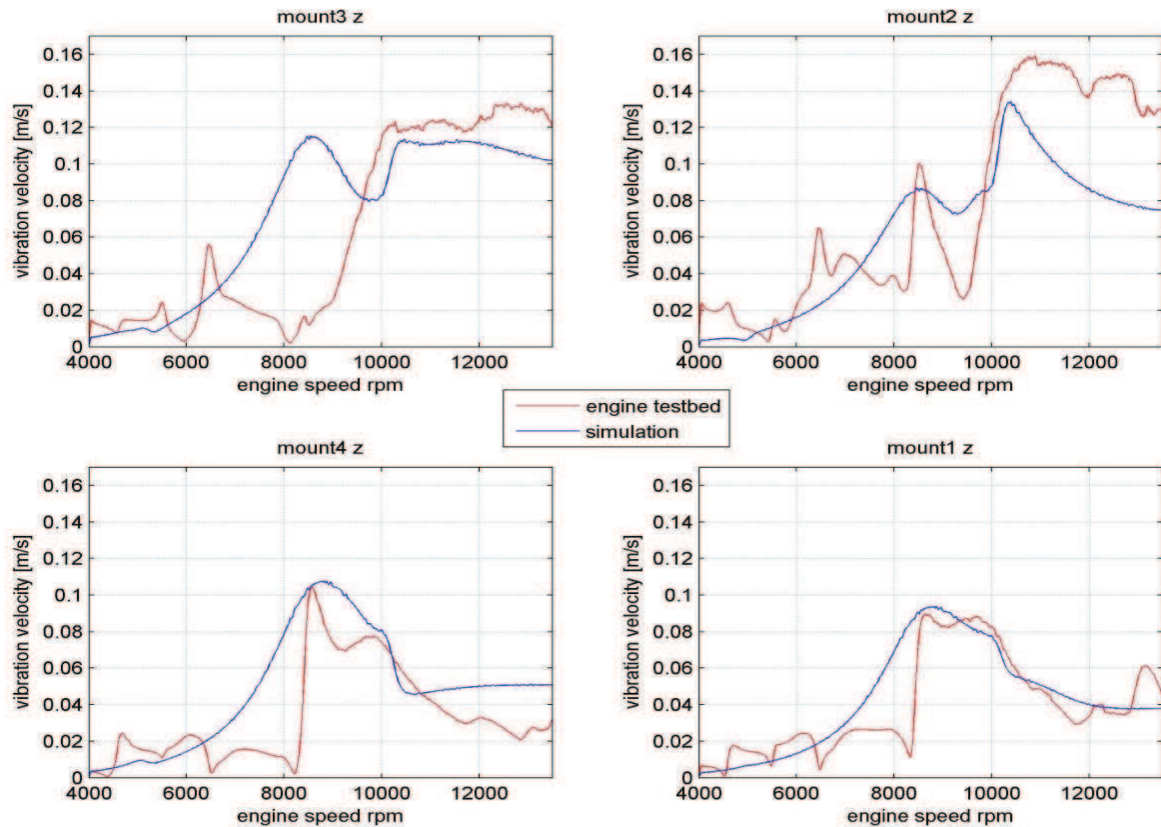


figure 9.8 vibration velocity amplitude in z-direction, simulation versus testbed

It can be seen that the real case behaviour cannot be exactly represented by the simulation. But it succeeded to generate resonances with adequate amplitudes at the appropriate frequencies in many points. While the lower mounting points 1 and 4 show quite good approaches, in mounting point 1 a resonance occurs in the simulation at an engine speed of approximately 8200 rpm, where a minimum should be. Further the measurements show more resonance peaks than the simulation. This can be caused due to influences which are not taken into account in the simulation, for instance resonance of attaching parts.

9.4 Conclusion:

The model validation shows that the excitation due to second order inertia forces can be modelled correctly, as well as the crank shaft torque.

But the vibration situation of the engine does not represent the real case. This is due to an insufficient model of the rubber pads. A modification of the parameters of the rubber pads gives a better approach but still doesn't reflect the real case behaviour exactly. Nevertheless the simulation is practical for our application, since the simulated vibration velocity amplitudes reach values which are adequate to the occurring amplitudes in real case at the appropriate frequencies.

10 Adaptive engine mounting stiffness

The Idea was to influence the vibration situation by varying the stiffness of the engine mounting. The engine mounting can be assumed to be a spring damper system and the engine to be a body mass. This together results an oscillating system. Basic idea is to shift the natural frequency in a desired range, by changing the spring stiffness of the mounting. Due to this the resonance occurs at another frequency and consequently the peak amplitude of the vibration is being shift to another frequency range. In other words, the amplitude is changed at a specific engine speed.

A Variation of the damping rate of the mounting influences the peak amplitude at resonance where higher damping rates result in smaller vibration amplitudes. The damping coefficient also influences the natural frequency of the system but only slightly.

In this way the vibration amplitude of any oscillating system can be controlled to a desired value through an active variation of the spring stiffness and the damping rate.

10.1 Simplified model of the engine mounted on the testbed

A calculation of the amplitude frequency response of a simplified model shows the influence of the spring stiffness and the damping rate of the mounting on the vibration amplitude.

The simplified model is a mass, representing the engine which is stored on a spring and a damper, representing the elastic mounting. A sinusoidal force, which describes the excitation through the second order inertia forces of the engine, is acting in the centre of gravity of the mass.

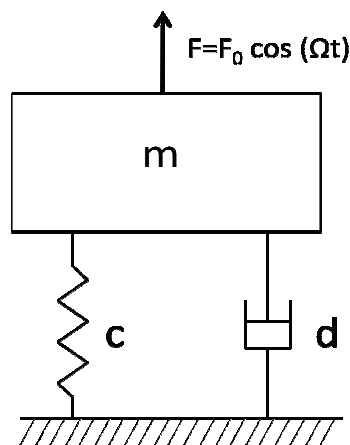


figure 10.1 model of driven damped harmonic oscillator

The force F describes the sinusoidal excitation through the second order inertia forces of the four cylinder in-line engine with the amplitude F_0 . According equation (5.22) equals the amplitude to $F_0 = -4 \cdot m_t \cdot r \cdot \omega^2 \cdot \frac{r}{l}$ and the angular velocity $\omega = 2\varphi$.

The considered system equates a damped and driven harmonic oscillator, driven by the second order inertia force of the four cylinder in-line engine, where the damping coefficient d and the spring stiffness c are variable. The deductions of the amplitude frequency response are based on the book "Technische Mechanik 3" [Hau02] .

The equilibrium conditions in x-direction for the mass m result in the following equation:

$$m \cdot \ddot{x} = -c \cdot x - d \cdot \dot{x} + F_0 \cdot \cos(\Omega t) \quad (10.1)$$

Introduction of the damping ratio $\zeta = \frac{d}{2 \cdot m}$ and the undamped angular oscillation frequency $\omega^2 = \frac{c}{m}$ and rewriting the equilibrium equation results in:

$$\ddot{x} + 2 \cdot \zeta \cdot \dot{x} + \omega^2 \cdot x = \omega^2 \cdot \frac{F_0}{c} \cdot \cos(\Omega t) \quad (10.2)$$

Substitution of the initial displacement $x_0 = \frac{F_0}{c}$ results in the equation of motion of the mass m :

$$\boxed{\ddot{x} + 2 \cdot \zeta \cdot \dot{x} + \omega^2 \cdot x = \omega^2 \cdot x_0 \cdot \cos(\Omega t)} \quad (10.3)$$

The equation of movement is a nonhomogeneous ordinary differential equation and its fundamental solution can be cast in terms of a homogeneous (transient) solution x_h and a particular solution x_p .

$$x = x_h + x_p \quad (10.4)$$

Since the transient solution decays exponentially over the time, the amplitudes get negligible small compared to the particular solution after a while. For this reason we only consider the particular solution x_p of the nonhomogeneous differential equation.

For the particular solution we use the following ansatz equation:

$$x_p = x_0 \cdot V \cdot \cos(\Omega t - \varphi) \quad (10.5)$$

Where φ is the phase lag in respect to the driving force.

Since $\cos(\Omega t - \varphi) = \cos(\Omega t) \cdot \cos(\varphi) + \sin(\Omega t) \cdot \sin(\varphi)$, equation (10.5) becomes:

$$x_p = x_0 \cdot V \cdot [\cos(\Omega t) \cdot \cos(\varphi) + \sin(\Omega t) \cdot \sin(\varphi)] \quad (10.6)$$

And the derivations for x_p result in:

$$\begin{aligned} \dot{x}_p &= x_0 \cdot V \cdot \Omega \cdot [-\sin(\Omega t) \cdot \cos(\varphi) + \cos(\Omega t) \cdot \sin(\varphi)] \\ \ddot{x}_p &= x_0 \cdot V \cdot \Omega^2 \cdot [-\cos(\Omega t) \cdot \cos(\varphi) - \sin(\Omega t) \cdot \sin(\varphi)] \end{aligned} \quad (10.7)$$

If we substitute equations (10.7) in the equation of movement (10.3) and introduce the factor $D = \frac{\zeta}{\omega}$, we obtain:

$$\begin{aligned} &x_0 \cdot V \cdot \frac{\Omega^2}{\omega^2} \cdot [-\cos(\Omega t) \cdot \cos(\varphi) - \sin(\Omega t) \cdot \sin(\varphi)] \\ &+ 2 \cdot D \cdot x_0 \cdot V \cdot \frac{\Omega}{\omega} \cdot [-\sin(\Omega t) \cdot \cos(\varphi) + \cos(\Omega t) \cdot \sin(\varphi)] \\ &+ x_0 \cdot V \cdot [\cos(\Omega t) \cdot \cos(\varphi) + \sin(\Omega t) \cdot \sin(\varphi)] = x_0 \cdot \cos(\Omega t) \end{aligned} \quad (10.8)$$

Rearranging equation (10.8) gives:

$$\begin{aligned} &\left[-V \cdot \frac{\Omega^2}{\omega^2} \cdot \cos(\varphi) + 2 \cdot D \cdot V \cdot \frac{\Omega}{\omega} \cdot \sin(\varphi) + V \cdot \cos(\varphi) - 1 \right] \cdot \cos(\Omega t) \\ &+ \left[-V \cdot \frac{\Omega^2}{\omega^2} \cdot \sin(\varphi) - 2 \cdot D \cdot V \cdot \frac{\Omega}{\omega} \cdot \cos(\varphi) + V \cdot \sin(\varphi) \right] \cdot \sin(\Omega t) = 0 \end{aligned} \quad (10.9)$$

Now the only way in which equation (10.9) can be satisfied at all time is if the coefficients of $\cos(\Omega t)$ and $\sin(\Omega t)$ separately equal to zero. This results in:

$$V \left[\frac{\Omega^2}{\omega^2} \cdot \cos(\varphi) + 2 \cdot D \cdot \frac{\Omega}{\omega} \cdot \sin(\varphi) + \cos(\varphi) \right] = 1 \quad (10.10)$$

And

$$-\frac{\Omega^2}{\omega^2} \cdot \sin(\varphi) - 2 \cdot D \cdot \frac{\Omega}{\omega} \cdot \cos(\varphi) + \sin(\varphi) = 0 \quad (10.11)$$

Since $\tan(\varphi) = \frac{\sin(\varphi)}{\cos(\varphi)}$ equation (10.11) can be rewritten as:

$$\tan(\varphi) = \frac{2 \cdot D \cdot \Omega}{\omega^2 - \Omega^2} \quad (10.12)$$

Equation (10.12) and (10.10) can be combined to give:

$$V = \left[\left(1 - \left(\frac{\Omega}{\omega} \right)^2 \right)^2 + 4 \cdot D^2 \cdot \left(\frac{\Omega}{\omega} \right)^2 \right]^{-1/2} \quad (10.13)$$

This follows because $\cos(\varphi) = \frac{1}{\sqrt{1+\tan^2(\varphi)}}$ and $\sin(\varphi) = \frac{\tan(\varphi)}{\sqrt{1+\tan^2(\varphi)}}$

The factor V represents the amplitude gain factor and the angle φ the phase lag of the frequency response.

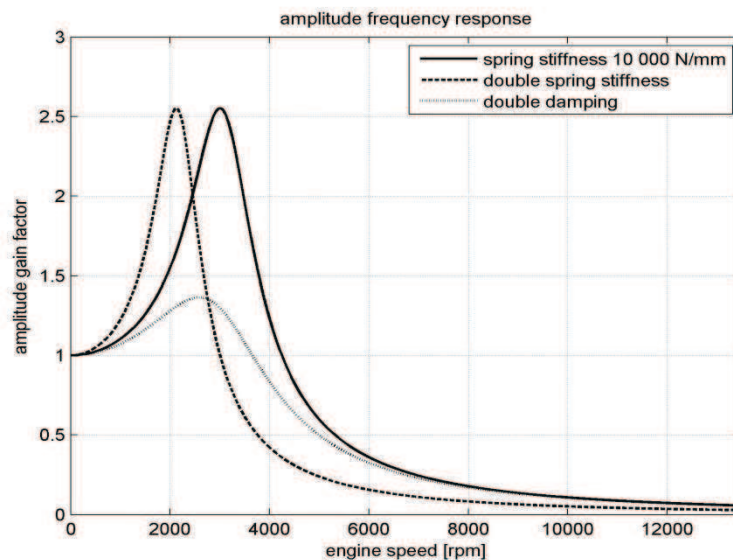


figure 10.2 amplitude frequency response, spring stiffness 10 000 N/mm

figure 10.2 shows the amplitude frequency response of the system with a spring stiffness of 10 000 N/mm compared to the double spring stiffness and double damping ratio. It can be seen that the higher stiffness shifts the point of resonance towards lower frequencies and higher damping reduces the peak amplitude. If we consider an engine speed of 4000 rpm it can be seen that a variation of the spring stiffness causes a high influence on the vibration amplitude. Smaller but still appreciable is the influence of the damping ratio. The further we continue onward higher excitation frequencies the less gets the influence of both on the damping ratio and the spring stiffness on the vibration amplitude. That means that the effect of an adaptive stiffness and damping ratio is greatest close to the resonant frequency.

If we consider a system with a lower spring stiffness for instance, where the resonant frequency is far away from the operating point the situation is a different.

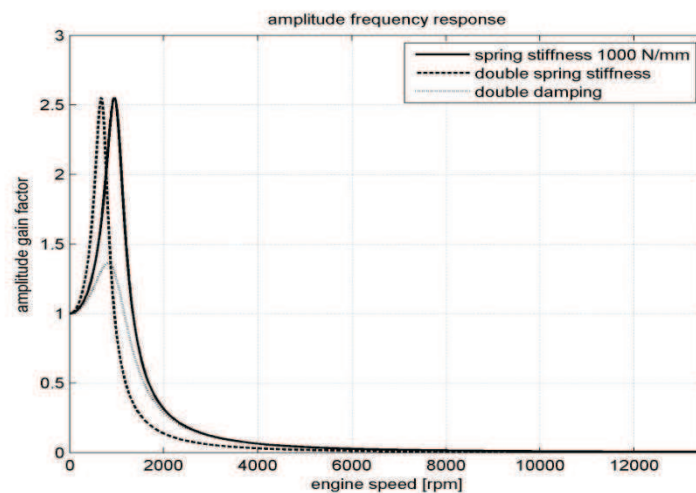


figure 10.3 amplitude frequency response, spring stiffness 1000 N/mm

figure 10.3 describes the amplitude frequency response of the system with a spring stiffness of 1000 N/mm. If looking on the operating range between 4000 and 13 500rpm one can see, that neither a variation of the spring stiffness nor of the damping ratio has big influence on the variation amplitude. In that case, the adaptation of the mounting stiffness or the damping ratio does not result in the desired effect.

10.2 Conclusion:

The analysis shows that an adaptation of the engine mounting stiffness and the damping ratio can be an effective tool in order to modify the vibration amplitude. But it's only effective, if the operation point is close to the resonant frequency. In highly over-resonant operation, the adaptive mounting stiffness has nearly no influence. Consequently it's not possible to do modifications on the vibration amplitude over the whole speed band of the engine. The system is rather qualified to influence either the vibration amplitude in lower speed range when the engine is operated above the resonant frequency or in high speed range when the engine is operated under the point of resonance.

11 Vibration Absorber

One idea to reduce or amplify the vibration amplitude was to induce sinusoidal forces in the engine block on different places in a specific direction. These forces basically reduce or enhance the excitation of the engine. This simulation analyses how many absorbers and their position, direction, magnitude and phase shift of the implied forces are necessary in order to reach the desired vibration situation. The analysis is independent on the problem how the forces are generated.

By using at least two vibration absorbers at different positions with different amplitudes and phasing, also angular vibrations can be generated or absorbed.

Disadvantage of the vibration absorber is the fact, that one absorber can amplify or reduce only one frequency at the same time. If there is a need to amplify different amplitudes at different frequencies for example first and second order mass forces, at least two absorbers are needed.

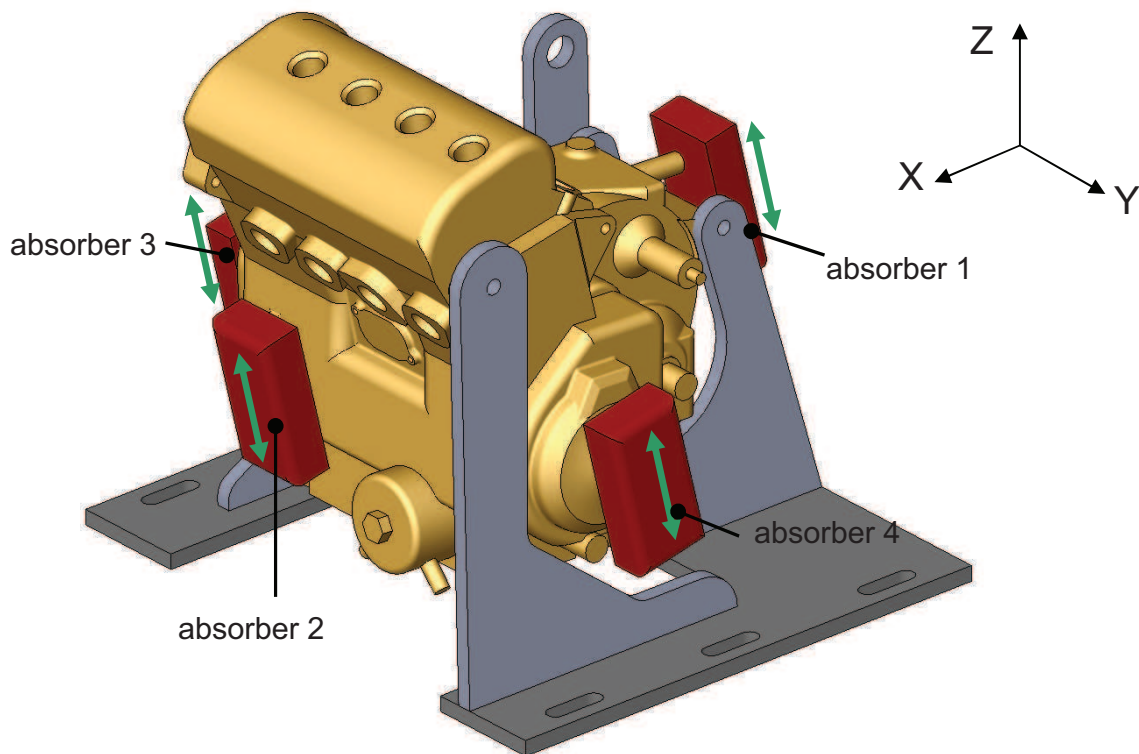


figure 11.1 position of vibration absorbers

figure 11.1 shows a possible placement of four vibration absorbers. The generated forces are acting in direction of the excitation which is in direction of the cylinder axis.

Two of them are acting in line of the crank shaft axle. These absorbers work in phase or with 180 degrees of phase shift to the excitation in order to amplify or reduce the excitation and consequently reduce or amplify the vibration amplitude in direction of the cylinder axis.

The other two absorbers are displaced in x-direction. These absorbers have the function to excite angular vibration around the crank shaft axle. Since the two forces act in contrariwise direction, the resultant force is zero. Only a torque around the y-axis remains. For this reason no excitation occurs in translational direction but the torque excites angular vibration around the y-axis.

It has to be taken into account, that the phase lag of the angular vibration is not the same than in translational direction. Since an excitation is only effective if it acts in the same phase than the vibration, a detection of the phase lag of the rotational vibration is necessary.

11.1 Model of Vibration Absorber

The vibration absorber was modelled in Dymola and consists of a sinusoidal force that acts on a rigid massless frame. The Inputs are the accordant force signals. The generation of the force signal is done in Simulink. The model is defined in a way that the number, the positions and the directions of the acting forces can be modified easily.

In sum four absorbers are in use.

11.1.1 Dymola Model of Vibration Absorber

The vibration absorbers are an extension of the mechanical Dymola model. Thus the Dymola block which is implemented in the Simulink model gets four more in-ports for the force signals.

The model consists of a rigid frame element for each absorber which describes the position of the point where the force is acting in respect to the engine reference point. The attached fixed rotation element describes the angle of the direction of the force resolved in the engine coordinate system. The acting force was modelled using a frame force element, which represents an external force defined by three input signals for the three directions. The force vector is resolved in the coordinate system, which is rotated by the fixedRotation element.

- Used blocks from the Modelica library:

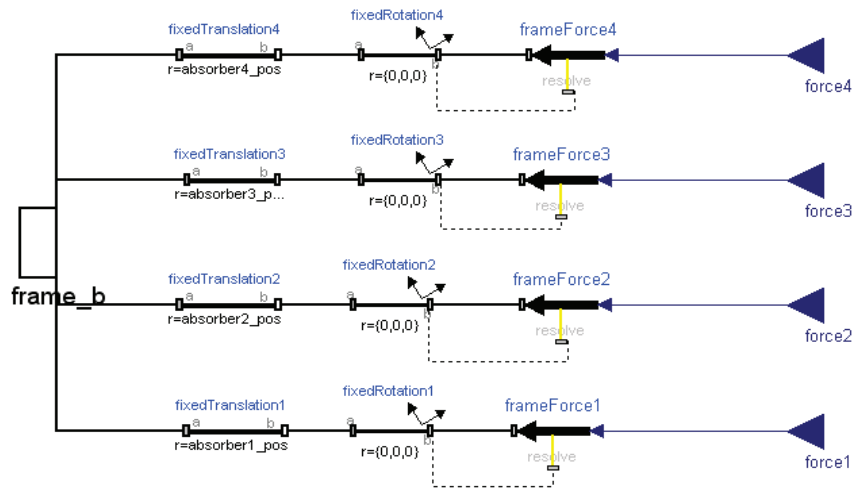


figure 11.2 Dymola Model of Vibration Absorber

frameForce1 - 4: These elements represent external forces which are acting in frame_b of the fixedRotation elements. The Input is a force signal vector. This vector is resolved in the frame which is connected to the resolve out port.

fixedTranslation1 - 4: These elements describe the position vectors from the engine reference point to the points where the forces are acting.

fixedRotation1 - 4: These elements describe the rotation of the coordinate system in which the forces are acting in respect to the engine reference point.

Parameters

Name	Type	Unit	Default	Description
absorber1_pos[3]	position	[m]	{-0.35,0,0}	Position vector of absorber 1 resolved in engine reference point
Absorber2_pos[3]	position	[m]	{0.35,0,0}	Position vector of absorber 2 resolved in engine reference point
Absorber3_pos[3]	position	[m]	{0,-0.2,0}	Position vector of absorber 3 resolved in engine reference point
Absorber4_pos[3]	position	[m]	{0,0.2,0}	Position vector of absorber 4 resolved in engine reference point
Absorber1_ang[3]	angle	[deg]	{0,15,0}	Rotation angle of coordinate system, in which force 1 is acting resolved in engine reference point
Absorber2_ang[3]	angle	[deg]	{0,15,0}	Rotation angle of coordinate system, in which force 2 is acting resolved in engine reference point

Absorber3_ang[3]	angle	[deg]	{0,15,0}	Rotation angle of coordinate system, in which force 3 is acting resolved in engine reference point
Absorber4_ang[3]	angle	[deg]	{0,15,0}	Rotation angle of coordinate system, in which force 4 is acting resolved in engine reference point

Connectors

Type	Name	Description
Frame_b	Frame_b	Describes the fixed connection to engine reference point
Real	Force_1	In port of the signal of absorber force 1
Real	Force_2	In port of the signal of absorber force 2
Real	Force_3	In port of the signal of absorber force 3
Real	Force_4	In port of the signal of absorber force 4

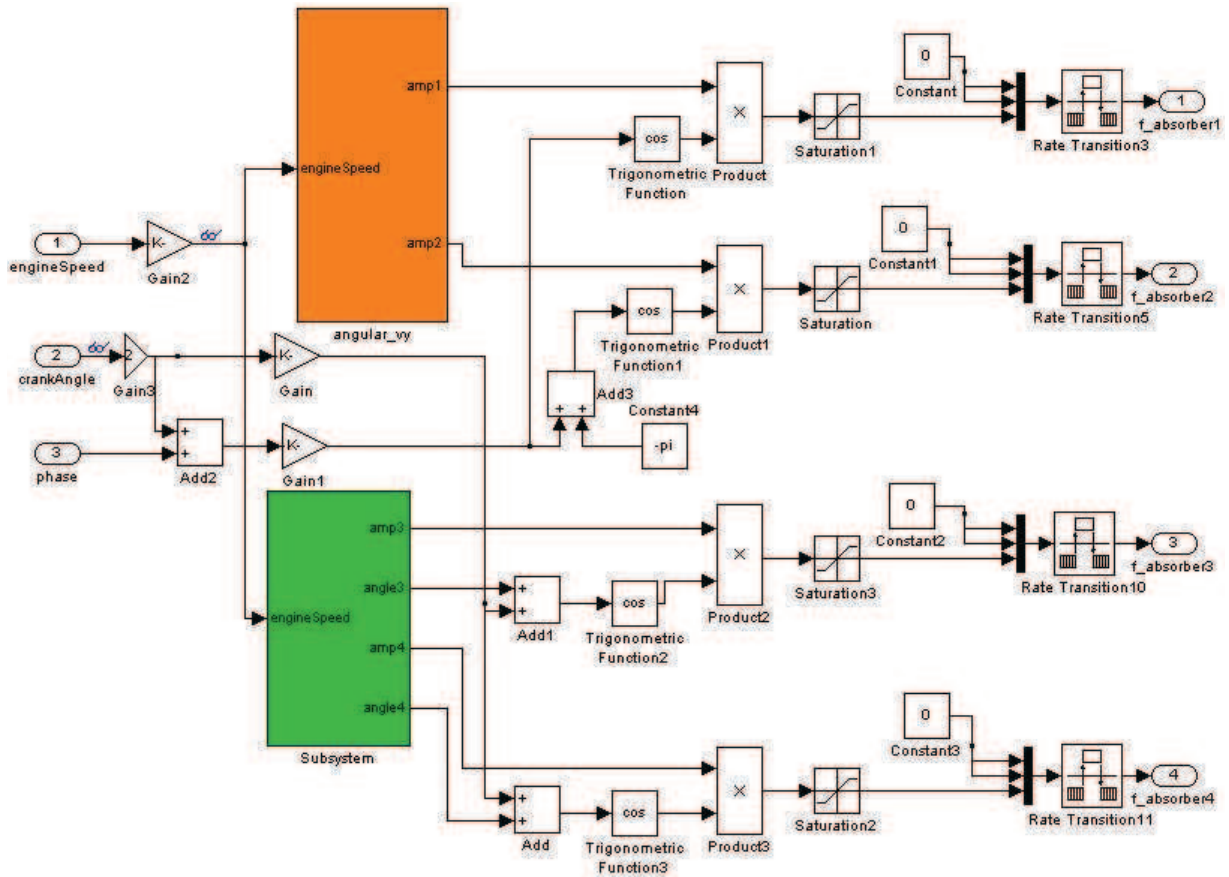
11.1.2 Simulink Model of vibration absorber

The Dymola block in the Simulink model got four additional in ports for the vibration absorber forces.

Additionally sub models for the force generation and for the phase shift detection are needed.

The subsystem “vibrationAbsorber” includes the model of generator for the vibration absorber forces. The phase shift between the angular vibration and the excitation due to the second order inertia force is determined in the “phaseShift” subsystem.

11.1.2.1 Subsystem “VibrationAbsorber”



11.3 subsystem “vibrationAbsorber”

The “vibrationAbsorber” submodel exists out of two subsystems, which content the lookup tables for the amplitude of the absorber forces.

The input signals are the actual filtered engine speed in rpm the crank angle signal from the crank angle calculator (see 8.2.2) in degrees and the phase lag from the phase shift detector (see 11.1.2.2) in degree.

The angular_v subsystem contains two 1D-lookup tables, one for vibration absorber 1 and one for absorber 2, which excite or absorb angular vibration around the y-axis. It returns the force amplitudes as a function of the engine speed. The tables perform a 1-D linear interpolation of the input values using the specific table. The subsequent rate limiter allows a limitation of the gradient of the signal if required. Since the phase angle of the angular vibration is determined by the phase detector, no additional lookup tables for the phase angles are needed.

The block “translation_v” outputs the force amplitude in N and the phase angle in radiant of vibration absorber 3 and 4 as a function of the engine speed. Since these absorbers

either amplify or reduce vibration, the phase angle either equals to zero or to 180 degree. For this reason additional lookup tables for the phase angle have to be defined. In sum the block contains four lookup tables, two for the force amplitudes and two for the phase angles.

If we follow the angle signal of the “translation_v” block downstream the crank angle signal is added. This results in the angle signal of the absorber force. This is done by the “Add” and “Add1” elements. The “Trigonometric Function” block returns the cosines of the force angle signal, which is multiplied by the corresponding amplitude signal. The resulting signal is the sinusoidal force signal f_{absorber_i} of absorber i in the shape:

$$f_{\text{absorber}_i} = \text{amp}_i \cdot \cos(\varphi + \text{angle}_i) \quad (11.1)$$

Where φ equals to the crank angle, angle_i to the phase lag and amp_1 to the force amplitude of absorber i . The “Saturation” block keeps the force signal into a definable limit.

The force in-port of the Dymola model requires a 3-dimensional force vector. But since we just want to define a force in z-direction, the x- and y- components are kept to zero. This was done by multiplexing two constant zero signals and the force signal to a 3-dimensional force vector.

In a similar way the force signals of the absorbers 1 and 2 are modelled, with the difference that the phase angle signal comes from the phase shift detector. Since the force signal of absorber 2 is always 180 degree phase shift to the signal of absorber 1, the constant value of $-\pi$ is added to the angle signal.

11.1.2.2 Subsystem “PhaseShift”

The phase shift detector is modelled in the “PhaseShift” subsystem. Its function is to detect the phase angle between the excitation and the angular oscillation of the engine around the y-axis. The inputs are the vibration signal of the centre of gravity of the engine and the crank angle signal from the crank angle calculator (see 8.2.2). The phase shift detector outputs the phase lag between the angular oscillation velocity of the engine around the y-axis and the excitation in degree.

The method of the phase detection is based on a Discrete Fourier Transformation (DFT). The DFT transforms time based data into frequency based data. The basic principle is that complicated periodic functions can be written as a sum of simple waves mathematically represented by sin and cosine waves with defined amplitude, phase angle and frequency.

The phase detector determines the phase lag of the domination frequency with help of a Fast Fourier Transformation (FFT). The FFT computes the Discrete Fourier Transformation of a time based matrix with a FFT algorithm. Plotting the amplitude

spectrum gives information about the amplitudes which occur at a specific frequency. The phase plot of the FFT returns the corresponding phase angle to a specific frequency. The phase detector determines the frequency, where the maximum amplitude occurs and returns the corresponding phase angle. In this way the phase angle of the angular velocity signal and the crank angle signal are computed. The difference of these values represents the phase shift between the angular vibration velocity and the crank angle signal.

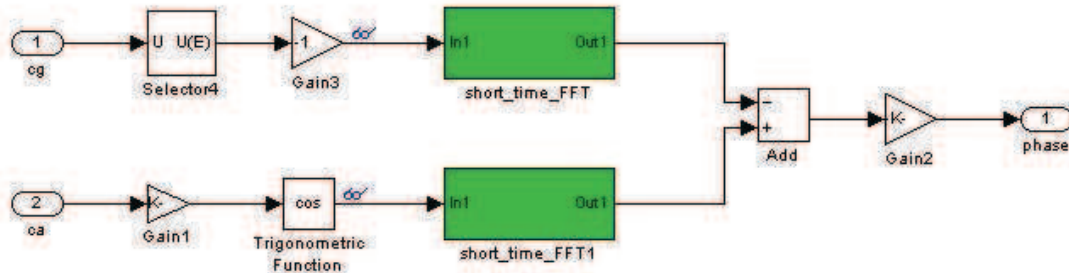


figure 11.4 Simulink model of phase shift detector

figure 11.4 shows the schematic diagram of the phase shift detector model. The inputs are the vibration signal of the centre of gravity of the engine and the crank angle signal. The “Selector4” block selects the angular velocity signal around the y-axis of the vibration signal vector. Since the velocity signal has a phase shift of 180 degrees to the angle signal, the velocity signal is multiplied by -1 in the “Gain3” block. The crank angle signal is translated in radian by the “Gain1” block. The “Trigonometric function” converts the crank angle signal into a cosine wave. The “short_time_FFT” subsystem processes the spectral analyses with help of a short time FFT and outputs the phase angle of the input signal. The difference of the two phase angle signals equals to the searched phase shift. The block “Gain2” converts the signal to degree units.

The “Short_time_FFT” subsystem:

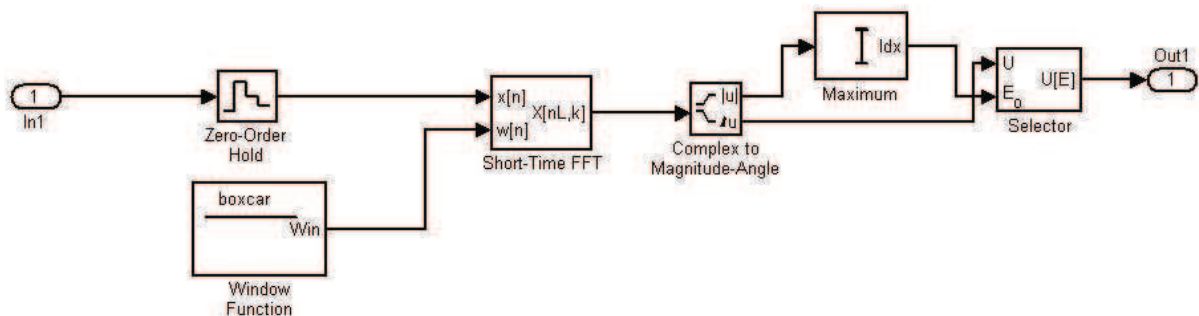


figure 11.5 “Short_Time_FFT” submodel

In-port1 inputs the time based vibration or crank angle signal. The “Zero-Order-Hold” block converts the time based signal into a sample based signal, since there are sample or frame based signals required for the short time FFT. In this block, a sample time has to be defined. In order to reach the maximum resolution, the sample time is set equal to the fixed simulation step size of 2^{-16} sec.

The “Short-Time FFT” block computes a nonparametric estimate of the spectrum. The block buffers, applies an analysis window and zero pads the input signal. Then the block takes the FFT of the signal, transforming it into the frequency domain. The $w(n)$ port requires an analysis window. The block buffers the analysis window signal into a frame based signal with the frame length W . For the window function the type “Boxcar” was chosen, which equates to a rectangular window. The rectangular window provides a function which equals to one inside the interval and to zero elsewhere. That means that this window takes the chunk of the signal without any other modifications. The window size is chosen equal to 2^{14} samples. That means if we consider a sample time of 2^{-16} sec, one frame includes the data of 0.25 sec.

The overlap of the consecutive windows is chosen equal to the window length minus 1024, that is $2^{14} - 1024$ samples. Hence every 1024 samples one FFT is proceeded with a frame length of 2^{14} samples. That equates to a time range of 0.0156 sec, or in other words, 64 FFT are run through in one second.

The FFT length was set equal to the sample frequency.

The output of the short-Time-FFT block is the frame based complex frequency spectrum of the input signal $x[n]$

The magnitude and phase lag was determined using a “Complex to Magnitude-Angle” block. This block computes the magnitude and the phase angle in radiant of the complex input. The subsequent “Maximum” block searches for the maximum Amplitude of the current frame and outputs its index. Finally the “Selector” block selects the phase angle to the corresponding index.

11.1.3 Vibration Absorber Map

The parameters of the lookup tables were modified in order to approach similar vibration behaviours than the data of the chassis dyno measurements show. This was achieved due to the following procedure:

- First of all the parameters of the force amplitude of vibration absorber 3 and 4 were modified, so that the excitation force due to the second order inertia forces was compensated over the whole speed band. With help of equation (5.22) a good approach could be achieved. It was obtained that the vibration level of the engine was almost equal to zero.
- Next step was to increase or decrease the force amplitude of the vibration absorbers in a way so that the z-vibration amplitude of the centre of gravity has the same level than on the chassis dyno.

- Afterwards the vibration absorbers 1 and 2, which generate angular excitation around the y-axis were activated. The force amplitude was modified in a way, so that the angular vibration velocity around the y-axis approaches the values of the chassis dyno measurements.
- Finally the focus was on the engine mounting points. A fine tuning of the lookup tables resulted in the following characteristics:

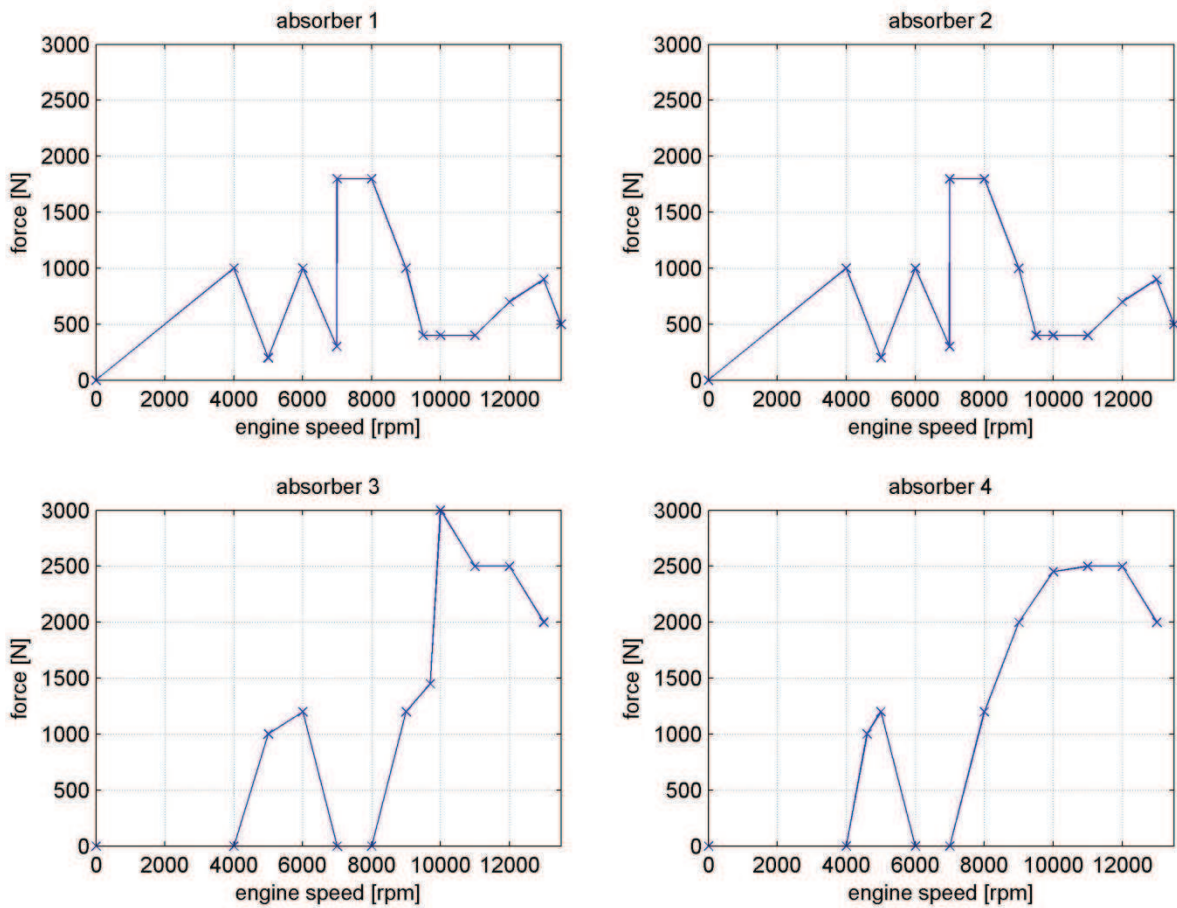


figure 11.6 vibration absorber map

11.1.4 Results

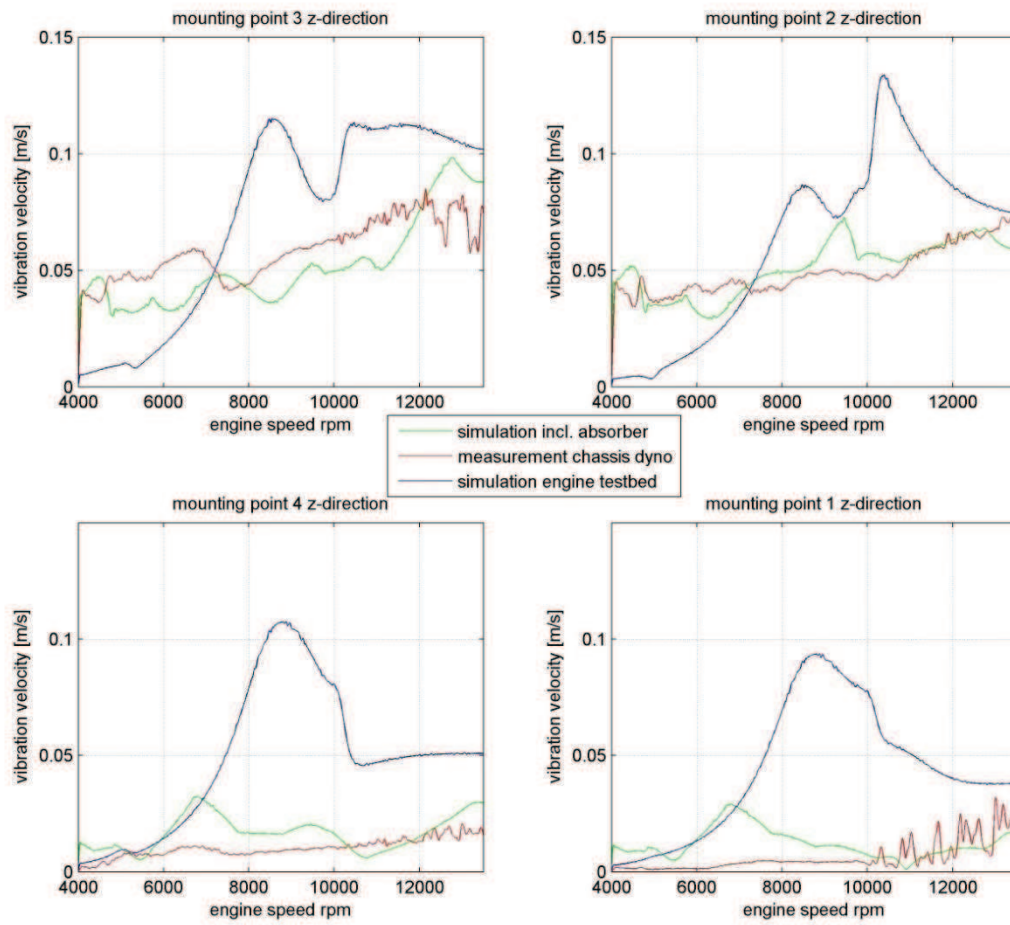


figure 11.7 second order vibration velocity amplitude z-direction, absorbers vs. chassis dyno

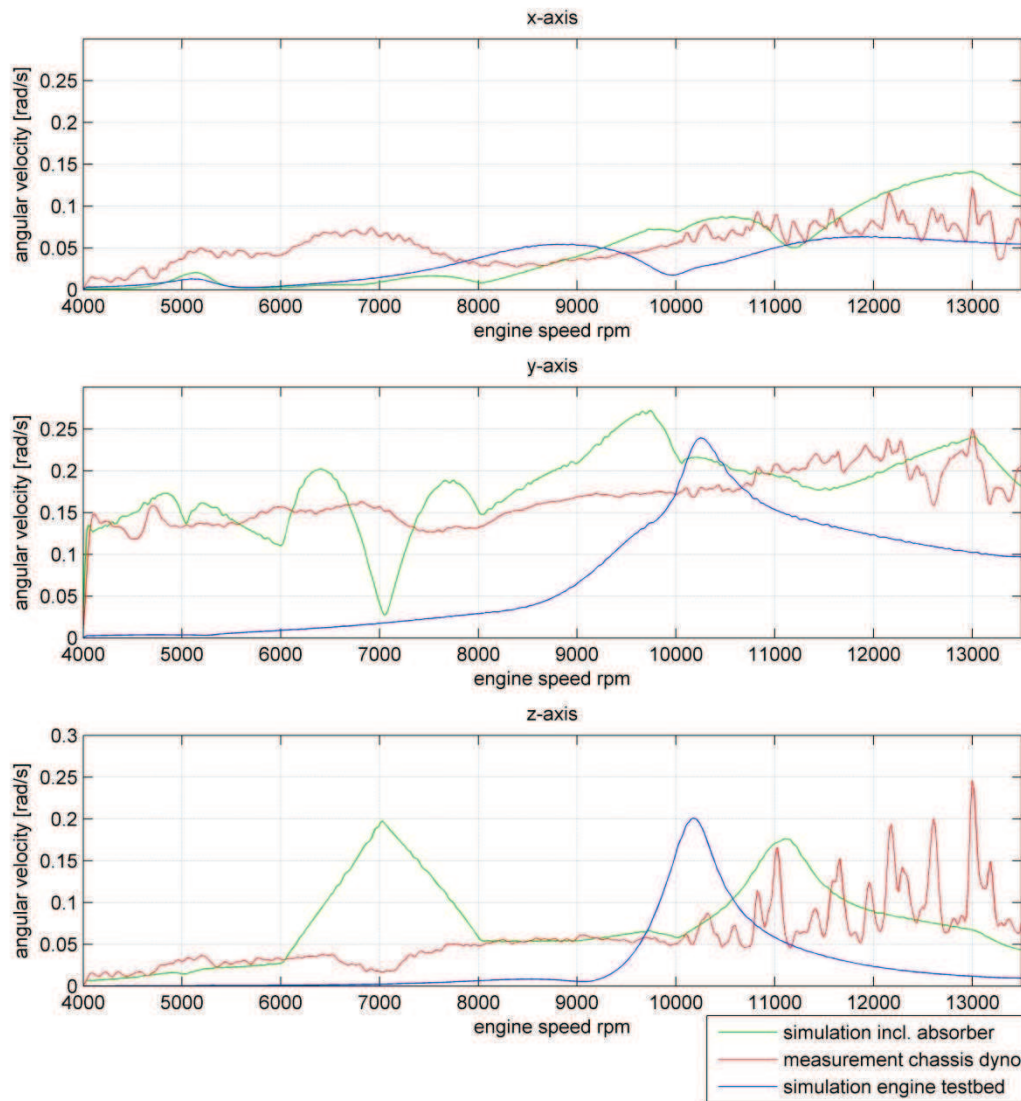


figure 11.8 second order angular velocity amplitude, absorbers vs. chassis dyno

Figures figure 11.7 and figure 11.8 show the second order vibration amplitude of the mounting points and the angular velocity amplitudes of the system. In these graphs the simulation results with and without vibration absorbers are plotted and compared to the vibration situation in the racecar measured on the chassis dyno.

It can be clearly seen that the vibration amplitude can be modified over the whole engine speed band and conditions which equal to the situation in the race car can be approached in nearly every point. Simply the angular velocity around the y-axis cannot be amplified at an engine speed of approximately 7000 rpm. This also the reason for the deviation of the vibration velocity of mounting points 1 and 4 from the desired value. In this point the angular vibration around the y-axis changes its direction and consequently a modification would require too high force amplitudes of the absorbers 1 and 2.

Nevertheless the analyses show, that the desired situation can be reached in nearly every point even if the characteristic is not very smooth. The design of a sophisticated controller for the force amplitudes of the absorbers would give a better response and consequently a better approach.

12 Conclusion

It's shown in this thesis, that the vibrations which occur on an engine testbed can be modified, so that a vibration situation arises which is similar to the situation inbuilt in a racecar. The two analysed methods are a variation of the engine mounting stiffness and an application of sinusoidal forces on the engine block.

In order to analyse the two different vibration situations a comparison of the measured acceleration on the engine testbed and on the chassis dyno was done. The running mode analysis, described in chapter 7.4 clearly shows that the second order vibrations are dominating at both mounting situations. A more detail analyses of the second order vibrations brings out, that resonances occur on the engine testbed while the amplitudes increase nearly linear over the engine speed on the chassis dyno. The transformation of the vibration velocity amplitude of the mounting points to the centre of gravity movement allows an allocation of the occurring resonances to the corresponding movement.

As described in chapter 10 the adaptive engine mounting stiffness is only effective close to the point of resonance. But there are other aspects in favour. For example the complexity of the controller of the adaptive engine mounting stiffness system is much less compared to the vibration absorber system, since the parameters to control are changing much slower. While the control parameters of the vibration absorbers change resolved over the crank angle, the parameters of the adaptive engine mounting system change only engine speed resolved. This also restricts the choice of the absorber actuators since they must respond very quickly especially at high engine speeds. For instance we consider the point of the maximum engine speed of 13500 rpm. This equals to a frequency of 225 Hz. In order to compensate the second order inertia forces in this point, an actuator has to be found which generates a sinusoidal force with a frequency of 450 Hz.

Since the force and frequency requirements of the vibration absorbers are very ambitious, this system is probably only applicable at low engine speeds.

To draw a conclusion, the adaptive mounting stiffness system is most effective close to the point of resonance and the vibration absorber system is probably only applicable at low engine speeds.

Because of these facts a meaningful configuration will be a combination of both systems, where the stiffness of the engine mounting is determined so that the point of resonance lies close above the maximum engine speed. In this case the vibration amplitudes can be controlled by the adaptive engine mounting stiffness system at high engine speeds and by the vibration absorbers at low engine speeds. Due to this combination the advantages of both systems are coming into effect.

13 Future projects

This thesis brings up two possible basic approaches for an adaptive engine mounting system. The first is to vary the engine mounting stiffness or the damping ratio, the other is to induce forces. But also a combination of both can be taken into consideration.

The next step will be to do a preliminary study and to search for solutions for both systems.

For the adaptive mounting stiffness system a solution for the problem how the stiffness can be varied has to be found. For this reason an analysis of existing spring-damper elements has to be done and the possibility of application has to be proven. If no standard elements are available solutions for an element with variable stiffness have to be discussed.

For the vibration absorbers system a capable actuator has to be found, which satisfies the force and frequency requirements.

After an evaluation of all systems a selection has to be done.

The selected system has to be subject to more detailed analyses. Therefore it's recommended to design a model of the system and to implement it in the multi body simulation. If the simulation fulfils all objectives, a digital mock-up can be designed.

Next a prototype of the designed system will be manufactured and tested on an engine testbed. Therefore AVL cooperates again with the TU Graz Racing Team, since they will test their engine on an AVL testbed in February 2011.

After the tests of the system on the TU Graz Racing engine the measured results have to be compared to the measurements on the chassis dyno.

An evaluation will show if all objectives could be achieved and if necessary, possible improvements should be discussed. After all tests are positive the system is ready for utilization by the customers.

14 List of references

Books:

- [Gla07] Glad, T., & Lennard, L. (2007). *Reglerteknik Grundläggande Teori*. Lund: Studentlitteratur.
- [Hau02] Hauger, Schnell, & Gross. (2002). *Technische Mechanik 3*. Springer.
- [Kol00] Kollmann, F. G. (2000). *Maschinenakustik 2. Auflage*. Springer.
- [Mül04] Müller, G., & Michael, M. (2004). *Taschenbuch der Technischen Akustik*. Springer.
- [Sch10] Schlecht, B. (2010). *Maschinenelemente 2: Getriebe-Verzahnungen-Lager*. München: Pearson Studium.
- [Sch97] Schwarz, H. R. (1997). *Numerische Mathematik 4. Auflage*. Stuttgart: B. G. Teubner.
- [Rol09] Wittel, H., Muhs, D., Jannasch, D., & Voßiek, J. (2009). *Roloff/Matek Maschinenelemente 19. Auflage*. Wiesbaden: Vieweg + Teuber GWV Fachverlage GmbH.
- [Wit01] Wittenburg, J., & Pestel, E. (2001). *Festigkeitslehre: Ein Lehr- und Arbeitsbuch, 3. Auflage*. Berlin Heidelberg New York: Springer.

Papers:

- [Fed10] Federation Internationale de l'automobile. (2010, June 23). *Formula One Technical Regulations*. FIA Sport.

From the Internet:

- [Kan10] Kane, Jack; EPI Inc. (2010). *A comparison of V8 engines used in Formula One and NASCAR Cup (RET-029)*. Retrieved July 2010, from http://www.epi-eng.com/piston_engine_technology/comparison_of_cup_to_f1.htm
- [Mat10] MathWorks. (n.d.). *MATLAB and SIMULINK for Technical Computing*. Retrieved April 2010, from <http://www.mathworks.com/help/techdoc/fft.html>

15 Table of figures

figure 5.1 simplified model of single cylinder crank mechanism	8
figure 5.2 layout crank shaft 4-cylinder in-line engine.....	12
figure 5.3 vector diagram 1st order inertia forces 4-cylinder in-line engine	12
figure 5.4 vector diagram 2nd order inertia forces 4-cylinder in-line engine.....	13
figure 5.5 Second order inertia forces 8-cylinder V90° engine.....	14
figure 6.1 layout engine testbed	16
figure 6.2 sensor position on engine testbed.....	17
figure 6.3 test procedure engine testbed.....	18
figure 6.4 schematic diagram of chassis dyno.....	18
figure 6.5 mounting situation on chassis dyno.....	19
figure 6.6 test procedure on chassis dyno.....	20
figure 7.1 shape of raw data matrix.....	21
figure 7.2 lowpass Butterworth filter design.....	22
figure 7.3 raw data vs. Filtered data.....	22
figure 7.4 Classification of data for FFT.....	23
figure 7.5 FFT at 10 000 rpm on engine testbed	25
figure 7.6 translation of a reference frame.....	27
figure 7.7 translation and rotation of a reference frame.....	28
figure 7.8 translation and rotation of engine cg.....	30
figure 7.9 running mode analysis of mounting point 3 in z-direction	34
figure 7.10 second order vibration velocity on testbed and chassis dyno in z-direction	35
figure 7.11: second order vibration velocity of cg on testbed and chassis dyno.....	37
figure 7.12: second order angular velocity of cg on testbed and chassis dyno	39
figure 8.1 Dymola model of test bed.....	43
figure 8.2 degrees of freedom of engine model.....	45
figure 8.3 Dymola model of engine.....	46
figure 8.4 degrees of freedom cylinder.....	49
figure 8.5 Dymola model of Cylinder	50
figure 8.6 friction mean effective torque	53
figure 8.7 measurement of engine cg height	54
figure 8.8 CAD-model of engine.....	55
figure 8.9 indicated cylinder pressure of cylinder 1.....	55
figure 8.10 Dymola Model of gas force calculator.....	56

figure 8.11 Dymola Model of Clutch	57
figure 8.12 Dymola Model of Gearbox.....	59
figure 8.13 model of gear switch	60
figure 8.14 Dymola Model of drive shaft.....	62
figure 8.15 Dymola model of torque gauge	63
figure 8.16 Dymola Model of engine mounting frame	65
figure 8.17 schematic diagram of rubber pad model.....	67
figure 8.18: 1D schematic diagram of rubber pad model	67
figure 8.19 Simulink Model of engine and testbed.....	69
figure 8.20 Simulink Model of engine speed controller	71
figure 8.21 Simulink Model of PID controller	71
figure 8.22 Step response according Ziegler/Nichols	73
figure 8.23 Step response with improved PID controller.....	74
figure 9.1 residual of vibration velocity amplitude in z-direction	76
figure 9.2 piston displacement simulation at 4000rpm.....	77
figure 9.3 firing order simulation at 4000rpm	77
figure 9.4 engine characteristics map.....	78
figure 9.5 crank shaft torque at 13000 rpm simulation vs. Calculation.....	80
figure 9.6 simulated excitation force, engine speed 4000 rpm.....	80
figure 9.7 vibration velocity amplitude on engine testbed, measurement vs.simulation	81
figure 9.8 vibration velocity amplitude in z-direction, simulation versus testbed.....	83
figure 10.1 model of driven damped harmonic oscillator	84
figure 10.2 amplitude frequency response, spring stiffness 10 000 N/mm.....	87
figure 10.3 amplitude frequency response, spring stiffness 1000 N/mm.....	88
figure 11.1 position of vibration absorbers.....	89
figure 11.1 Dymola Model of Vibration Absorber	91
11.2 subsystem "vibrationAbsorber".....	93
figure 11.3 Simulink model of phase shift detector	95
figure 11.4 "Short_Time_FFT" submodel	95
figure 11.5 vibration absorber map.....	97
figure 11.6 second order vibration velocity amplitude z-direction, absorbers vs. chassis dyno.....	98
figure 11.7 second order angular velocity amplitude, absorbers vs. chassis dyno.....	99

16 Appendix A: Previous projects

16.1 Data sheet of acceleration Sensor

Manufacturers' Specifications Bruel & Kjaer 4393 : Accelerometer

Piezoelectric Charge Accelerometer

*Charge sensitivity : 0.316 pC/ms⁻² or 3.1 pC/g ± 2 % ***

*Voltage sensitivity : 0.48 mV/ms⁻² or 4.8 mV/g ± 2 % ***

Mounted resonance : 55 kHz

Frequency range - 5 % : 0.2 Hz to 12000 Hz

Frequency range - 10 % : 0.1 Hz to 16500 Hz

Capacitance - typical : 650 pF with supplied integral cable

Max transverse sensitivity : < 4 %

Transverse resonance : 18 kHz

Piezoelectric material : PZ23

Construction : Delta shear

Typical temperature transient sensitivity : 5 ms⁻²/°C

Typical magnetic sensitivity (50 Hz to 0.03T) : 30 ms⁻²/tesla

Typical acoustic sensitivity (154 dB SPL) : 0.04 ms⁻²

Minimum leakage resistance at 20 °C : 20 G Ω

Ambient temperature range : -74 °C to 250 °C

Maximum operational shock (Peak) : ± 250 kms⁻²

Maximum continuous sinusoidal acceleration (Peak) : 50 kms⁻²;

Electrical Connector : M3 subminiature coaxial connector - side entry, recommended clearance for integral plug 18 mm

Mounting thread : M3, 2.2 mm deep

Mounting torque : 1 Nm, max = 2 Nm, min = 0.5 Nm

Dimensions - body : 7.3 mm diameter

Dimensions - overall height : 11 mm

Dimension - across base flats : 7.5 mm - spanner size

Weight : 2.4 grams

Case Material : Titanium ASTM Grade 2

Recommended cable : AO 0038

16.2 Mean vibration velocity amplitude of Engine Testbed Measurements

By Josef Retzl, AVL List GmbH

Project: TU Graz Racing



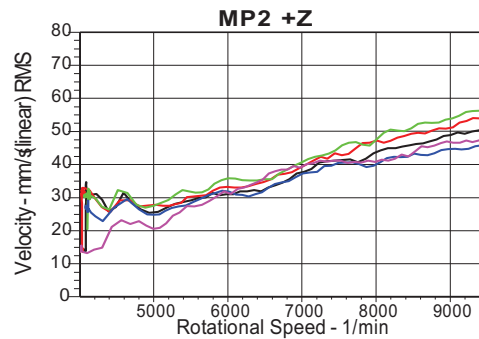
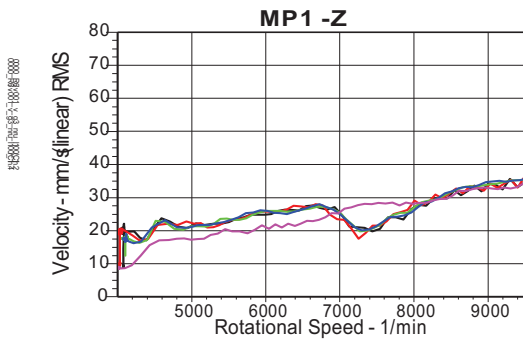
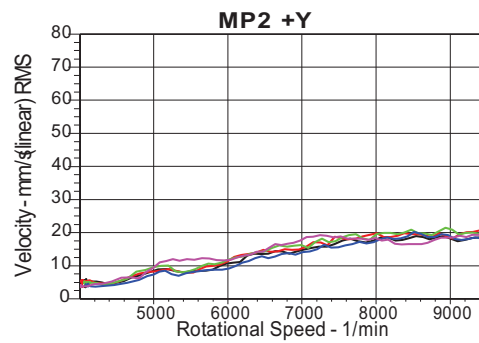
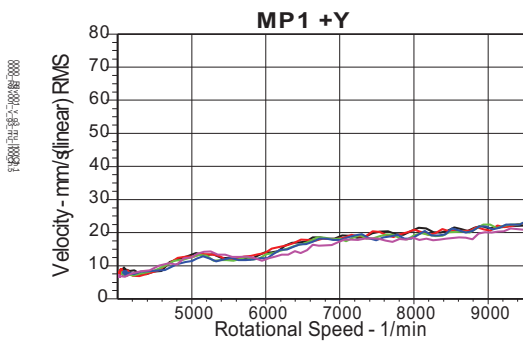
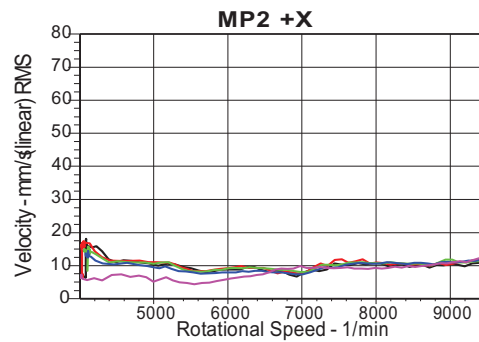
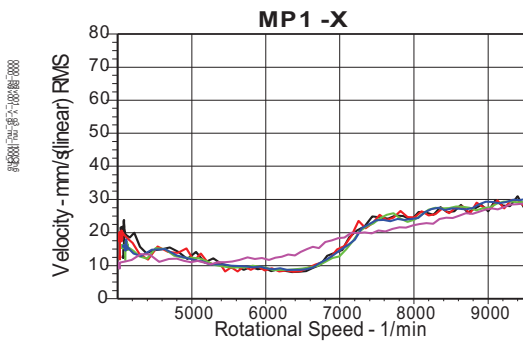
Version Version 01

Measurement: Running Mode Analysis

Testsite: Engine Test Bed - non Acoustic

- Run Up Full Load , 3rd Gear
- Run Up Full Load , 4th Gear
- Run Up Full Load , 5th Gear

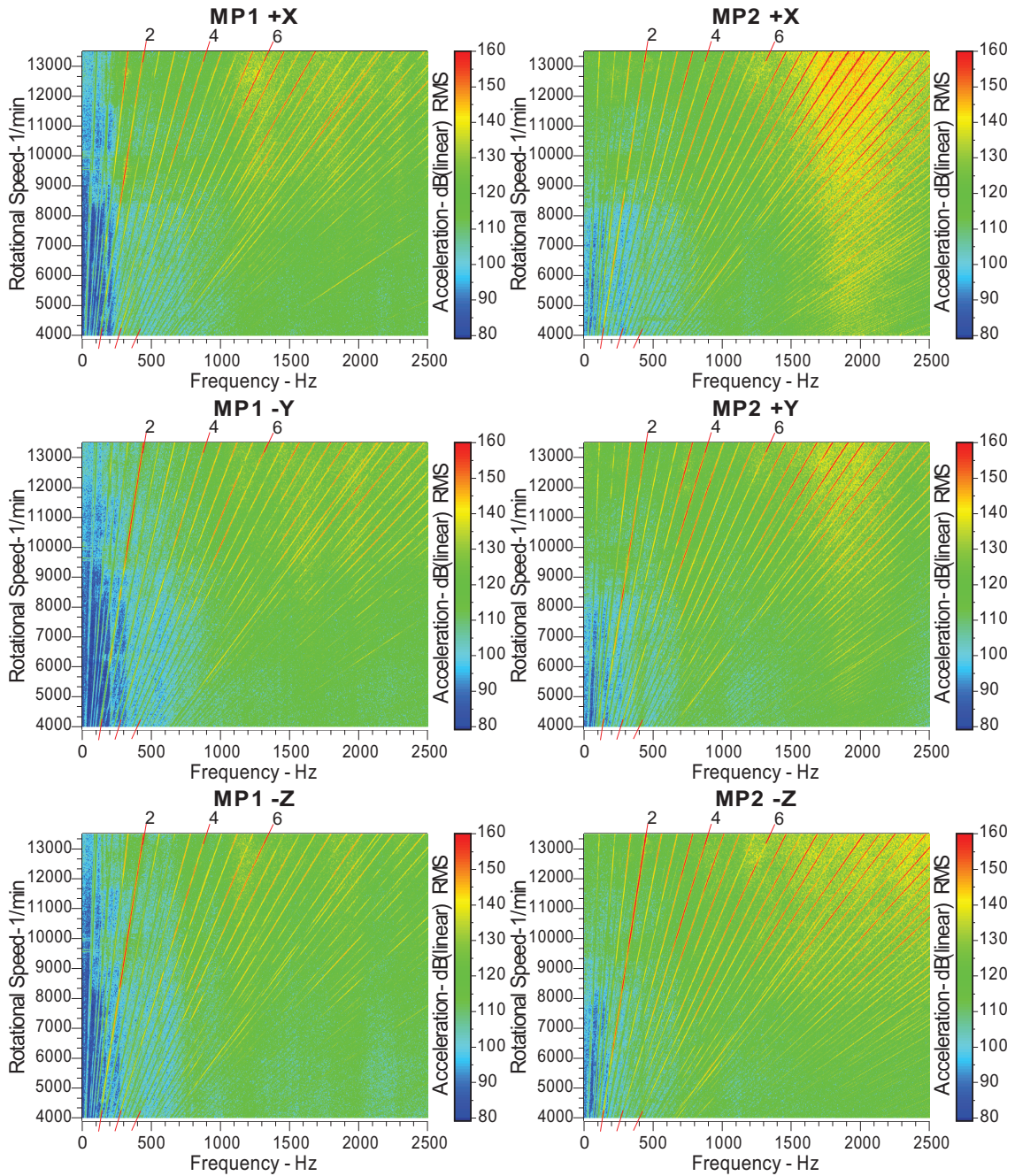
- Run Up Full Load , 6th Gear
- Run Up Motored , 6th Gear



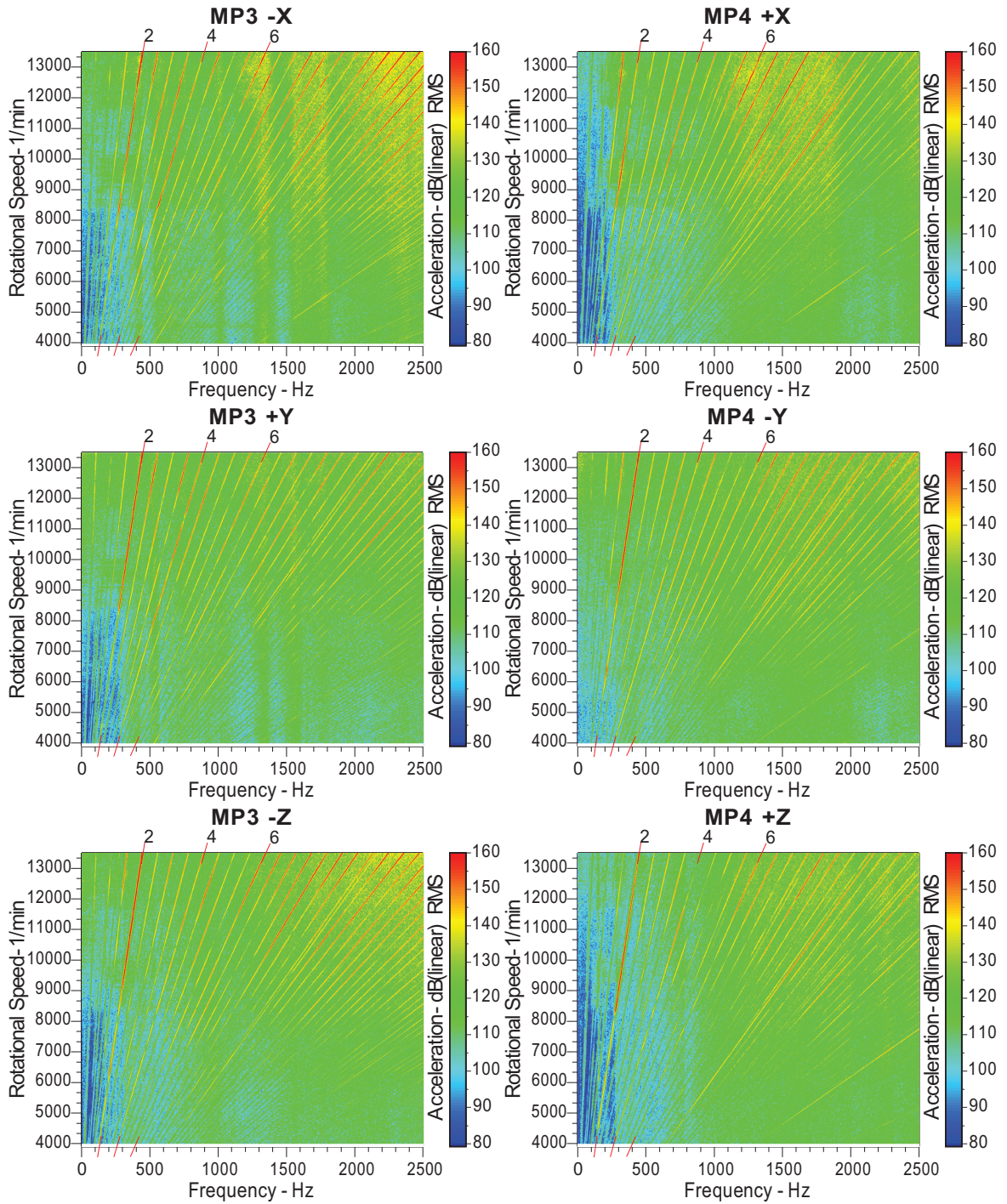
16.3 Running Mode analyses Engine Testbed Measurements

By Josef Retzl, AVL List GmbH

Version **Version 01**
Measurement: Running Mode Analysis
Testsite: Engine Test Bed - non Acoustic
Condition: **Run Up Full Load**



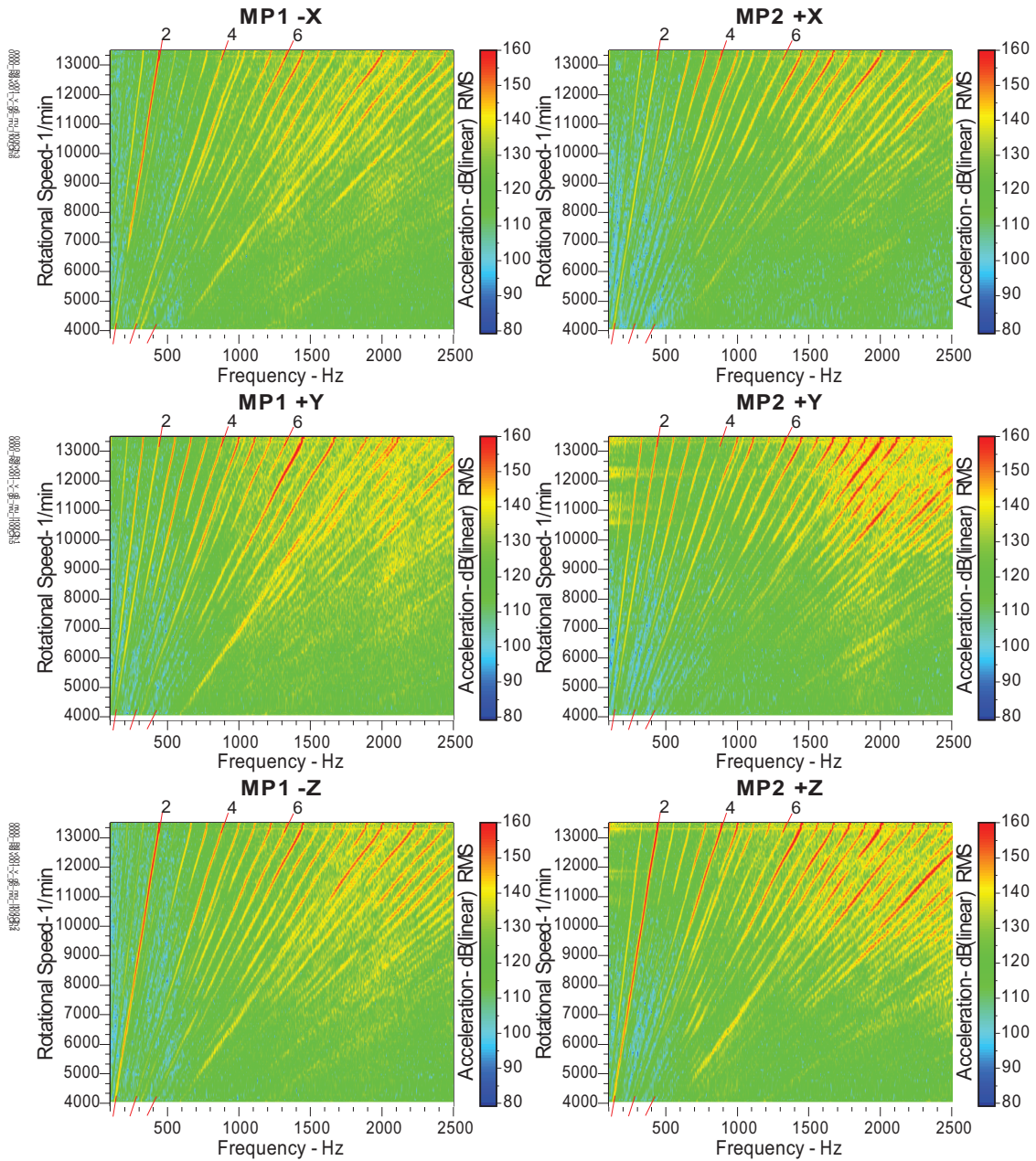
Version **Version 01**
Measurement: Running Mode Analysis
Testsite: Engine Test Bed - non Acoustic
Condition: Run Up Full Load



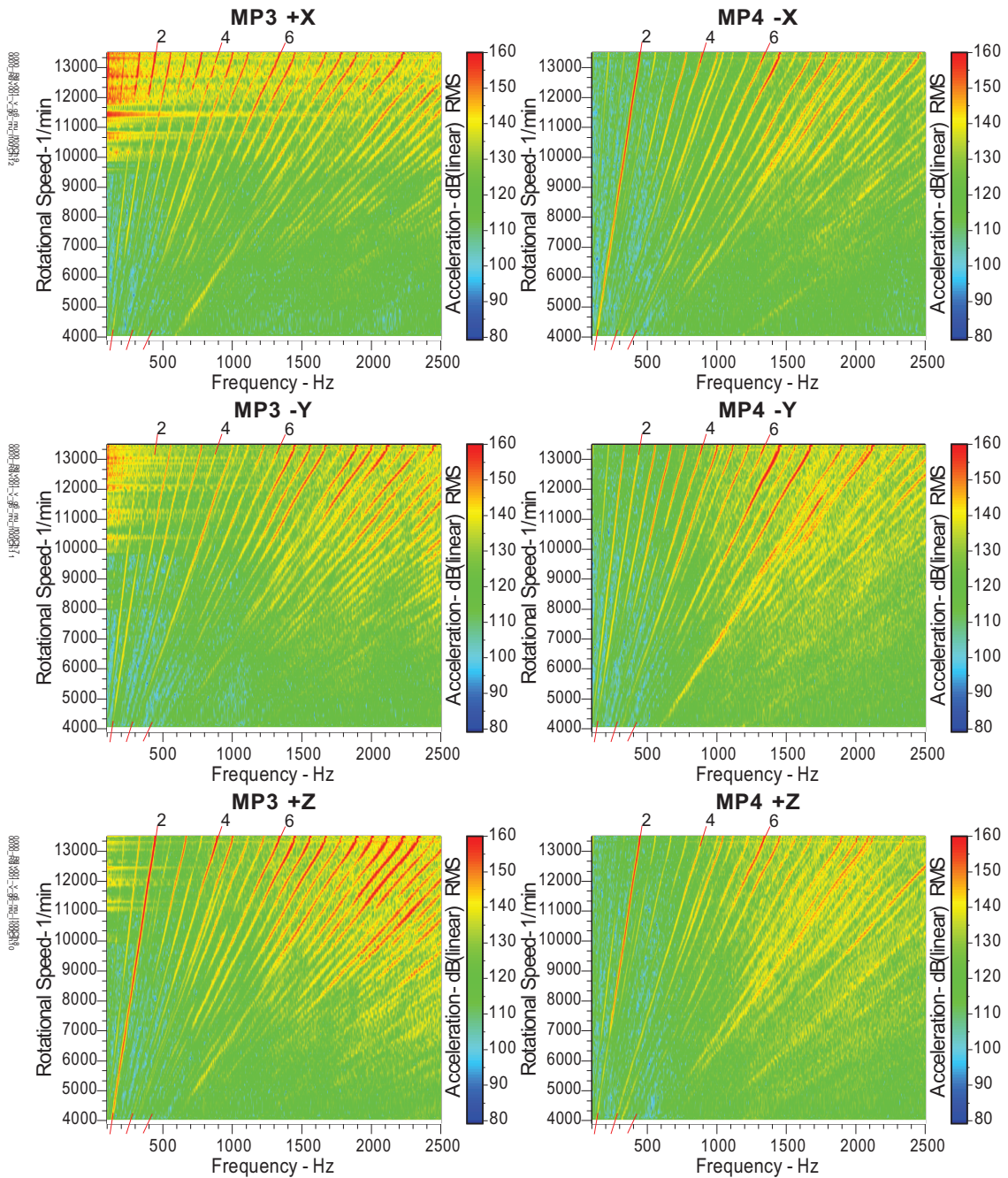
16.4 Running Mode analyses Chassis Dyno Measurements

By Josef Retzl AVL List GmbH

Version **Version 01**
Measurement: Running Mode Analysis
Testsite: Engine Test Bed - non Acoustic
Condition: Run Up Full Load , 6th Gear



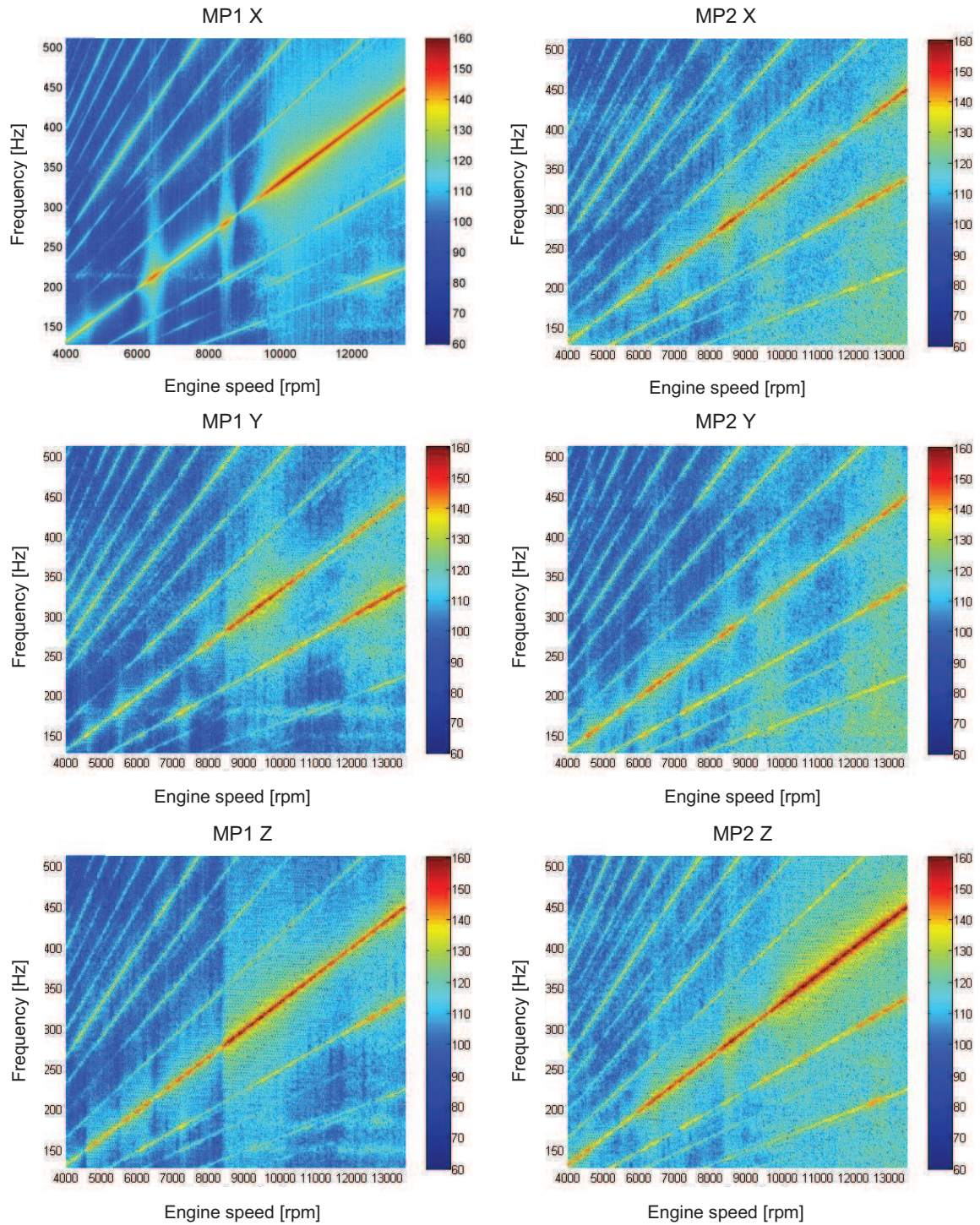
Version **Version 01**
Measurement: Running Mode Analysis
Testsite: Engine Test Bed - non Acoustic
Condition: Run Up Full Load , 6th Gear

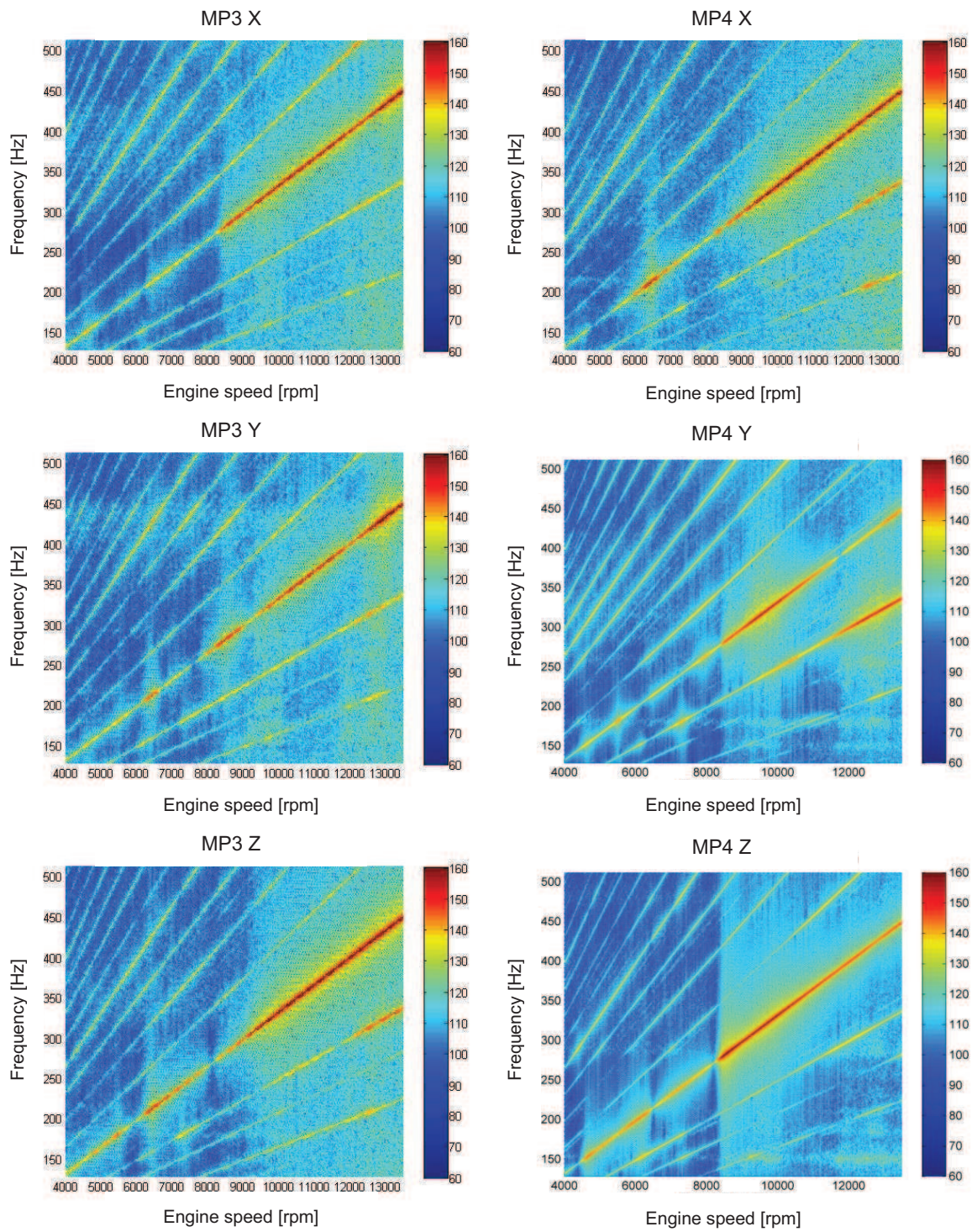


17 Appendix B: Measurements Data

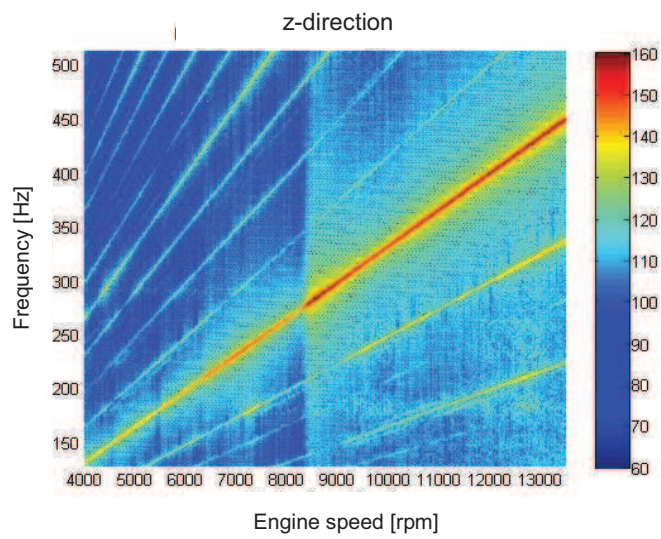
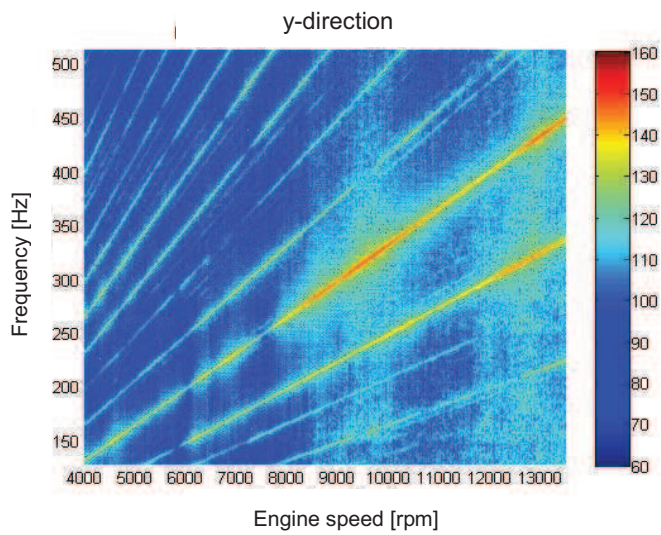
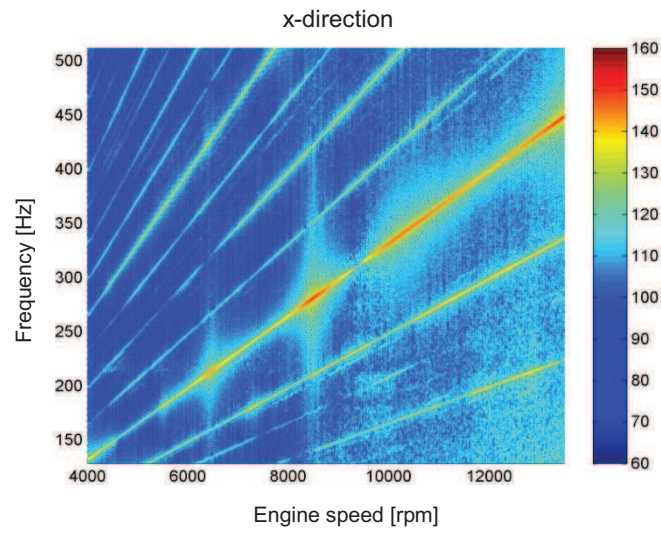
17.1 Running Mode analyses Engine Testbed Measurements

17.1.1 Vibration velocity level of mounting points



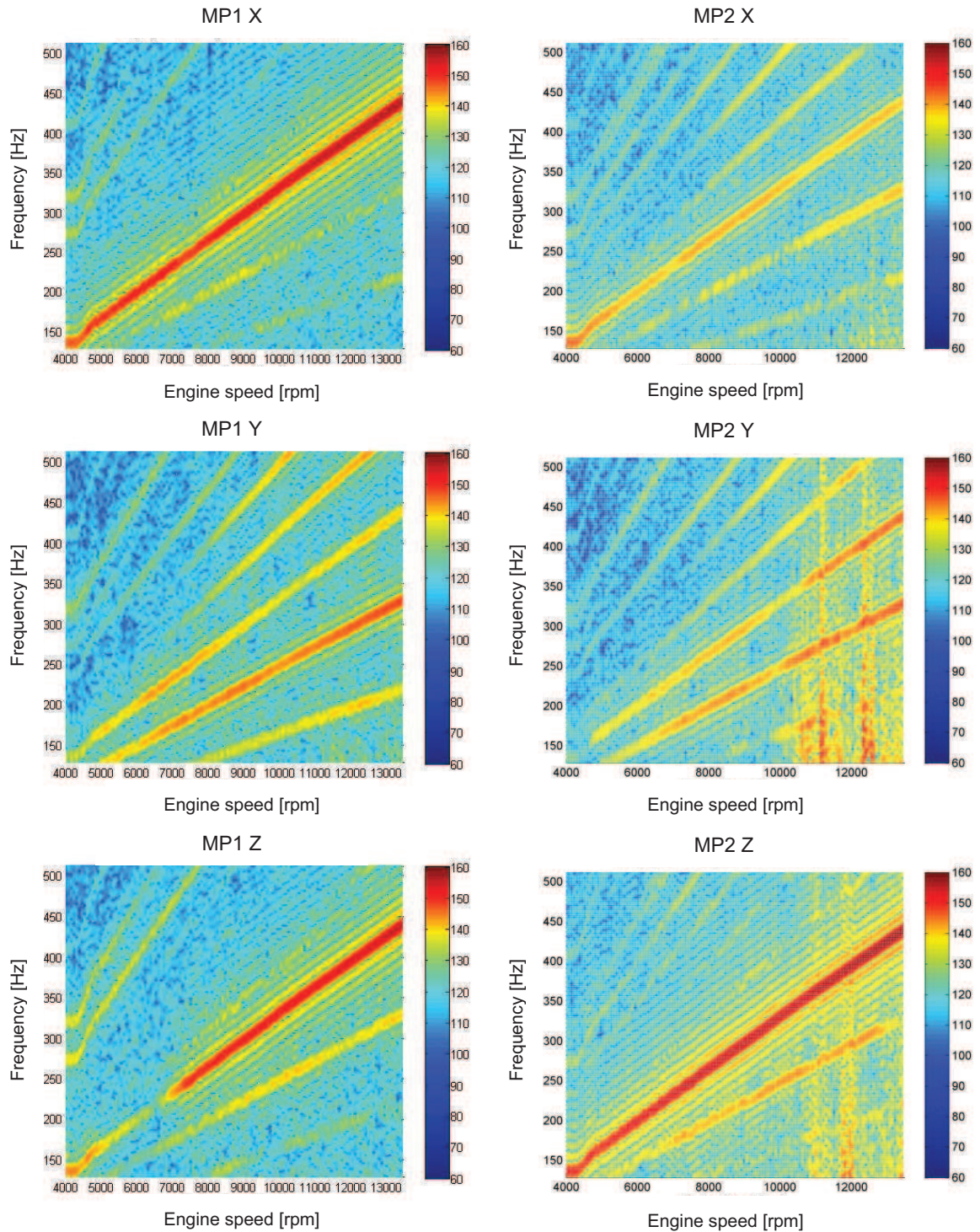


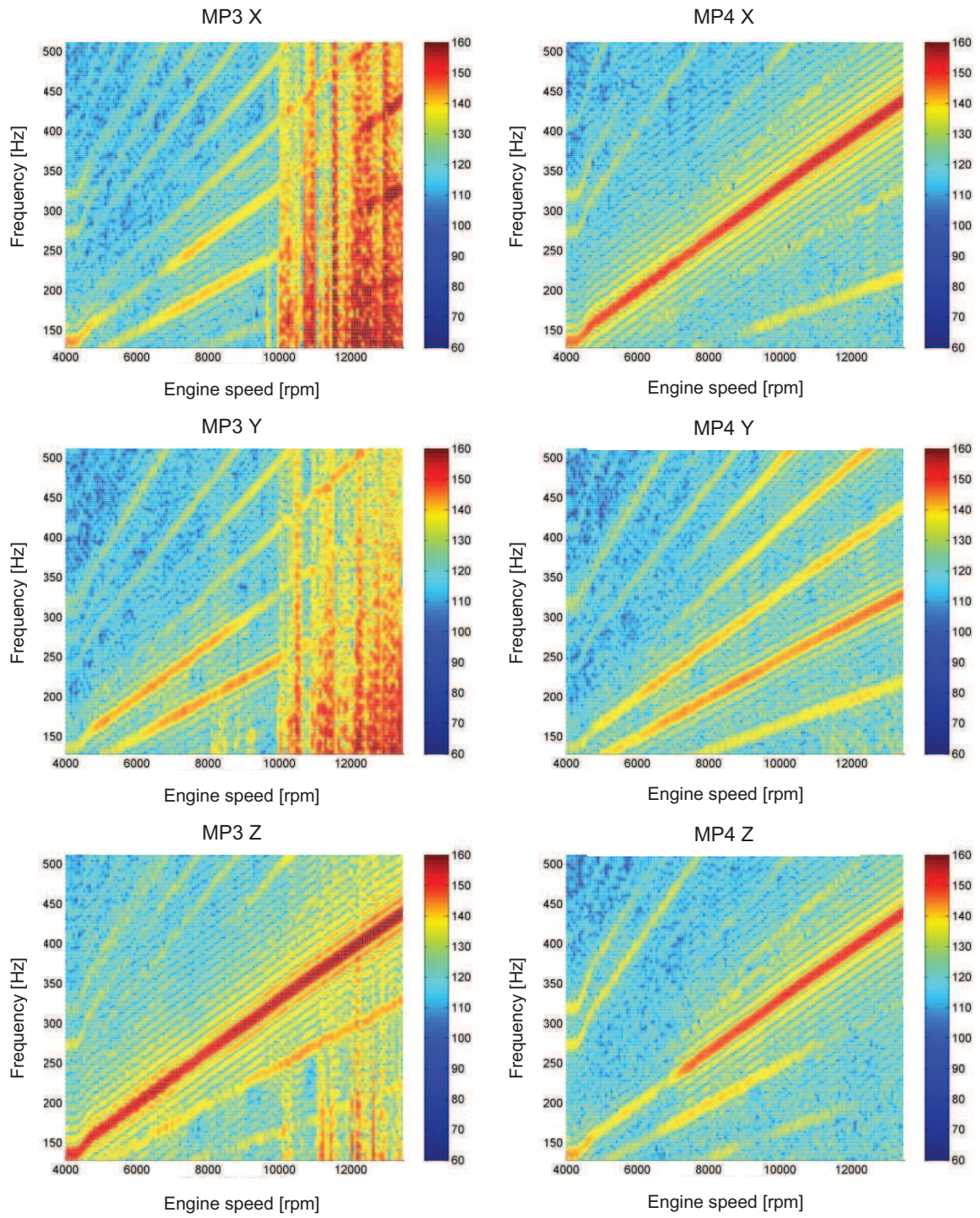
17.1.2 Vibration velocity level of centre of gravity



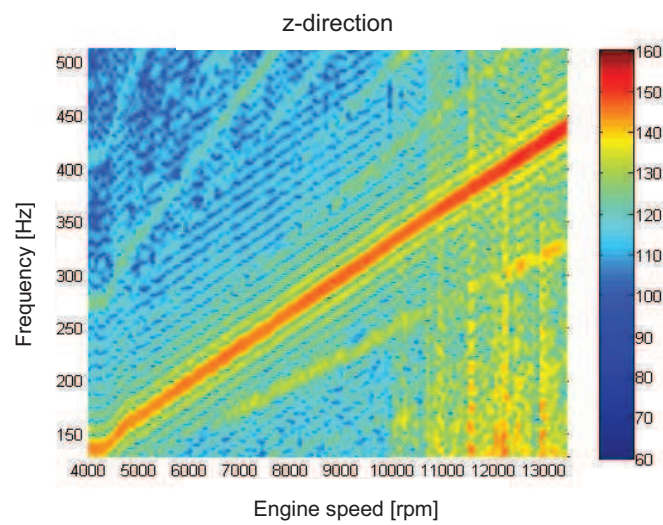
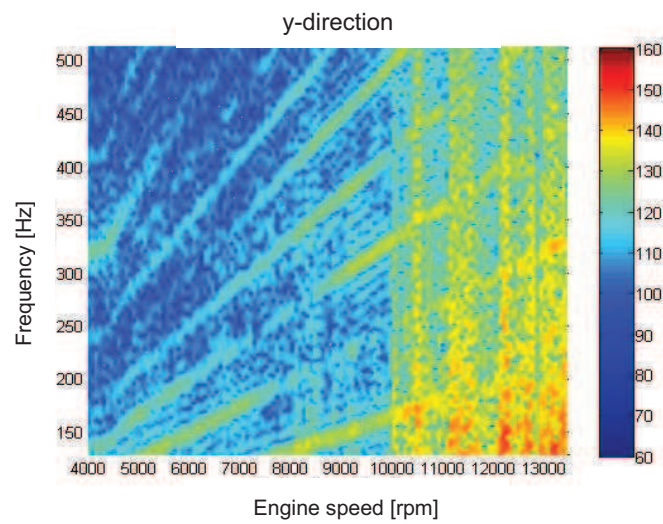
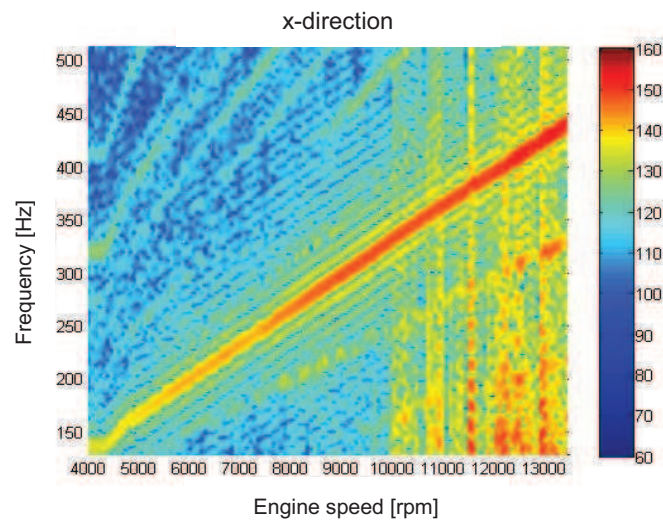
17.2 Running Mode analyses Chassis Dyno Measurements

17.2.1 Vibration velocity level of mounting points



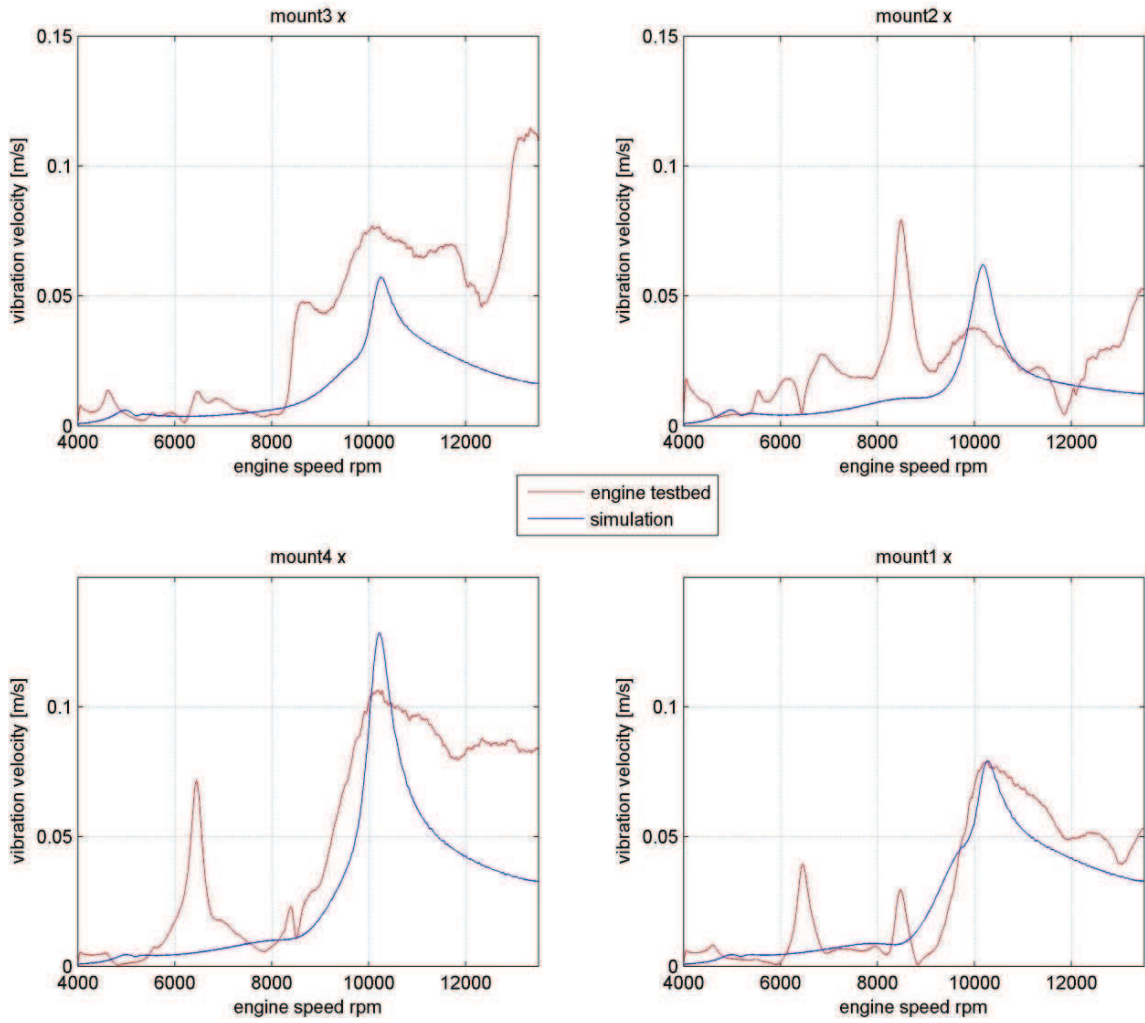


17.3 Vibration Velocity of centre of gravity

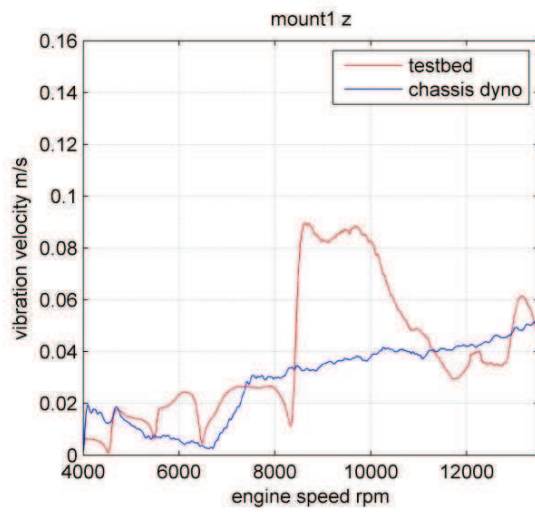
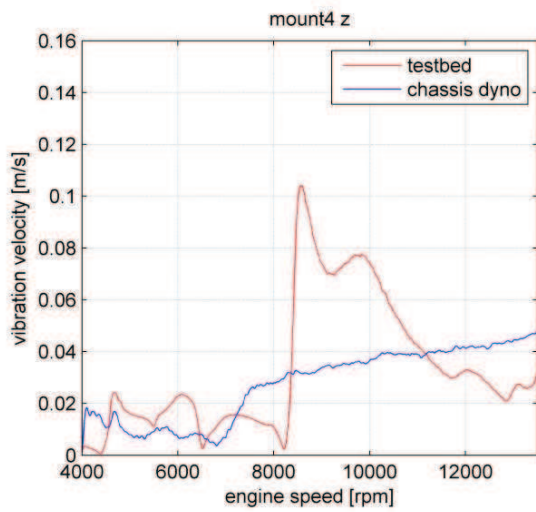
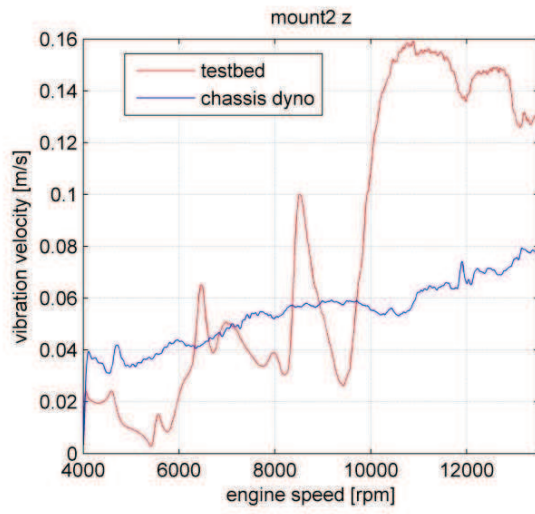
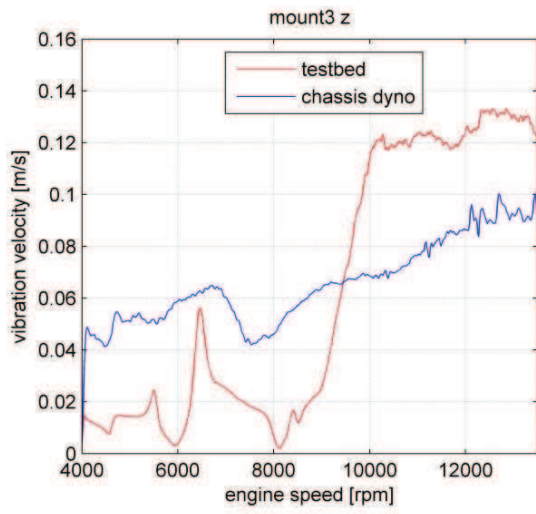


17.4 Second order vibration velocity of mounting points, Engine Testbed vs. Chassis Dyno

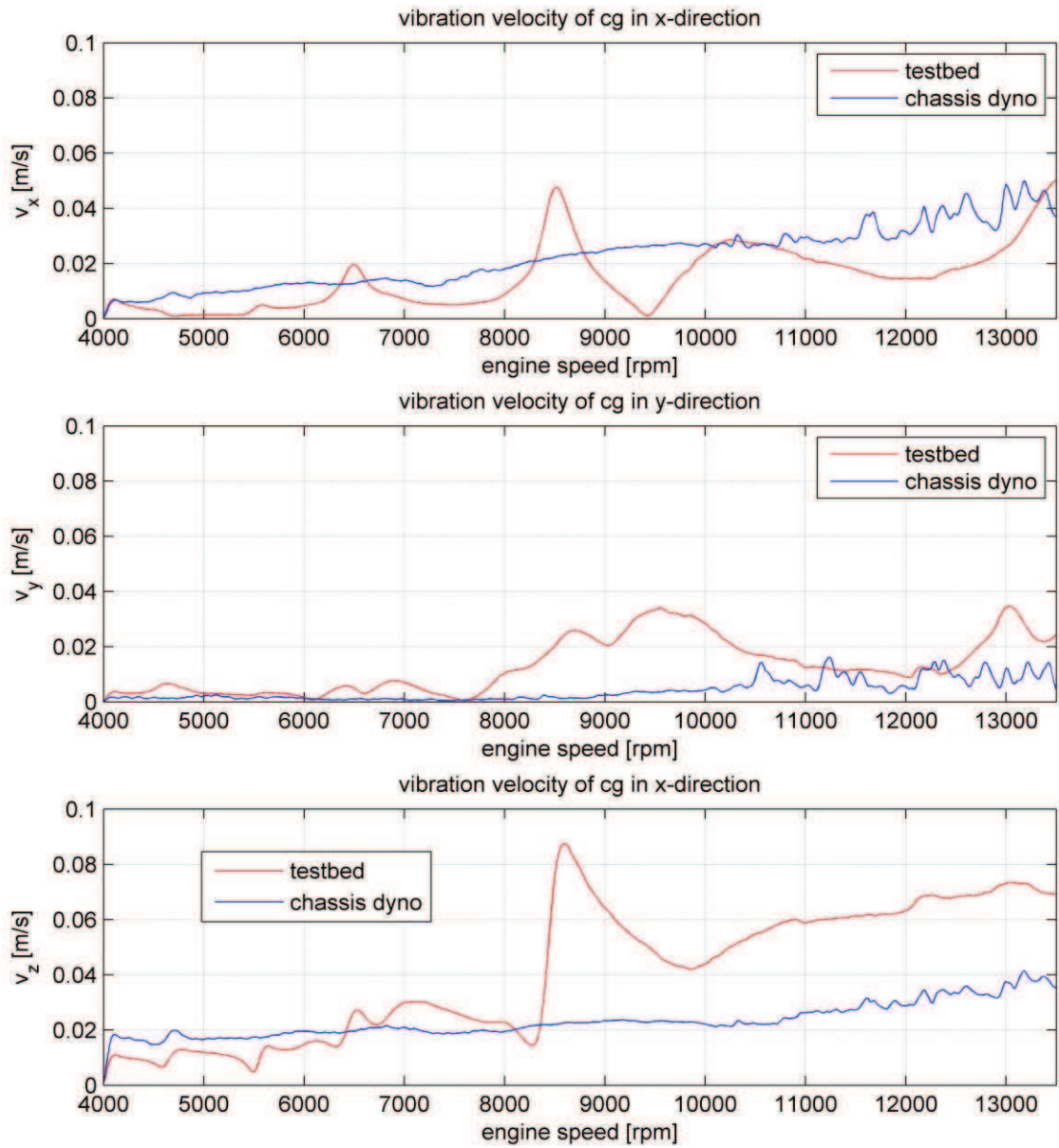
17.4.1 x-direction

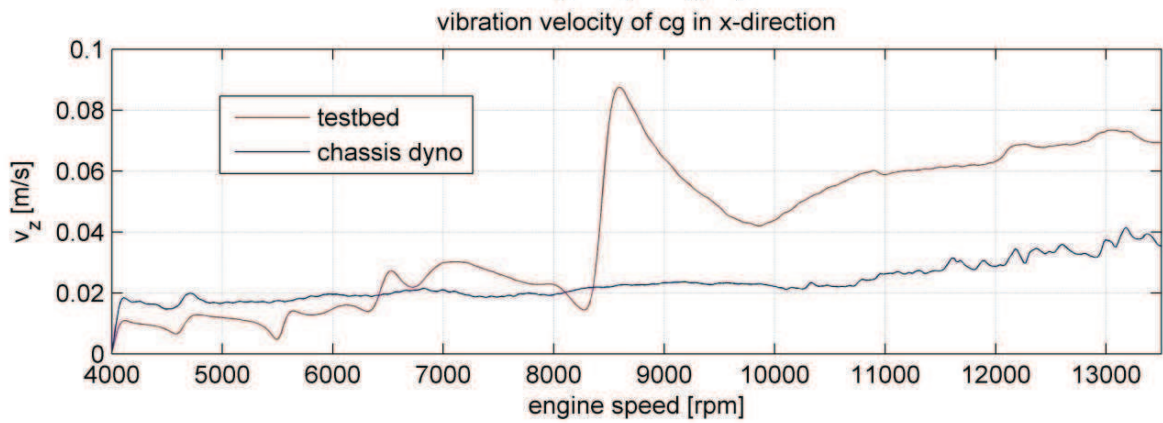
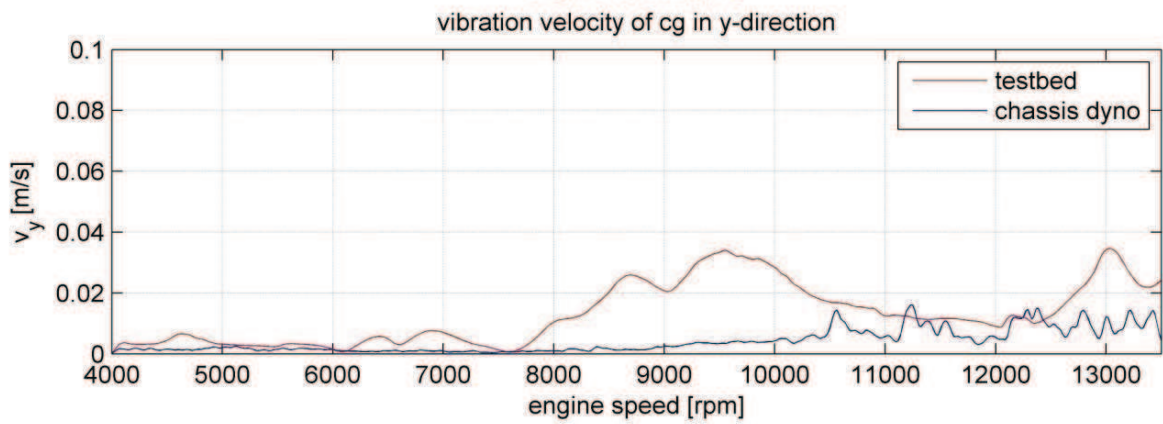
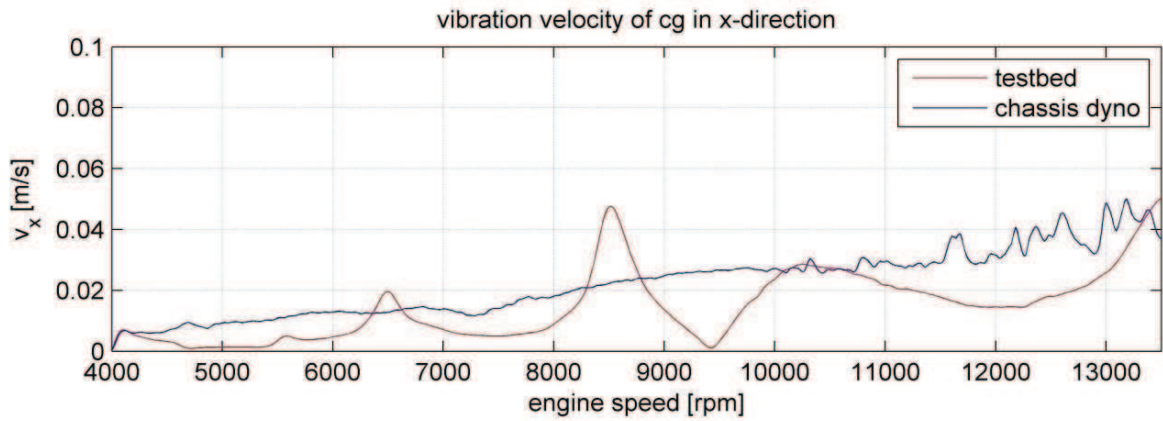


17.4.2 y-direction



17.5 Second order vibration velocity of Cg, Engine Testbed vs. Chassis Dyno





18 Appendix C: Multi-Body Simulation

18.1 Used elements from the Modelica library

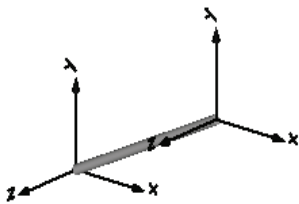
The description of the parts is quoted from the Modelica documentation.

18.1.1 FixedTranslation

Fixed translation of frame_b with respect to frame_a

Component for a fixed translation of frame_b with respect to frame_a, i.e., the relationship between connectors' frame_a and frame_b remains constant and frame_a is always parallel to frame_b.

By default, this component is visualized by a cylinder connecting frame_a and frame_b, as shown in the figure below. Note, that the two visualized frames are not part of the component animation and that the animation may be switched off via parameter animation = false.



Parameters

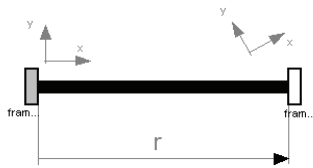
Type	Name	Default	Description
Boolean	animation	true	= true, if animation shall be enabled
Position	R[3]	{0,0,0}	Vector from frame_a to frame_b resolved in frame_a [m]

Connectors

Type	Name	Description
Frame_a	frame_a	
Frame_b	frame_b	

Path: Modelica.Mechanics.MultiBody.Parts.FixedTranslation
Version: 2.2

18.1.2 FixedRotation



Fixed translation followed by a fixed rotation of frame_b with respect to frame_a

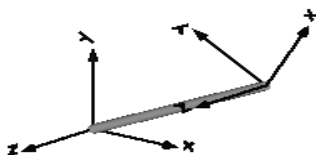
Component for a fixed translation and fixed rotation of frame_b with respect to frame_a, i.e., the relationship between connectors frame_a and frame_b remains constant. There are several possibilities to define the orientation of frame_b with respect to frame_a:

Planar rotation along axis 'n' (that is fixed and resolved in frame_a) with a fixed angle 'angle'.

Vectors n_x and n_y that are directed along the corresponding axes direction of frame_b and are resolved in frame_a (if n_y is not orthogonal to n_x , the y-axis of frame_b is selected such that it is orthogonal to n_x and in the plane of n_x and n_y).

Sequence of three planar axes rotations. For example, "sequence = {1,2,3}" and "angles = {90, 45, -90}" means to rotate frame_a around the x axis with 90 degrees, around the new y axis with 45 degrees and around the new z axis around -90 degrees to arrive at frame_b. Note, that sequence={1,2,3} is the Cardan angle sequence and sequence = {3,1,3} is the Euler angle sequence.

By default, this component is visualized by a cylinder connecting frame_a and frame_b, as shown in the figure below. In this figure frame_b is rotated along the z-axis of frame_a with 60 degree. Note, that the two visualized frames are not part of the component animation and that the animation may be switched off via parameter animation = false.



Parameters

Type	Name	Default	Description
Boolean	animation	true	= true, if animation shall be enabled
Position	r[3]	{0,0,0}	Vector from frame_a to frame_b resolved in frame_a [m]
Temp	rotationType	Modelica.Mechanics.MultiBody..	Type of rotation description
if rotationType = RotationAxis			
Axis	n[3]	{1,0,0}	Axis of rotation in frame_a (= same as in frame_b)
Angle_deg	angle	0	Angle to rotate frame_a around axis n into frame_b [deg]
if rotationType = TwoAxesVectors			
Axis	n_x[3]	{1,0,0}	Vector along x-axis of frame_b resolved in frame_a
Axis	n_y[3]	{0,1,0}	Vector along y-axis of frame_b resolved in frame_a
if rotationType = PlanarRotationSequence			
RotationSequence	sequence[3]	{1,2,3}	Sequence of rotations
Angle_deg	angles[3]	{0,0,0}	Rotation angles around the axes defined in 'sequence' [deg]

Connectors

Type	Name	Description
Frame_a	frame_a	
Frame_b	frame_b	

Release Notes:

July 28, 2003

Path: Modelica.Mechanics.MultiBody.Parts.FixedRotation

Filename: D:/Program Files/Dymola/Modelica/Library/Modelica 2.2/Mechanics/MultiBody/parts.mo

Version: 2.2

18.1.3 Body

Rigid body with mass and inertia tensor. All parameter vectors have to be resolved in frame_a. The inertia tensor has to be defined with respect to a coordinate system that is parallel to frame_a with the origin at the center of mass of the body.

By default, this component is visualized by a cylinder located between frame_a and the center of mass and by a sphere that has its center at the center of mass. If the cylinder length is smaller as the radius of the sphere, e.g., since frame_a is located at the center of mass, the cylinder is not displayed. Note, that the animation may be switched off via parameter `animation = false`.

Every body has potential states. If possible a tool will select the states of joints and not the states of bodies because this is usually the most efficient choice. In this case the position, orientation, velocity and angular velocity of frame_a of the body will be computed by the component that is connected to frame_a. However, if a body is moving freely in space, variables of the body have to be used as states. The potential states of the body are:

The position vector `frame_a.r_0` from the origin of the world frame to the origin of frame_a of the body, resolved in the world frame and the absolute velocity `v_0` of the origin of frame_a, resolved in the world frame ($= \text{der}(\text{frame_a.r_0})$).

If parameter `useQuaternions` in the "Advanced" menu is true (this is the default), then 4 quaternions are potential states. Additionally, the coordinates of the absolute angular velocity vector of the body are 3 potential states.

If `useQuaternions` in the "Advanced" menu is false, then 3 angles and the derivatives of these angles are potential states. The orientation of frame_a is computed by rotating the world frame along the axes defined in parameter vector "`sequence_angleStates`" (default = {1,2,3}, i.e., the Cardan angle sequence) around the angles used as potential states. For example, the default is to rotate the x-axis of the world frame around `angles[1]`, the new y-axis around `angles[2]` and the new z-axis around `angles[3]`, arriving at frame_a.

The quaternions have the slight disadvantage that there is a non-linear constraint equation between the 4 quaternions. Therefore, at least one non-linear equation has to be solved during simulation. A tool might, however, analytically solve this simple constraint equation. Using the 3 angles as states has the disadvantage that there is a singular configuration in which a division by zero will occur. If it is possible to determine in advance for an application class that this singular configuration is outside of the operating region, the 3 angles might be used as potential states by setting `useQuaternions = false`.

In text books about 3-dimensional mechanics often 3 angles and the angular velocity are used as states. This is not the case here, since 3 angles and their derivatives are used as potential states (if `useQuaternions = false`). The reason is that for real-time simulation the discretization formula of the integrator might be "inlined" and solved together with the body equations. By appropriate symbolic transformation the performance is drastically increased if angles and their derivatives are used as states, instead of angles and the angular velocity.

Whether or not variables of the body are used as states is usually automatically selected by the Modelica translator. If parameter `enforceStates` is set to `true` in the "Advanced" menu, then body variables are forced to be used as states according to the setting of parameters `"useQuaternions"` and `"sequence_angleStates"`.

Parameters

Type	Name	Default	Description
Boolean	<code>animation</code>	<code>true</code>	= true, if animation shall be enabled (show cylinder and sphere)
Position	<code>r_CM[3]</code>	<code>{0,0,0}</code>	Vector from frame_a to center of mass, resolved in frame_a [m]
Mass	<code>m</code>	<code>1</code>	Mass of rigid body [kg]
Inertia tensor (resolved in center of mass, parallel to frame_a)			
Inertia	<code>I_11</code>	<code>0.001</code>	(1,1) element of inertia tensor [kg.m ²]
Inertia	<code>I_22</code>	<code>0.001</code>	(2,2) element of inertia tensor [kg.m ²]
Inertia	<code>I_33</code>	<code>0.001</code>	(3,3) element of inertia tensor [kg.m ²]
Inertia	<code>I_21</code>	<code>0</code>	(2,1) element of inertia tensor [kg.m ²]
Inertia	<code>I_31</code>	<code>0</code>	(3,1) element of inertia tensor [kg.m ²]
Inertia	<code>I_32</code>	<code>0</code>	(3,2) element of inertia tensor [kg.m ²]
Initialization			
Temp	<code>initType</code>	<code>Types.Init.Free</code>	Type of initialization (defines usage of start values below)
Position	<code>r_0_start[3]</code>	<code>{0,0,0}</code>	Initial values of frame_a.r_0 (vector from origin of world frame to origin of frame_a resolved in world frame) [m]
RotationSequence	<code>sequence_start[3]</code>	<code>{1,2,3}</code>	Sequence of rotations to rotate world frame into frame_a at initial time
Angle_deg	<code>angles_start[3]</code>	<code>{0,0,0}</code>	Initial values of angles to rotate world frame around 'sequence_start' axes into frame_a [deg]
Velocity	<code>v_0_start[3]</code>	<code>{0,0,0}</code>	Initial values of velocity $v_0 = \text{der}(\text{frame_a.r}_0)$ [m/s]
AngularVelocity_degs	<code>w_0_start[3]</code>	<code>{0,0,0}</code>	Initial values of angular velocity of frame_a resolved in world frame [deg/s]
Acceleration	<code>a_0_start[3]</code>	<code>{0,0,0}</code>	Initial values of acceleration $a_0 = \text{der}(v_0)$ [m/s ²]

			der(v_0) [m/s²]
AngularAcceleration_degs2	z_0_start[3]	{0,0,0}	Initial values of angular acceleration z_0 = der(w_0) [deg/s²]
Advanced			
Type	Type	Name	Default
Name	Boolean	animation	true
Default	Position	r_CM[3]	{0,0,0}

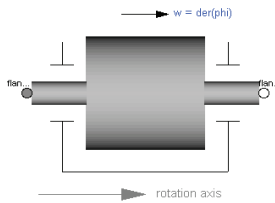
Connectors

Type	Name	Description
Frame_a	frame_a	

Path: Modelica.Mechanics.MultiBody.Parts.Body
 Filename: D:/Program Files/Dymola/Modelica/Library/Modelica 2.2/Mechanics/MultiBody/parts.mo
 Version: 2.2

18.1.4 Inertia

1D-rotational component with inertia



Parameters

Type	Name	Default	Description
Inertia	J	1	Moment of inertia [kg.m ²]

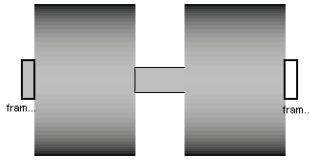
Connectors

Type	Name	Description
Flange_a	flange_a	(left) driving flange (flange axis directed INTO cut plane)
Flange_b	flange_b	(right) driven flange (flange axis directed OUT OF cut plane)

Rotational component with inertia and two rigidly connected flanges.
 Release Notes:
 June 30, 1999 by Martin Otter:
 Path: Modelica.Mechanics.Rotational.InertiaFilename:

D:/Program Files/Dymola/Modelica/Library/Modelica 2.2/Mechanics/Rotational.mo
Version: 2.2

18.1.5 RevoluteJoint



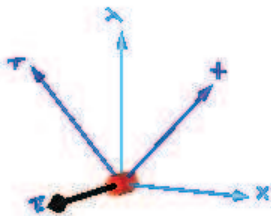
Revolute joint (1 rotational degree-of-freedom, 2 potential states)

Joint where frame_b rotates around axis n which is fixed in frame_a. The two frames coincide when " $\phi + \phi_{\text{offset}} = 0$ ", where " ϕ_{offset} " is a parameter with a zero default and " ϕ " is the rotation angle.

In the "Advanced" menu it can be defined via parameter enforceStates that the rotation angle " ϕ " and its derivative shall be definitely used as states (this means that the Modelica attributes stateSelect=StateSelect.always are set on these variables). The states are usually selected automatically. In certain situations, especially when closed kinematic loops are present, it might be slightly more efficient, when using the "enforceStates" setting.

If a planar loop is present, e.g., consisting of 4 revolute joints where the joint axes are all parallel to each other, then there is no longer a unique mathematical solution and the symbolic algorithms will fail. Usually, an error message will be printed pointing out this situation. In this case, parameter planarCutJoint in the "Advanced" menu of one of the revolute joints has to be set to true. The effect is that from the 5 constraints of a usual revolute joint, 3 constraints are removed and replaced by appropriate known variables (e.g., the force in the direction of the axis of rotation is treated as known with value equal to zero; for standard revolute joints, this force is an unknown quantity).

In the following figure the animation of a revolute joint is shown. The light blue coordinate system is frame_a and the dark blue coordinate system is frame_b of the joint. The black arrow is parameter vector "n" defining the translation axis (here: $n = \{0,0,1\}$, $\phi_{\text{start}} = 45^\circ$).



Parameters

Type	Name	Default	Description
Boolean	animation	true	= true, if animation shall be enabled (show axis as cylinder)
Axis	n[3]	{0,0,1}	Axis of rotation resolved in frame_a (= same as in frame_b)
Angle_deg	phi_offset	0	Relative angle offset (angle = phi + from_deg(phi_offset)) [deg]
Initialization			
Temp	initType	Types.Init.Free	Type of initialization (defines usage of start values below)
Angle_deg	phi_start	0	Initial value of rotation angle phi (fixed or guess value) [deg]
AngularVelocity_degs	w_start	0	Initial value of relative angular velocity $w = \text{der}(\text{phi})$ [deg/s]
AngularAcceleration_degs2	a_start	0	Initial value of relative angular acceleration $a = \text{der}(w)$ [deg/s ²]
Advanced			
Boolean	enforceStates	false	= true, if generalized variables (phi,w) shall be used as states
Boolean	planarCutJoint	false	= true, if joint shall be used as cut-joint in a planar loop

Connectors

Name	Type	Description
Frame_a	frame_a	
Frame_b	frame_b	

Path: Modelica.Mechanics.MultiBody.Joints.Revolute
 Filename: D:/Program Files/Dymola/Modelica/Library/Modelica 2.2/Mechanics/MultiBody/Joints.mo
 Version: 2.2

18.1.6 ActuatedRevolute

Actuated revolute joint (1 rotational degree-of-freedom, 2 potential states)

Joint where frame_b rotates around axis n which is fixed in frame_a. The two frames coincide when " $\text{phi} + \text{phi_offset} = 0$ ", where " phi_offset " is a parameter with a zero default and " phi " is the rotation angle.

The revolute joint has two additional 1-dimensional mechanical flanges (flange "axis" represents the driving flange and flange "bearing" represents the bearing) where it can be driven with elements of the Modelica.Mechanics.Rotational library.

In the "Advanced" menu it can be defined via parameter `enforceStates` that the rotation angle "phi" and its derivative shall be definitely used as states (this means that the Modelica attributes `stateSelect=StateSelect.always` are set on these variables). The states are usually selected automatically. In certain situations, especially when closed kinematic loops are present, it might be slightly more efficient, when using the "enforceStates" setting.

If a planar loop is present, e.g., consisting of 4 revolute joints where the joint axes are all parallel to each other, then there is no longer a unique mathematical solution and the symbolic algorithms will fail. Usually, an error message will be printed pointing out this situation. In this case, parameter `planarCutJoint` in the "Advanced" menu of one of the revolute joints has to be set to true. The effect is that from the 5 constraints of a usual revolute joint, 3 constraints are removed and replaced by appropriate known variables (e.g., the force in the direction of the axis of rotation is treated as known with value equal to zero; for standard revolute joints, this force is an unknown quantity).

In the following figure the animation of an actuated revolute joint is shown. The light blue coordinate system is `frame_a` and the dark blue coordinate system is `frame_b` of the joint. The black arrow is parameter vector "n" defining the translation axis (here: $n = \{0,0,1\}$, `phi_start = 45o`).

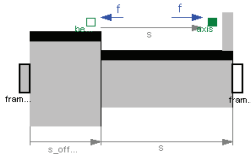
Parameters

Type	Name	Default	Description
Boolean	<code>animation</code>	<code>true</code>	= true, if animation shall be enabled (show axis as cylinder)
Axis	<code>n[3]</code>	<code>{0,0,1}</code>	Axis of rotation resolved in <code>frame_a</code> (= same as in <code>frame_b</code>)
Angle_deg	<code>phi_offset</code>	<code>0</code>	Relative angle offset (angle = <code>phi_start + from_deg(phi_offset)</code>) [deg]
Initialization			
Temp	<code>initType</code>	<code>Types.Init.Free</code>	Type of initialization (defines usage of start values below)
Angle_deg	<code>phi_start</code>	<code>0</code>	Initial value of rotation angle phi (fixed or guess value) [deg]
AngularVelocity_degs	<code>w_start</code>	<code>0</code>	Initial value of relative angular velocity $w = \text{der}(\text{phi})$ [deg/s]
AngularAcceleration_degs2	<code>a_start</code>	<code>0</code>	Initial value of relative angular acceleration $a = \text{der}(w)$ [deg/s ²]
Advanced			
Boolean	<code>enforceStates</code>	<code>false</code>	= true, if generalized variables (phi,w) shall be used as states
Boolean	<code>planarCutJoint</code>	<code>false</code>	= true, if joint shall be used as cut joint in a planar loop

Connectors

Type	Name	Description
Frame_a	frame_a	
Frame_b	frame_b	
Flange_a	axis	
Flange_b	bearing	

18.1.7 ActuatedPrismatic



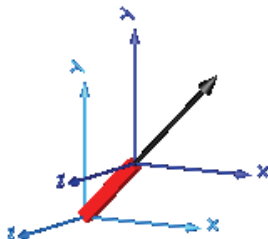
Actuated prismatic joint (1 translational degree-of-freedom, 2 potential states)

Joint where frame_b is translated along axis n which is fixed in frame_a. The two frames coincide when " $s + s_offset = 0$ ", where " s_offset " is a parameter with a zero default and " s " is the relative distance.

The prismatic joint has two additional 1-dimensional mechanical flanges (flange "axis" represents the driving flange and flange "bearing" represents the bearing) where it can be driven with elements of the Modelica.Mechanics.Translational library.

In the "Advanced" menu it can be defined via parameter enforceStates that the relative distance " s " and its derivative shall be definitely used as states (this means that the Modelica attributes stateSelect=StateSelect.always are set on these variables). The states are usually selected automatically. In certain situations, especially when closed kinematic loops are present, it might be slightly more efficient, when using the "enforceStates" setting.

In the following figure the animation of an actuated prismatic joint is shown. The light blue coordinate system is frame_a and the dark blue coordinate system is frame_b of the joint. The black arrow is parameter vector "n" defining the translation axis (here: $n = \{1, 1, 0\}$).



Parameters

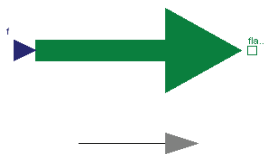
Type	Name	Default	Description
Boolean	animation	true	= true, if animation shall be enabled
Axis	n[3]	{1,0,0}	Axis of translation resolved in frame_a (= same as in frame_b)
Position	s_offset	0	Relative distance offset (distance between frame_a and frame_b = s_offset + s) [m]
Initialization			
Temp	initType	Types.Init:Free	Type of initialization (defines usage of start values below)
Position	s_start	0	Initial value of distance (fixed or guess value) [m]
Velocity	v_start	0	Initial value of relative velocity $v = \text{der}(s)$ [m/s]
Acceleration	a_start	0	Initial value of relative acceleration $a = \text{der}(v)$ [m/s ²]
Advanced			
Boolean	enforceStates	false	= true, if generalized variables (s,v) shall be used as states

Connectors

Type	Name	Description
Frame_a	frame_a	
Frame_b	frame_b	
Flange_a	axis	
Flange_b	bearing	

Path: Modelica.Mechanics.MultiBody.Joints.ActuatedPrismatic
 Filename: D:/Program Files/Dymola/Modelica/Library/Modelica 2.2/Mechanics/MultiBody/Joints.mo
 Version: 2.2

18.1.8 Force



External force acting on a drive train element as input signal

The input signal "s" in [N] characterizes an external force which acts (with positive sign) at a flange, i.e., the component connected to the flange is driven by force f.

Input signal s can be provided from one of the signal generator blocks of `Modelica.Blocks.Source`.

Connectors

Type	Name	Description
Flange_b	flange_b	
input ReallInput	f	driving force as input signal

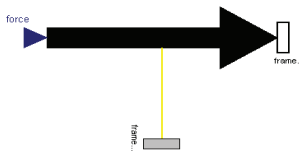
First Version from August 26, 1999 by P. Beater (based on `Rotational.Torque1D`)

Path: `Modelica.Mechanics.Translational.Force`

Filename: `D:/Program Files/Dymola/Modelica/Library/Modelica 2.2/Mechanics/Translational.mo`

Version: 2.2

18.1.9 ExternalForce



External force acting at `frame_b`, defined by 3 input signals and resolved in `frame_b` or in `frame_resolve`

The 3 signals of the force connector are interpreted as the x -, y - and z -coordinates of a force acting at the frame connector to which this component is attached. If connector `frame_resolve` is not connected, the force coordinates are with respect to `frame_b`. If connector `frame_resolve` is connected, the force coordinates are with respect to `frame_resolve`. In this case the force and torque in connector `frame_resolve` are set to zero, i.e., this connector is solely used to provide the information of the coordinate system, in which the force coordinates are defined.

This force component is by default visualized as an arrow acting at the connector to which it is connected. The diameter and color of the arrow are fixed and can be defined via parameters `diameter` and `color`. The arrow points in the direction defined by the `inPort.signal` signals. The length of the arrow is proportional to the length of the force vector using parameter `N_to_m` as scaling factor. For example, if `N_to_m = 100 N/m`, then a force of 350 N is displayed as an arrow of length 3.5 m.

Parameters

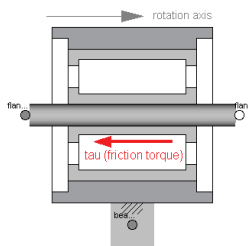
Type	Name	Default	Description
Boolean	animation	true	= true, if animation shall be enabled

Connectors

Type	Name	Description
Frame_b	frame_b	
input ReallInput	force[3]	x-, y-, z-coordinates of force resolved in frame_b or frame_resolve (if connected)

Path: Modelica.Mechanics.MultiBody.Forces.FrameForce
 Filename: D:/Program Files/Dymola/Modelica/Library/Modelica 2.2/Mechanics/MultiBody/Forces.mo
 Version: 2.2

18.1.10 BearingFriction



Coulomb friction in bearings

This element describes Coulomb friction in bearings, i.e., a frictional torque acting between a flange and the housing. The positive sliding friction torque "tau" has to be defined by table "tau_pos" as function of the absolute angular velocity "w"

$\tau_{pos} = [0, 0; 1, 2; 2, 5; 3, 8];$

Currently, only linear interpolation in the table is supported. Outside of the table, extrapolation through the last two table entries is used. It is assumed that the negative sliding friction force has the same characteristic with negative values. Friction is modelled in the following way:

When the absolute angular velocity "w" is not zero, the friction torque is a function of w and of a constant normal force. This dependency is defined via table tau_pos and can be determined by measurements, e.g. by driving the gear with constant velocity and measuring the needed motor torque (= friction torque).

When the absolute angular velocity becomes zero, the elements connected by the friction element become stuck, i.e., the absolute angle remains constant. In this phase the friction torque is calculated from a torque balance due to the requirement, that the absolute acceleration shall be zero. The elements begin to slide when the friction torque exceeds a threshold value, called the maximum static friction torque, computed via:

$$\text{maximum_static_friction} = \text{peak} * \text{sliding_friction}(w=0) \quad (\text{peak} \geq 1)$$

This procedure is implemented in a "clean" way by state events and leads to continuous/discrete systems of equations if friction elements are dynamically coupled which have to be solved by appropriate numerical methods. The method is described in:

Otter M., Elmqvist H., and Mattsson S.E. (1999):

Hybrid Modeling in Modelica based on the Synchronous Data Flow Principle. CACSD'99, Aug. 22.-26, Hawaii.

Parameters

Type	Name	Default	Description
Real	tau_pos[:, :]	[0, 1]	[w,tau] Positive sliding friction characteristic (w>=0)
Real	peak	1	peak*tau_pos[1,2] = Maximum friction torque for w==0
Advanced			
AngularVelocity	w_small	1e10	Relative angular velocity near to zero if jumps due to a reinit(..) of the velocity can occur (set to low value only if such impulses can occur) [rad/s]

Connectors

Type	Name	Description
Flange_a	flange_a	
Flange_b	flange_b	
Flange_a	bearing	

June 30, 1999 by Martin Otter:
 Name: BearingFriction
 Path: Modelica.Mechanics.Rotational.BearingFriction
 Filename: D:/Program Files/Dymola/Modelica/Library/Modelica 2.2/Mechanics/Rotational.mo
 Version: 2.2

18.2 Source Code of Self designed blocks of the Dymola Model

```

model springDamp3D
  import SI = Modelica.SIunits;
  import Modelica.Mechanics.MultiBody.Frames;

  parameter Real c11(final unit="N/m")=83000 "xx Component of stiffness Tensor";
  parameter Real c22(final unit="N/m")=83000 "yy Component of stiffness Tensor";
  parameter Real c33(final unit="N/m")=500000 "zz Component of stiffness Tensor";
  parameter Real d11(final unit="Ns/m")=200
    "xx Component of damping coefficient Tensor";
  parameter Real d22(final unit="Ns/m")=200
    "yy Component of damping coefficient Tensor";
  parameter Real d33(final unit="Ns/m")=2000
    "zz Component of damping coefficient Tensor";
  parameter Boolean initialisation=false;
  parameter SI.Position s_rel0[3]={0,1,0} "unstretched spring lenght vector";
  final parameter Real c[3,3]=[c11,0,0;0,c22,0;0,0,c33];
  final parameter Real d[3,3]=[d11,0,0;0,d22,0;0,0,d33];
  SI.Position s_rel[3](start=s_rel0);
  Real f[3](final unit="N");

  initial equation

    if initialisation then
      frame_b.r_0 = frame_a.r_0 + Frames.resolve1(frame_a.R, -s_rel0);
    end if;

  equation

    frame_b.r_0 = frame_a.r_0 + Frames.resolve1(frame_a.R, -s_rel);
    zeros(3)=frame_a.t;
    zeros(3)=frame_b.t;

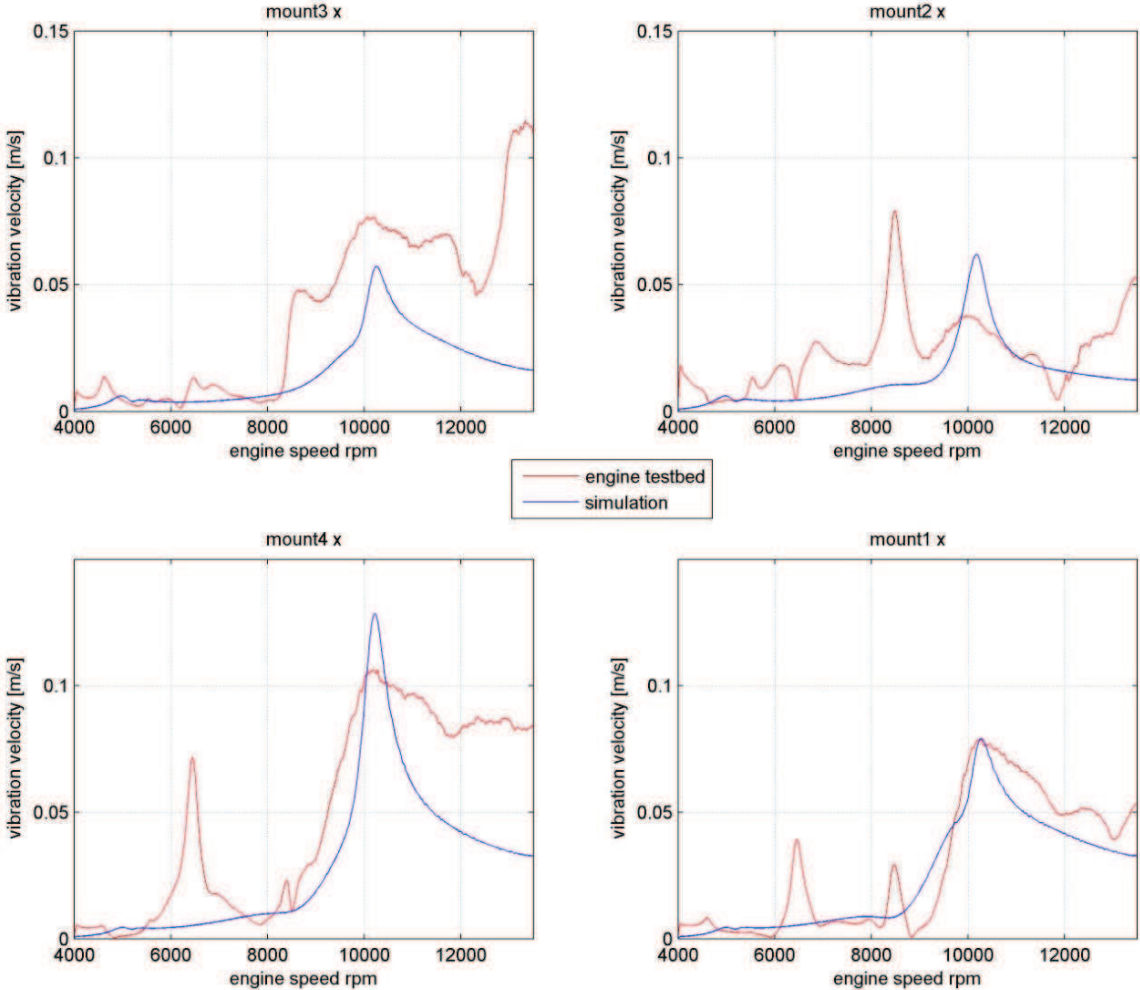
    frame_a.f=f;
    frame_b.f=-f;
    f=c*(s_rel-s_rel0)+d*der(s_rel-s_rel0);

end springDamp3D;

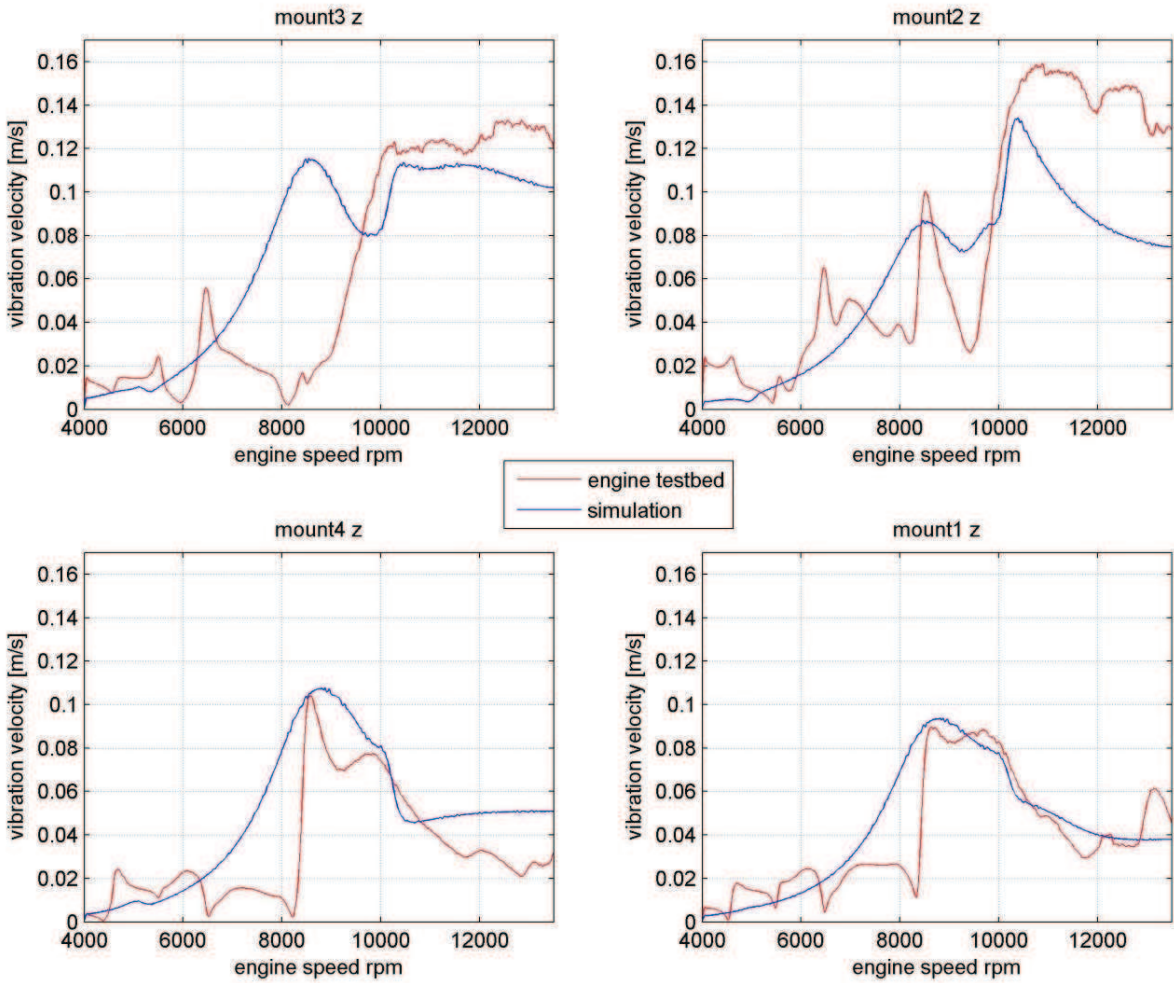
```

19 Appendix D: Simulation vs. Testbed

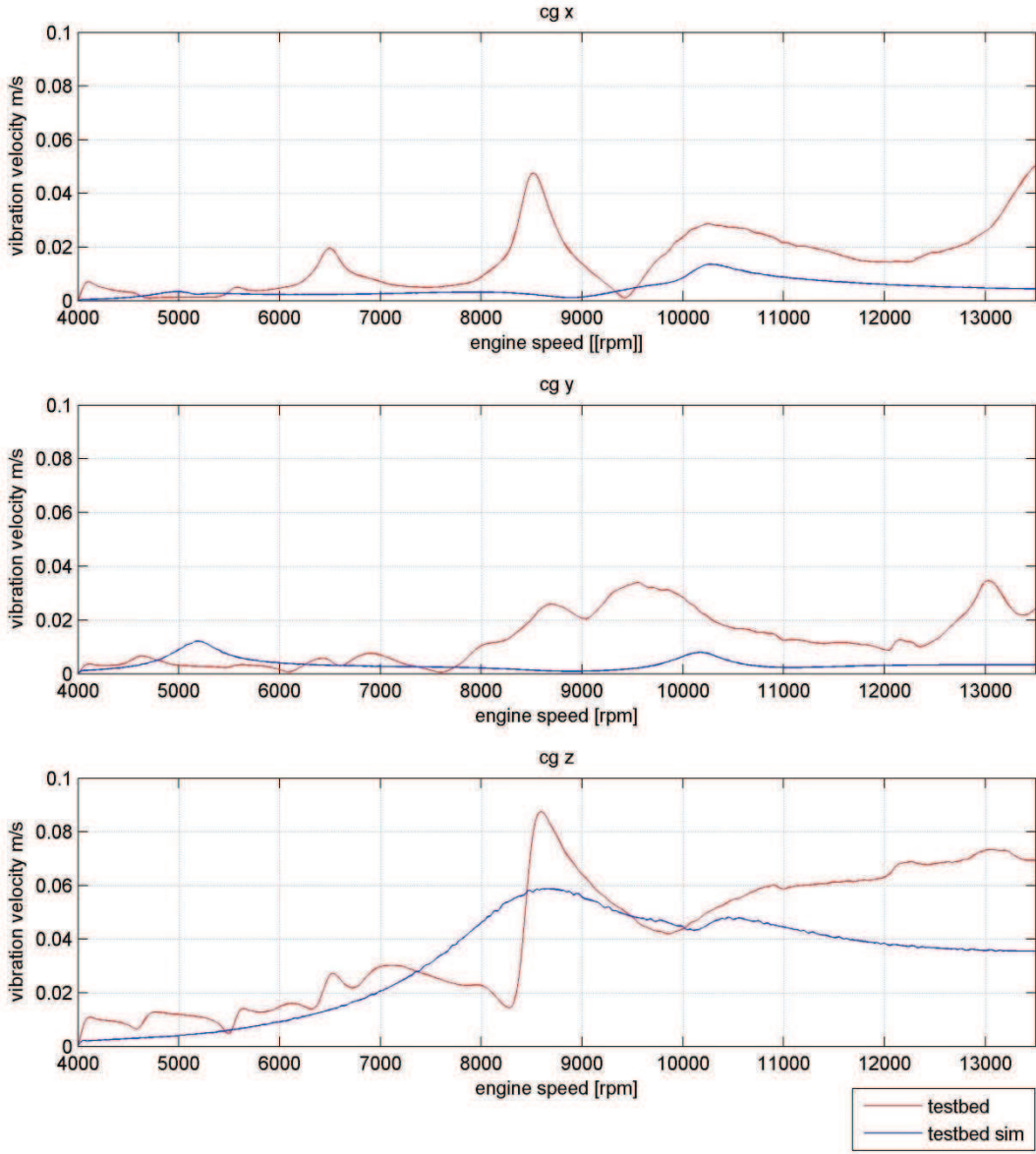
19.1 Second order vibration velocity of mounting points in x-direction



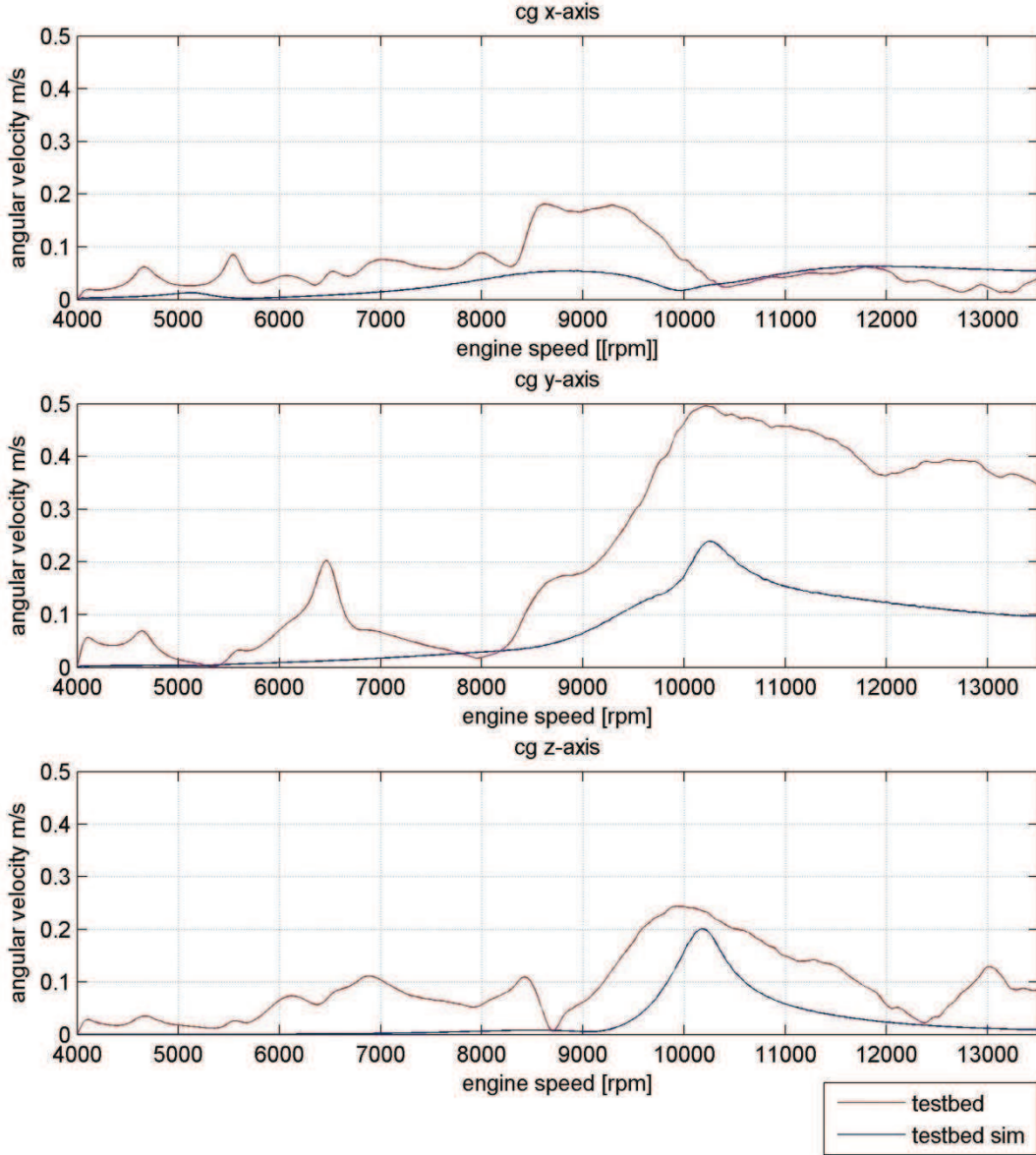
19.2 Second order vibration velocity of mounting points in z-direction



19.3 Second order vibration velocity of centre of gravity

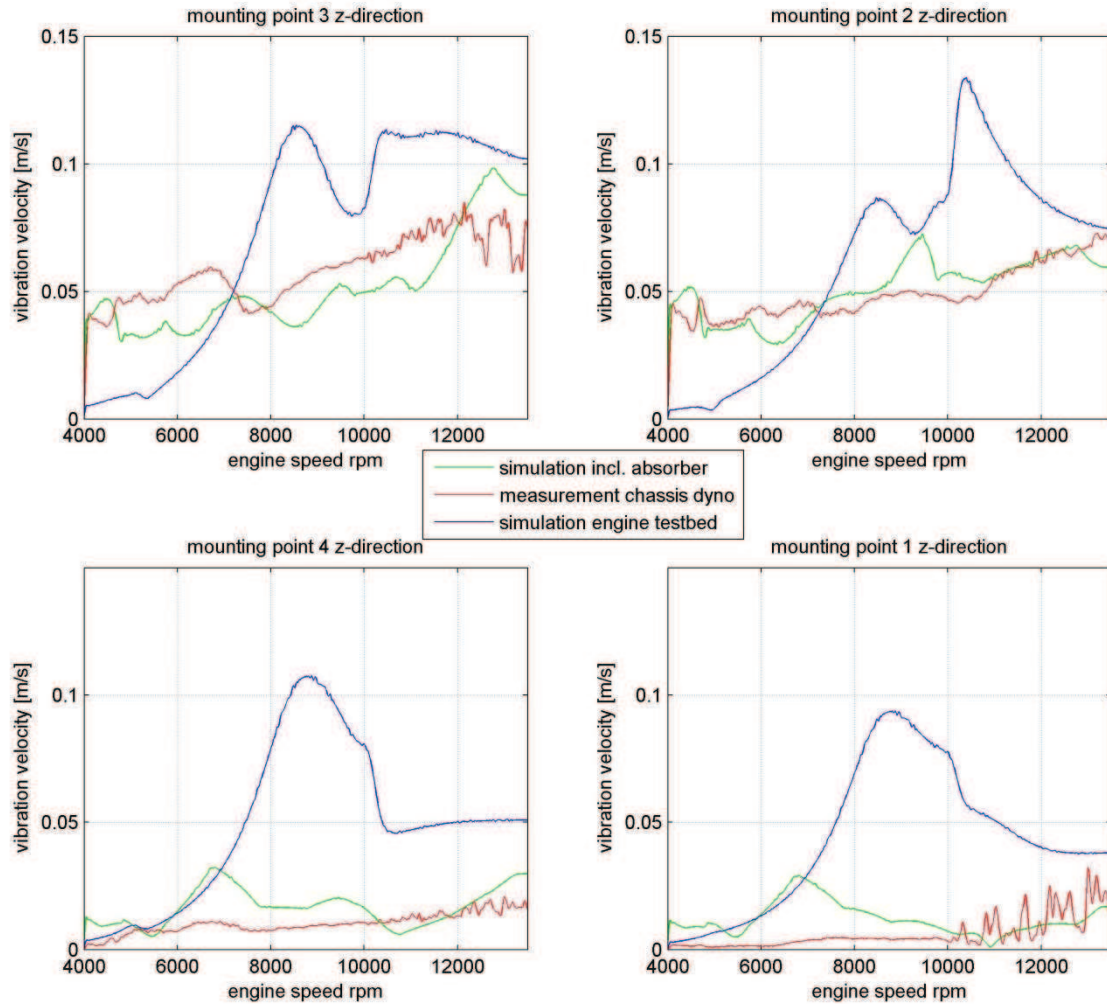


19.4 Second order angular vibration velocity of centre of gravity

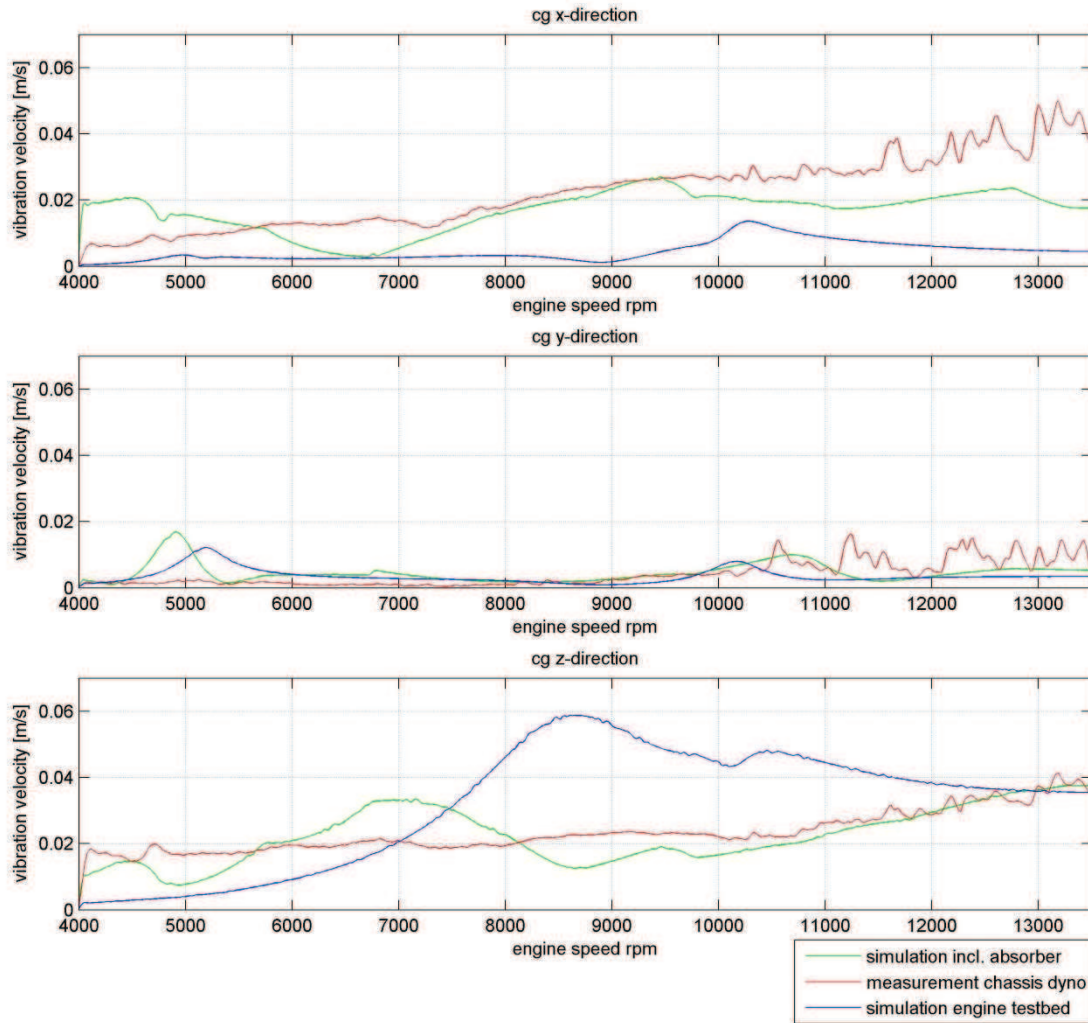


20 Appendix E: Simulation Results incl. vibration absorbers

20.1 Second order vibration velocity of mounting points in z-direction



20.2 Second order vibration velocity of centre of gravity



20.3 Second order angular vibration velocity of centre of gravity

